UNIVERSIDADE DE LISBOA
FACULDADE DE CIÊNCIAS
DEPARTAMENTO DE FÍSICA

Synchronization of Oscillators in a Fluid

Tomé Alberto Fernandes da Silva

Mestrado em Engenharia Física

Dissertação orientada por:
Dr. Rodrigo Carlos Viana Coelho
Prof. Dr. Nuno Miguel Azevedo Machado de Araújo

2023

Ao Alberto e à Rosalina, à Bárbara e à Natacha,
este pouco que tenho para dar

Acknowledgments

My deepest gratitude goes to my supervisor Prof. Rodrigo Coelho, for the constant, patient and all-present advise and guidance. My understanding of LBM is almost completely owed to him. I also have to thank my supervisor Prof. Nuno Araújo, for the incisive and thorough corrections and direction.

Through some of the hardest moments and toughest work, there they were, my friends. Knowingly or not, my "dogmatic" friends helped me greatly.

Without my family this would not had been possible. My sister Natacha made me go through thick and thin; long before getting into university, my sister Bárbara was already there. My parents, Alberto and Rosalina Silva, trusted me without ever questioning me, they supported me in every aspect going through this endeavor.

We also acknowledge financial support from the Portuguese Foundation for Science and Technology (FCT) under the contracts UIDB/00618/2020 and UIDP/00618/2020.

Resumo

Partículas em movimento num fluido podem interagir através de escoamentos (interação hidrodinâmica), levando a comportamentos não-lineares complexos. Um problema de interesse é a sincronização em escoamentos biológicos à escala microscópica, tal como a sincronização de flagelos bacterianos ou cílios que desempenham um papel importante nos mecanismos de transporte em sistemas vivos. Neste trabalho, utilizámos o método lattice-Boltzmann para simular osciladores em movimento num fluido e estudar o efeito da interação partícula-fluido. Relacionámos os resultados obtidos por este método com o modelo de Kuramoto –, um modelo de sincronização que almejávamos parametrizar através do seu fator de acoplamento. Isto permitir-nos-ia obter um modelo genérico para caraterizar o sistema de osciladores num fluido.

O sistema em estudo, simulado com o método lattice-Boltzmann, tem as seguintes caraterísticas: é bidimensional e constituído por um fluido contido entre duas placas paralelas com condição de não-deslizamento (em cima e em baixo) e com condições de fronteira periódicas à direita e à esquerda. Neste, dois osciladores são incluídos igualmente espaçados na horizontal (tendo-se em conta as suas imagens periódicas) e na posição central entre as duas palcas. Cada oscilador toma a forma de uma partícula sólida circular, sendo que o seu movimento se faz na horizontal. Cada um dos osciladores está ligado a um centro de oscilação através de uma força do tipo mola; o seu movimento autónomo é propulsionado por uma força externa de magnitude constante e que muda de sentido após atingir uma certa amplitude em relação ao centro de oscilação; além disso, cada oscilador está, evidentemente, sujeito à força de arrasto do fluido. Podemos considerar este sistema como um modelo para flagelos (secção transversal). Para implementar tal sistema, complementamos o método lattice-Boltzmann com a computação da força de arrasto para partículas móveis e o próprio movimento destas partículas. Neste último caso, utilizamos o método de Verlet e um algoritmo de criação e destruição de nodos do fluido (o que acontece quando a partícula sólida move-se pela rede de nodos). O código para as simulações foi testado e a sua coerência física comprovada através de um conjunto de escoamentos conhecidos.

O nosso estudo é direcionado para os efeitos que têm as propriedades do sistema na sincronização, nomeadamente: a viscosidade do fluido, a distância entre centros de oscilação, a frequência natural e a velocidade linear dos osciladores e a diferença de fase inicial. Este estudo é dividido em duas partes: na primeira, estudamos sistemas com partículas com a mesma frequência natural; e na segunda, sistemas com partículas com frequências naturais diferentes. Esta variável, a frequência natural, é definida como sendo a frequência de um oscilador quando este se encontra num sistema suficientemente grande, de tal forma que podemos considerar que a influência de outro qualquer oscilador no seu movimento é negligenciável, isto é, o oscilador encontra-se isolado no fluido.

A variável que utilizamos para caraterizar o sistema com osciladores com a mesma frequência natural é o tempo de sincronização, considerado como sendo o instante em que o sistema atinge uma diferença de fase suficientemente pequena (no nosso caso, $\Delta\phi \leq 0.283$ rad), uma vez que, para este caso, a diferença de fase final é nula. O tempo de sincronização demonstra os seguintes comportamentos face às propriedades do sistema: 1) aumenta com a diferença de fase inicial; 2) aumenta com a distância entre os centros de oscilação; 3) diminui com a viscosidade; 4) não é significativamente alterado pela velocidade linear; e 5) é não-monótono com a frequência natural. No nosso estudo da viscosidade, começámos por apenas variar a viscosidade entre ensaios; mas visto que a viscosidade também altera a frequência natural dos osciladores, fizemos um segundo estudo da influência da viscosidade, em que a frequência natural era mantida constante através do ajuste da aceleração das partículas. Neste segundo estudo, o tempo de sincronização também diminui com a viscosidade.

O sistema com osciladores com frequências naturais diferentes tem a caraterística de a diferença de fase final não ser necessariamente nula (e, em geral, não o é); pelo que, além do tempo de sincronização, também a diferença de fase final é utilizada para caraterizar a sincronização do sistema. Curiosamente, estas duas variáveis têm o mesmo comportamento em função das quantidades de interesse: 1) ambas aumentam com a distância entre os centros de oscilação; 2) são não-monótonas com a viscosidade; e 3) aumentam com a diferença entre as frequências naturais (o mesmo é dizer, com a diferença entre as acelerações dos osciladores).

Procedemos então à simulação do modelo de Kuramoto com dois osciladores. Isto com o intuito de obter soluções numéricas que não só nos indicassem a existência (ou não) de sincronização, mas também nos dessem o tempo de sincronização, a diferença de fase final e a evolução temporal do sistema. Ao estabelecermos previamente as frequências naturais dos osciladores e a diferença de fase inicial, o sistema é passível de ser classificado exclusivamente pelo fator de acoplamento. Ao simularmos o sistema com osciladores com a mesma frequência natural, observamos que o tempo de sincronização diminui com o fator de acoplamento, segundo uma lei de potência (sobretudo válida para os casos em que os osciladores não começam em oposição de fase). Vemos que a potência é essencialmente igual a -1 – isto é, o tempo de sincronização é inversamente proporcional ao fator de acoplamento. Além do mais, é possível obter esta constante de proporcionalidade em função da diferença de fase inicial por meio de uma regressão linear – isto é, a constante de proporcionalidade (entre o tempo de sincronização e o fator de acoplamento) é, ela própria, diretamente proporcional à diferença de fase inicial.

Ao compararmos as simulações do fluido com aquelas do modelo de Kuramoto, observamos que o modelo de Kuramoto mais simples utilizado apresenta algumas limitações. Estas limitações devem-se ao facto de, mesmo quando as simulações dos dois modelos têm o mesmo tempo de sincronização, a transição (em termos da diferença de fase instantânea) entre o instante inicial e a sincronização ocorrerem de forma evidentemente diferente. Na simulação do fluido, esta transição mostra-se muito dependente das condições iniciais do sistema, a tal ponto de se evidenciam dois regimes de sincronização distintos.

Propusemos então duas alterações diferentes ao modelo de Kuramoto: uma onde o fator de acoplamento não é constante; e outra onde a frequência natural não é constante. Em ambos os casos, a variável em questão converge para o seu valor final a partir de um outro valor: no caso da frequência natural, a frequência inicial de um dos osciladores é considerada nula; e no caso do fator de acoplamento, o valor inicial é considerado superior ao final –, isto visto que o primeiro regime de sincronização tende mais depressa para a sincronização do que o segundo. Com qualquer um destes modelos modificados, obtemos um fator de acoplamento efetivo.

Para o sistema com dois osciladores com a mesma frequência natural, o fator de acoplamento efetivo mostra-se proporcional à frequência natural e à viscosidade, e inversamente proporcional ao quadrado da distância entre os centros de oscilação. Por esta razão, relacionamos o fator de acoplamento a estas três variáveis. Esta parametrização do fator de acoplamento mostra-se razoável; no entanto, a dependência do fator de acoplamento nestas variáveis não é unívoca, pelo que é de supor que existem relações mais complexas entre estas variáveis e/ou outras variáveis que não tidas em conta.

Para o sistema com dois osciladores com frequências naturais diferentes, este fator de acoplamento efetivo diminui tanto com a distância entre centros de sincronização como com a diferença entre as frequências naturais (e pelo que é sugerido, segundo uma lei de potência, para estes dois casos). Quanto à viscosidade, o fator de acoplamento efetivo começa por diminuir ligeiramente, mas depois aumenta.

A caraterização do nosso sistema por meio do modelo de Kuramoto demonstra-se razoável, ainda que incompleta; isto devido ao facto de, em alguns casos, o sistema em estudo não concordar com as previsões do modelo de Kuramoto. O caso mais evidente é o da frequência: segundo o modelo de

Kuramoto, quando sincronizados, dois osciladores atingem uma frequência final que é a média das suas frequências naturais; no entanto, o que é observado no nosso sistema é que a frequência final é, na vasta maioria dos casos, superior a qualquer uma das frequências naturais dos osciladores. Isto parece dever-se ao efeito de uma "interferência construtiva" entre os osciladores, em que estes impulsionam o movimento um do outro reciprocamente. Esta interferência evidencia-se também na amplitude de oscilação, que, por exemplo, aumenta com a proximidade entre os centros de oscilação.

Palavras-chave: osciladores, sincronização, modelo de Kuramoto, método Lattice-Boltzmann

Abstract

Particles moving in a fluid interact though flows leading to rich non-linear behaviours. A problem of interest is the synchronisation in biological flows at the microscale, such as the synchronisation of bacteria flagella and the transport of organelles in living organisms by cilia. In this work, we used the lattice Boltzmann method to simulate moving solid particles in a fluid and simulate the fluid-particles interaction. With these simulations, we studied the effect on synchronization of different parameters, such as the fluid viscosity, the distance between oscillators, their natural oscillation frequency, and the initial phase shift. This study is divided in to two parts: systems with particles with the same natural oscillation frequency and systems with particles of different natural oscillation frequencies. This was done with further propose of relating these quantities with the coupling factor of the Kuramoto model. As the simplest Kuramoto model used presented some limitations, we propose a modification to it, where either the natural frequency of the coupling factor is non-constant. With these modified models, we concluded that the necessary coupling factor to synchronize is proportional to the natural frequency and the fluid viscosity, while inversely proportional to the distance between centers of oscillation.

Keywords: oscillators, synchronization, Kuramoto model, Lattice Boltzmann method

Index

List of Figures

List of Tables

Acronyms

BGK	Bhatnagar-Gross-Krook.
CFD	Computational fluid dynamic.
CO	Center of oscillation.
KM	Kuramoto model.
LBE	Lattice Boltzmann equation.
LBM	Lattice Boltzmann method.
NSE	Navier-Stokes equation.

Chapter 1

Introduction

One can define spontaneous synchronization as the process by which two or more oscillators converge to the same repeating pattern under weak coupling. Phase synchronization is the convergence of the phase angles of multiple oscillators. We see this when a small group of people walking side-by-side end up synchronizing their stepping, or when applauding, a crowd tends to clap in-sync. This synchronization has the oscillators in-phase; there is also the case of frequency synchronization: the oscillators, starting with different frequencies, converge to the same frequency, but they do not converge to the same phase angle, and we achieve a final and definite phase shift. Phase synchronization only occurs if we have frequency synchronization.

The first historically known experiment of synchronization was that performed by Huygens [1]. It is said that all came from the "longitude problem", to which the pendulum clock would be the solution: while sick in bed, Huygens noted that the motion of two pendulum clocks hanging from a wall would eventually synchronize with each other. He later studied the problem of synchronization of coupled oscillators using the setup of two pendulum clocks hanging from a beam, which was in turn supported on two chairs. Hyugens' clocks have even been reexamined and revisited in the recent past [2] [3].

A commonly referred practical example of synchronization of oscillators interacting through a medium (similar to that of the experiment of Huygens) is that of an ensemble of metronomes on a moving platform [4]. The metronomes oscillate at different frequencies and out-of-phase with each other; the platform, like a swing that is influenced by all of the metronomes, itself oscillates in response to the ensemble. The result is that, in time, the coupling through the platform makes all the metronomes to oscillate in-phase (with instances of anti-phase synchronization being observed). In the case of oscillators in a fluid, it is the flow itself mediates the interaction.

The synchronization of signals can be seen in a variety of natural phenomena, an commonly cited one being that of flashing fireflies [6]. But there is also the synchronization of oscillators, which achieve a number of different repeating patterns, such as metachronal waves [7] (the "Mexican waves" in Figure 1.1) or phase-locking motion (the one we see in the ensemble of metronomes). These last two cases are observed in cilia and flagella, hairlike appendages that are generally found submerged in a fluid and subject to it. Their motion is described as "run-and-tumble". These biological structures and systems are of particular interest, as they are responsible for such processes as the transport of organelles in living organisms and the mucociliary transport in the human respiratory system – responsible for the clearing of the airways [8]. Recently, it has also been suggested that sperm movement is aided by the flocking movement of cilia in the walling of the uterus [9], and the presence of synchronization of flagella of unicellular green algae *Chlamydomonas* [10] [11]. These structures and their synchronization have been studied in a number of ways, be it by simulating them as colloidal spheres in a circular trajectory [12],

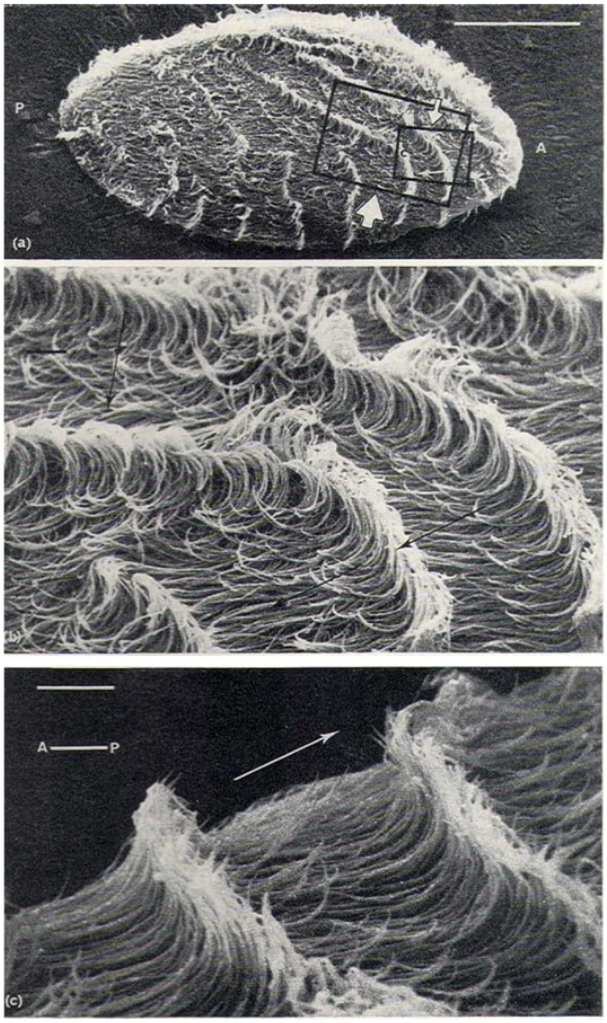

Figure 1.1: Pattern of metachronal waves on the ventral surface of an *Opalina* fixed in Ringer solution. (a) Image of the all animal, noted with the anterior and posterior of the being (the white A and B, respectively). (b) Enlargement of the region B of image (a) (indicated by the larger arrow), showing the leading sides of the waves turning through more than 45° as they spread posteriorly (motion indicated by the dark arrows). (c) Enlargement of image (a) (indicated by the smaller arrow), showing parts of the two waves illustrated in B, but seen from the opposite direction of (b) (motion indicated by the white arrow). This image is taken from [5].

studying experimentally the synchronization of beating flagella through direct hydrodynamic interactions [13], or analytically modelling the synchronization of rotating flagella [14].

Most of these studies focused on how the interaction between two or more flagella (in an ensemble) is dependent on the distance between them, through simple effective models, be it at the macro or the mesoscopic scale. We intended to study not only the distance dependency but also the influence of the fluid viscosity, the initial phase shift, the frequency and the linear velocity of the particles; and doing this by simulating the individual particles (at the microscopic scale) interacting through the fluid. As far as we can conclude, this type of study has not been thoroughly undertaken.

We saw how these oscillators synchronize (if at all), and how do the different parameters influence the overall behavior. There are two approaches that we take to this problem: computational fluid dynamic (CFD) modelling, which in our case is based on the lattice Boltzmann model (LBM); and stochastic modelling, which is the Kuramoto model (KM). This last model is often used in the study of the synchronization processes [15] –, and was developed from the model proposed by Winfree [16], which was hard to solve in its full generality. But this model has also been applied in a number of other systems,

like in Josephson junctions arrays [17] and laser arrays [18] [19]. The Kuramoto model can be applied to a wide range of systems, with different time scales and (oscillatory) motion lengths; as long as these systems can be parameterized into limit-cycle oscillators. For the LBM simulations, the geometry of the system was simplified to two particles in a one-directional motion, in a two dimensional system, periodic in the direction of the motion.

The model developed was inspired by a set of problems concerning biological oscillators (some of which were already referred and others that will be referred in section 3). The computational fluid dynamic code (explained on section 2.1), based on the lattice Boltzmann method, was written from scratch. The analysis of the results of the simulation of this CFD model was carried out with the aid of our own Python scripts. The comparison of the results of the CFD model with the Kuramoto model has taken us to suggest some possible limitations of the latter model, as well as some modifications to better predict the results found with the fluid simulations (cf. section 4.2). All of this work had as basis the necessary research of the scientific literature in the general problematic of oscillators in a fluid.

Our results suggest that the synchronization depends on the variables. We verified that adaptations to the Kuramoto model are necessary in order to describe the results from the fluid simulation. We started with oscillators of the same natural frequency. Our first approach was to try and define the behavior observed in the fluid simulations by their synchronization time: we adjusted this time to that predicted by the Kuramoto model, by assigning a corresponding coupling factor, K. As this proved to be too simplistic, we then modified the Kuramoto model to better predict the results obtained by the fluid simulations. Finally, we studied the system in which the particles had different natural frequencies; in this case, it was possible to compare them directly to the original Kuramoto model.

This thesis is structured as following. In chapter 2, we describe the fluid model and the Kuramoto model, while referring the most important specifics of each: the implementation of moving particles for the LBM and the KM with two particles. In chapter 3, we present the results of our simulations of the two systems studied: systems with particles with the same natural frequency and systems with particles with different natural frequencies. In chapter 4, we start by presenting our simulation of the KM, so as to then relate the coupling factor with the results obtained in chapter 3; it is also in this chapter that we propose the aforementioned modifications to the Kuramoto model. The main conclusions of the thesis are presented in chapter 5.

Chapter 2

Methods

2.1 Lattice Boltzmann method

We considered the lattice Boltzmann method to simulate the fluid flow and the fluid-particle interaction. With this method, the space is discretized in a regular lattice where each point of the lattice is a node with a given discrete distribution in the velocity space f_i. The type of lattice is defined by a velocity set $\{c_i\}$, itself characterized by the notation DdQq: the number of spatial dimensions, d, and the number of velocity vectors, q. The lattice chosen for this study was the D3Q19 (which stands for 3 spatial dimensions and 19 velocity vectors). Once we have our velocity set $\{c_i\}$ – and therefore our lattice – we also need to define the corresponding weights $\{w_i\}$. These weighs for the D3Q19 set are well known, and can be obtained from the Gauss-Hermite quadrature. A scheme of D3Q19 lattice is represented in Figure 2.1 and its weights in table 2.1.

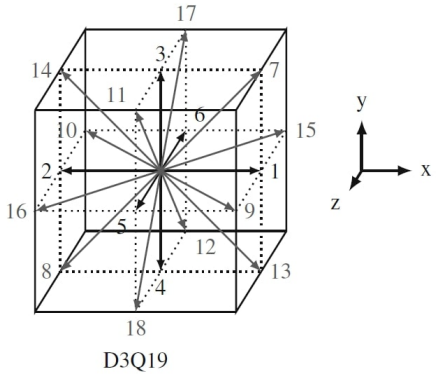

Figure 2.1: Scheme of the lattice D3Q19 lattice implemented. This figure is taken from section 3.4.7.3 of Ref. [20].

Table 2.1: This table has D3Q19 velocity set in an explicit form. The speed of sound for this lattice is $c_s = 1/\sqrt{3}$.

i	0	1	2	3	4	5	6	7	8	9	10	11	12	13	14	15	16	17	18
w_i	$\frac{1}{3}$	$\frac{1}{18}$	$\frac{1}{18}$	$\frac{1}{18}$	$\frac{1}{18}$	$\frac{1}{18}$	$\frac{1}{18}$	$\frac{1}{36}$	$\frac{1}{36}$	$\frac{1}{36}$	$\frac{1}{36}$	$\frac{1}{36}$	$\frac{1}{36}$	$\frac{1}{36}$	$\frac{1}{36}$	$\frac{1}{36}$	$\frac{1}{36}$	$\frac{1}{36}$	$\frac{1}{36}$
c_{ix}	0	+1	-1	0	0	0	0	+1	-1	+1	-1	0	0	+1	-1	+1	-1	0	0
c_{iy}	0	0	0	+1	-1	0	0	+1	-1	0	0	+1	-1	-1	+1	0	0	+1	-1
c_{iz}	0	0	0	0	0	+1	-1	0	0	+1	-1	+1	-1	0	0	-1	+1	-1	+1

With the collision and streaming method, one obtains the discrete distribution function for each node

f_i. This function tends to a equilibrium function f^{eq} by the collision operator Ω_i, which in our case is the Bhatnagar-Gross-Krook BGK collision operator [21]. The lattice Boltzmann Equation with BGK operator is then:

$$f_i(\vec{x} + \vec{c_i}\Delta t, t + \Delta t) = f_i(\vec{x}, t) - \frac{\Delta t}{\tau}(f_i(\vec{x}, t) - f_i^{eq}(\vec{x}, t)). \tag{2.1}$$

On the right-hand side of 2.1 is the collision operator. The equilibrium distribution function f_{eq} is obtained by a second-order expansion of the Maxwell-Boltzamann distribution, which gives:

$$f_i^{eq}(\vec{x}, t) = w_i\rho\left[1 + \frac{\vec{u}\cdot\vec{c_i}}{c_s^2} + \frac{(\vec{u}\cdot\vec{c_i})^2}{2c_s^4} - \frac{\vec{u}\cdot\vec{u}}{2c_s^2}\right]. \tag{2.2}$$

The link between LBE (lattice Boltzmann equation) and NSE (Navier-Stokes Equation) allows us to recover the macroscopic proprieties of the fluid. One can obtain the latter from the former by doing a multiscale expansion – this through the Chapman–Enskog theory [22]. One of those macroscopic behaviors that we recover is the fluid viscosity. The relaxation rate of the population is determined by the relaxation time τ, and the kinematic viscosity ν is then given from τ by:

$$\nu = c_s^2\left(\tau - \frac{1}{2}\right). \tag{2.3}$$

As the speed of sound in the D3Q19 lattice is $c_s = \frac{1}{\sqrt{3}}$, we have that $\nu = \frac{\tau - 1/2}{3}$.

In the case that we have an external force, and when we need to impose boundary conditions to our system, we need to consider a forcing scheme. We have implemented two algorithms for the collision method with a forcing scheme: the Guo [23] and Shan-Chen [24] algorithms. The Shan-Chen algorithm has a first-order accuracy: we shift the macroscopic velocity directly in the equilibrium function. In this case, we substitute the velocity $\vec{u}$ in equation 2.1 for $\vec{u}_{eq}$:

$$\vec{u}_{eq} = \vec{u} + \Delta\vec{u} = \vec{u} + \frac{\tau\vec{F}}{\rho}. \tag{2.4}$$

The Guo algorithm has a second-order accuracy: we determine the forcing term explicitly and add it to the right-hand side of the equation 2.1. In this case, the force term F_i for every node is determined by:

$$F_i = w_i\rho\left(1 - \frac{\Delta t}{2\tau}\right)\left[\frac{(\vec{c_i} - \vec{u})}{c_s^2} + \frac{(\vec{c_i}\cdot\vec{u})\vec{c_i}}{c_s^4}\right]\cdot\vec{F}. \tag{2.5}$$

It goes without saying that when there are no external forces on the fluid, the terms referring to the forcing schemes become null and both algorithms must be equivalent.

Another aspect about the method that should be mentioned is the implementation of the boundary conditions. When considering a periodic system, simple periodic conditions are implemented –, by which the density (mass) and momentum (velocity) are conserved. In the case that the boundary is a impenetrable solid obstacle, we implemented halfway bounce-back boundary conditions [25]. One can imagine that a wall is placed in the halfway point between the node that is fluid and the node that is obstacle: every velocity vector that would terminate in a obstacle node in the collision step of method will, in fact, be reflected, like an elastic collision, and end up as the symmetrical vector in the streaming step. Implementing the bounce-back method, we establish the no-slip condition in the contact between fluid and solid surface.

Finally, we refer the matter of units. The LBM has inherent units: the lattice units. Every cycle of the method corresponds to a time step, $\Delta t = 1$; the lattice spacing is the natural length, $\Delta x = 1$; and a

reference fluid density, $\rho = 1$. These simulation units will be the units used along our study; and all of simulations will be run with these units as default.[1]

An easy and straightforward method to validate the LBM code is to implement a steady, incompressible flow enclosed between two parallel walls: this is commonly referred to as 2D Poiseuille flow. This flow is driven by an external body force (e.g., gravity) on the x-axis. Considering a 2 dimensional scenario, and the no slip condition for the walls, the flow velocity on the x-axis is given in respect to the y-axis by:

$$u_x(y) = -\frac{g}{2\eta} y(y-d), \tag{2.6}$$

where η is the shear viscosity, g is the external body force and d is the distance separating the walls on the y-axis. We compared the theory with simulations with Guo and Shan-Chen algorithms. The system dimensions are: a length of $L_X = 250$ and a height of $L_Y = 100$ (which is $d = 99$ in the above expression), the relaxation time is $\tau = 0.55$ (which corresponds to $\nu = \eta = 0.016667$, as $\rho = 1$). The acceleration is $g = 2.778 \times 10^{-6}$. The flow profile was measured along a vertical line at $x = 225$. The results, once the simulations converged into a steady state, are presented on the Figure 2.2.

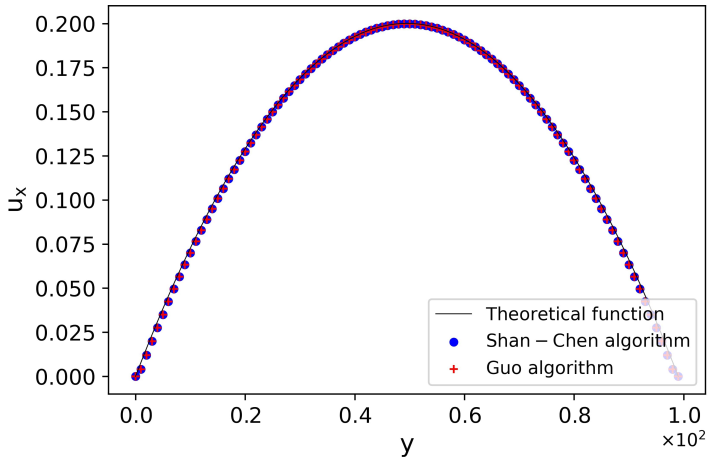

Figure 2.2: The simulations of the LBM with Shan-Chen (blue circles) and Guo (red crosses) algorithms are both in accordance with the theoretical result (black line) predicted by 2.6. Furthermore, both algorithms give the same results and their data points are overlapped.

The simulations present the characteristic parabolic velocity profile of the laminar flow. The results show a great agreement between both stream-swap algorithms and the theoretical model. Having tested both collision algorithms, and seeing that there is no difference in the results between them, from this point onward all of the lattice Boltzmann simulations use the Guo collision algorithm.

2.1.1 Implementation of moving particles

As we are interested in the interaction of moving particles in a fluid, it is important to know how the flow force behaves. To study the force of the fluid on solid boundaries, the force was determined by the momentum exchange on the bounce-back of the fluid with the solid nodes. Considering a moving

[1] On the matter of units, when discussing the Kuramoto model and the results of the LBM simulations, the arguments of the trigonometric functions will be expressed in radians.

obstacle, the drag force is given by [26][27][28][29]:

$$\vec{F}_d = \frac{1}{\Delta t}\sum_i (2f_i^* - 6\rho w_i \vec{u}_w \cdot \vec{c}_i)\vec{c}_i, \tag{2.7}$$

where the sum runs over all distribution functions that are bounced back from a particle wall, f_i^*, whose velocity is denoted by $\vec{u}_w$.

To simulate the movement of a particle most models need to use some kind of numerical integration method to solve Newton equations of motion. We chose to use the Verlet method [30], which has the advantage of time reversibility. For a given time step Δt, the velocity in the present instant $\vec{v}(t)$ and the position on the next instant $\vec{x}(t + \Delta t)$ is given, knowing the previous instant position $\vec{x}(t - \Delta t)$ and the acceleration in the present instant $\vec{a}(t)$, by:

$$\vec{x}(t + \Delta t) = 2\vec{x}(t) - \vec{x}(t - \Delta t) + \vec{a}(t)\Delta t^2, \tag{2.8}$$

$$\vec{v}(t) = \frac{\vec{x}(t + \Delta t) - \vec{x}(t - \Delta t)}{2\Delta t}. \tag{2.9}$$

To keep the study as simple as possible, we considered that the time step of the Verlet method would be the same as the time step of the LBM simulations, that is, $\Delta t = 1$. The acceleration is given simply by the applied forces on the particle through the Newton second law $\vec{F} = m\vec{a}$.

To incorporate moving particles, we implemented the creation and destruction of fluid nodes. A particle is treated as an array of prohibited nodes that are within the radius of the particle, i.e. as boundaries. When the particle moves, the newly occupied nodes have to be destroyed (they become prohibited nodes for the fluid), and the newly unoccupied nodes left behind the particle need to be created (i.e., become permitted to the fluid). This process is schematized in Figure 2.3.

As for the new solid nodes (resulting from the destruction of fluid nodes), the momentum is directly transferred to the solid: that is to say, the momentum in each direction of the old fluid node is added to the momentum in each direction of the particle. This is equivalent to transferring the force given by the product of the density of the old fluid node and its velocity density.

As for the fresh fluid node, each of them will have a density ρ_f equal to the mean of its neighbors [20]:

$$\rho_f = \rho(\vec{x}_f, t) = \frac{1}{N}\sum_i \rho(\vec{x}_f + \vec{c}_i\Delta t, t), \tag{2.10}$$

where the sum runs over all the first neighbors i. The velocity density of the fresh fluid node is that of the old solid node; the same is to say that the fresh nodes maintain the velocity of particle in the process of creation. We then initialize the populations f_i with their equilibrium values.

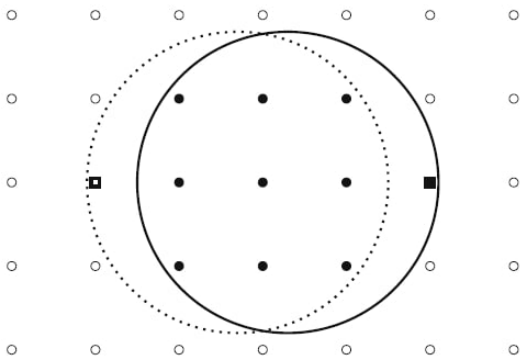

Figure 2.3: Creation and destruction of fluid nodes. A particle is moving from its previous position (dotted circle) to its new position (solid circle). As a consequence, one fresh fluid node (open square) appears behind the particle and a fluid node is destroyed (solid square) at the front of the particle. Fluid and solid nodes are shown as open and solid symbols, respectively. This figure was taken from section 11.2.4 of [20].

Finally, we have to account for the momentum transfer from the solid to the fresh fluid node: once again, what this means is that we need to subtract the force given by the product of the populations f_i and the velocity $\vec{u_i}$ of the new nodes from the net force on the solid as a all. It is convenient to define a destruction-creation net force, $\vec{F_p}$, that accounts for these momentum changes.

We should note that it is desirable that the movement of the solid particle through the fluid is slow enough, and that number of nodes that define the solid is large enough, so that this destruction-creation net force is negligible (and ideally it would be null); besides that, these desirable conditions will reduce the inevitable fluctuations in the total mass of the system, that affects its conservation.

To validate the code, we analyzed the drag force of two analogous situations: a stationary cylinder in a fluid enclosed between two walls (at the top and bottom) moving at constant velocity; and a moving cylinder with that same velocity in a fluid between two stationary walls. The system length was $L_X = 160$ and its height $L_Y = 160$, the viscosity of fluid was given by the relaxation time $\tau = 0.6$, and there were periodic boundary conditions to the right and left of the system. In this validation, the immovable particle's center is placed at $(x, y) = (50, 50)$. In the case where the particle was moving, its velocity was $u_x = 0.02083$; and when it was the walls that were moving, their velocity was symmetric, $u_w = -u_x = -0.02083$.

A characteristic feature of our simulations will be the radius R of the particles: the radius will be $R = 8$.

Two incompressible flow systems are said to be analogous if they both have the same Reynolds number and geometry, and this the condition that we adhered to here. This number is given by:

$$Re = \frac{Lv}{\nu}, \tag{2.11}$$

where L is a characteristic length (and in this case, the radius of the particle), v is the velocity of the flow and ν is the kinematic viscosity. The Reynolds number was set to 10. But in any case, as the geometry of the system did not change in the configurations we were comparing, the equivalency between them was guaranteed by the velocities of the wall and the particle having the same magnitude and direction, but symmetric values.

The comparison of these two scenarios are presented in the following Figure 2.4:

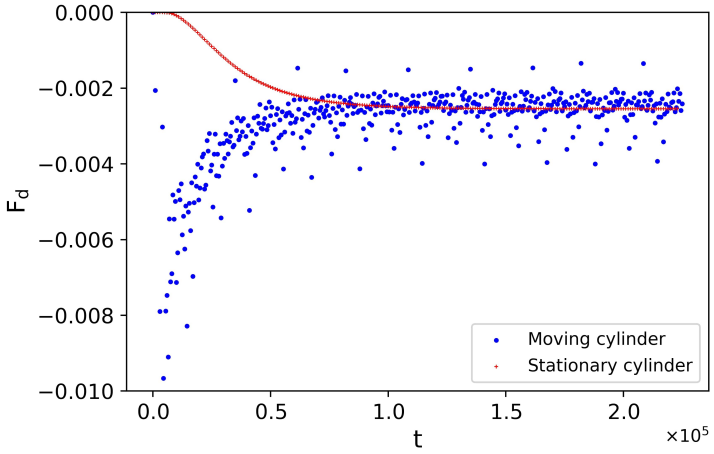

.

Figure 2.4: The drag force of the cylinder when moving (blue circles) converges to the same values as those obtained for the stationary cylinder in a flow with the same velocity magnitude (red crosses). The stationary cylinder converges to a drag coefficient of $C_D = 0.734$, and the moving cylinder converges to an average drag coefficient $\langle C_D \rangle = 0.722$.

In the case of the stationary cylinder in a fluid with moving walls, the drag coefficient converged to a mean value of $\langle C_D \rangle = 0.722$, and in the case with the moving cylinder, the drag coefficient converged to $C_D = 0.734$. This corresponds to a relative difference of $d_r = 1.6\%$, a reasonable value to consider that the two cases are analogous – and thus, we can say that the implementation of the nodes creation and destruction method simulates reasonably a moving particle in a fluid. The fluctuations on the force were present even when the particle was at constant velocity (as in the case with the last instants in Figure 2.4) –, they will be also present when we incorporate the oscillators in our simulations. These are mostly due to the discretization of the motion of the particle, which moves in a discrete way through the nodes: the nodes it occupies might not move, despite it having a non-zero velocity; and when it effectively moves, there is also a "readjustment" of the size of the particle.

2.2 Kuramoto model

The study of synchronization is often done with the Kuramoto model [15]. This mathematical model describes synchronization of large ensembles of weakly coupled oscillators. Each oscillator is viewed as a phasor $e^{i\theta_j(t)}$, with instantaneous phase $\theta_j(t)$ and natural frequency ω_j. This model predicts that the change of phase of each oscillator in a set of N oscillator is determined by the coupling factor K, by the following equation:

$$\frac{d\theta_j}{dt} = \omega_j + \frac{K}{N}\sum_{k=1}^{N}\sin(\theta_j - \theta_k). \tag{2.12}$$

The coupling factor K defines the strength of the interaction of any two oscillators: this means that, instead of K, we would have a matrix of coupling factors K_{jk}; but as our system only has 2 oscillators, K has only one value. [2] The number of oscillators is generally accounted for and is present in the N that divides the coupling factor K. But for commodity, from section 2.2.1 onward, anytime the coupling factor (or the KM) is mentioned, the constant $N = 2$ is implied.

[2] It is common to define K as a constant for the interaction of all pairs of oscillators, even if there is a large number of oscillators. That is to say that all oscillators interact with all the others in the same way.

An exact solution is given for $N \to \infty$. In this case, we resort to the order parameter R given by the mean phase of system ψ, where the amplitude $0 \leq |R\, e^{i\psi}| \leq 1$ measures the coherence of the system, in the following way:

$$R\, e^{i\psi} = \frac{1}{N} \sum_{j=1}^{N} e^{i\theta_j}. \tag{2.13}$$

Then, using this order parameter, the set of equations in 2.12, in the mean-field limit, can be rewritten as:

$$\frac{d\theta_j}{dt} = \omega_j + K\, R \sin(\psi - \theta_j). \tag{2.14}$$

Modified models have been developed for more complex systems of oscillators, like systems with disorder [31] and coupled networks with intra- and inter-network links [32] [33]. An extensive review about the Kuramoto model can be found in Ref. [34].

2.2.1 Two coupled oscillators

What happens if instead of having a very large set of oscillators, we have a very small set? Our study was directed to a system of 2 oscillators. One of the first consequences is the fact that we can no longer solve exactly the governing equations and periodic boundaries. In the case in each we have delay, what we have is frequency synchronization with a phase shift between oscillators. These situations were studied by Schuster and Wagner [35], who modelled this system with the Kuramoto model with time delay γ:

$$\begin{cases} \dfrac{d\theta_1}{dt}(t) = \omega_1 + K \sin[\theta_2(t-\gamma) - \theta_1(t)] \\ \dfrac{d\theta_2}{dt}(t) = \omega_2 + K \sin[\theta_1(t-\gamma) - \theta_2(t)] \end{cases}. \tag{2.15}$$

This model has already been used in the study of a living coupled oscillator system [36].

One can also ask: what measure can we then use to determine the synchronization coherence of such a given system? In this case, we use a synchronization parameter R, essentially equivalent to the order parameter R referred before in 2.13 for 2 oscillators, but some caution is need. With time delay, the a perfect coherence is no longer given by $R = 1$. The phase shift will decrease the value of R that corresponds to a synchronized state. And we can actually know what value of R to expect for each phase shift, and what value to expected when we don't have synchronization.

Let us assume that we have two very well-behaved oscillators, which have already achieved their final state (be it synchronized or not). Their instantaneous phase is given by their frequency ω_f and their absolute phase ϕ_f:

$$\begin{cases} \theta_1 = \omega_{f1} t + \phi_{f1} \\ \theta_2 = \omega_{f2} t + \phi_{f2} \end{cases}. \tag{2.16}$$

With some simple mathematical manipulations, which we present in detail in appendix B, and knowing that R is always non-negative, we arrive to the conclusion that R is given by:

$$R = \left| \cos\left(\frac{\Delta\omega_f}{2} t + \frac{\Delta\phi_f}{2} \right) \right|. \tag{2.17}$$

In the previous expression, $\Delta\omega_f$ is the different between the frequencies and $\Delta\phi_f$ is the phase shift between the two oscillators. If the oscillators are synchronized, then $\Delta\omega_f = 0$ rad, and the synchroniza-

tion parameter is given by:

$$R = \left| \cos\left(\frac{\Delta\phi_f}{2} \right) \right|. \tag{2.18}$$

In the case that the oscillators do not synchronize, we do not have a constant value of R, as we have a time dependency. However, the value of its mean, $\langle R \rangle$, is a constant, and given by:

$$\langle R \rangle = \frac{1}{b-a} \int_a^b \left| \cos\left(\frac{\Delta\omega_f}{2} t + \frac{\Delta\phi_f}{2} \right) \right| dt = \frac{2}{\pi}. \tag{2.19}$$

This number is approximately $\langle R \rangle \approx 0.637$. This result assumes that both $\Delta\omega_f$ and $\Delta\phi_f$ are constant –, which happens when the coupling is so weak that it is negligent.

The problem with these results is that if we get a value $\langle R \rangle = 0.637$, we cannot be sure if the oscillators are not synchronized or the oscillators are synchronized with a phase shift $\Delta\phi_f = \pm 1.76$ rad. In this case, if the frequencies of the oscillators are very close, the only way to know which case we have is to analyze the phase of the oscillators in a very long time scale. With this caveat, we have an alternative expression of R to corroborate the determined final phase shift (if there is a constant one), while being able to use the usual expression of the synchronization parameter (eq. B.2) to assess the evolution of the synchronization of a system (through the evolution in time of R).

Chapter 3

Fluid Simulation

As far as synchronization of oscillators in a fluid go, the problem of the behavior and synchronization of flagella and cilia has prompted a number of studies. The idealized models tend to represent the beating flagellum by a sphere revolving around a circular orbit [37][38][39]; a more recent and analogous theoretical modelling describes the flagellar beat as a generic limit-cycle oscillator, mostly proposed by Klindt [40][41]. Though we will not represent the motion of a flagella in a circular motion, this idea of limit-cycle oscillator has been adapted to a one-directional pendulous motion –, one can image the circular motion as 2D lateral parameterization, and the pendulous motion as simplified 1D upper parameterization. We model our oscillators as solid 2D circular particles with fixed radii.

There is a large set of parameters that can be controlled. We can choose the shape of the containing fluid, and its boundary conditions; the disposition of the particles relative to each other and the boundaries; the viscosity of the fluid; the type of forces (besides the drag force) that act on the particles; etc. A characteristic that will be constant throughout our work is the pinning of the particles. Wishing to have the particle oscillating around a specific point – that we will call its center of oscillation x_c –, every particle will be subject to a spring-like force $\vec{F_s}$ of the form:

$$\vec{F_s} = k_s(x - x_c)\vec{e_x}. \tag{3.1}$$

In case it is not said otherwise, the simulation value of the characteristic constant k_s of this force is 1×10^{-6}.

Another constant characteristic of our systems will be the mass of the oscillators, equal to $m = 1.5\pi R^2 \approx 301.6$[1], as the radius of the particles is $R = 8$ (the density of the solid particle is the same as the default fluid density, $\rho = 1$). In this regard, we remember that we will be using lattice units: a time step, $\Delta t = 1$, corresponds to a cycle of the LBM and the lattice spacing is the natural length, $\Delta x = 1$.

As we are mainly interested in the phenomenon of synchronization, some design choices are excluded by the simple fact that the system is incapable of synchronization. A possible restriction on synchronization systems is that of fixing the natural frequency of the particles (or phasor) – that is to say, the frequency at which a phasor oscillates by itself is always the same, and changes in its phase result only from its displacement by the effect of an external force, i.e., the coupling with neighboring particles. So, to this effect, we placed two particles side-by-side in a fluid enclosed by parallel walls, with each particle with a body acceleration of constant magnitude $A_x = 6 \times 10^{-6}$, but its direction would change

[1] From this point onward, and on the context of simulations and results, the value of π is approximated to 20 decimal places, $\pi \equiv 3.14159265358979323846$. If any other approximated value of the constant is referred, it should not be understood as being equivalent to the 20 decimal houses value of π, but the number exactly as it is written.

every time interval $\Delta t_1 = 4750$ for one particle and $\Delta t_2 = 4400$ for the other particle. We present a simulation of this model in Figure 3.2.

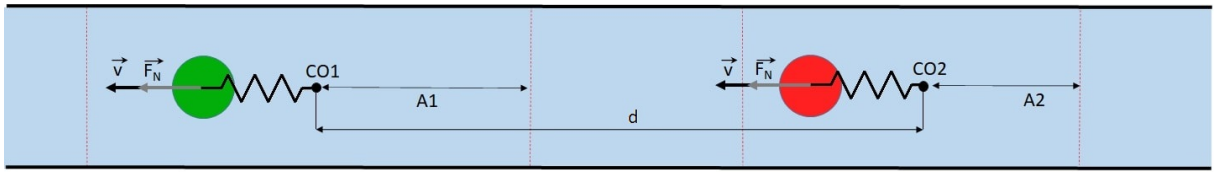

Figure 3.1: The system is represented here by a horizontal rectangle, with the fluid in light blue. The no slip boundary conditions are defined by the bold lines on top and at bottom of the system, and the periodic boundary conditions at the right and left can be identified by the absence of these same bold lines. There are two particles (one colored green and the other colored red), both moving right to left. Their centers of oscillation are called $CO1$ and $CO2$ (maintained by a spring-like force, represented by springs attached to the center of each particles' center), and their turnabout amplitudes are called $A1$ and $A2$. The distance between centers of oscillation is denoted d. On the other hand, for the system in which the direction of the body acceleration of each particle changes after a fixed time interval Δt, there's no turnabout amplitudes. (The scheme is not to scale with the simulations.)

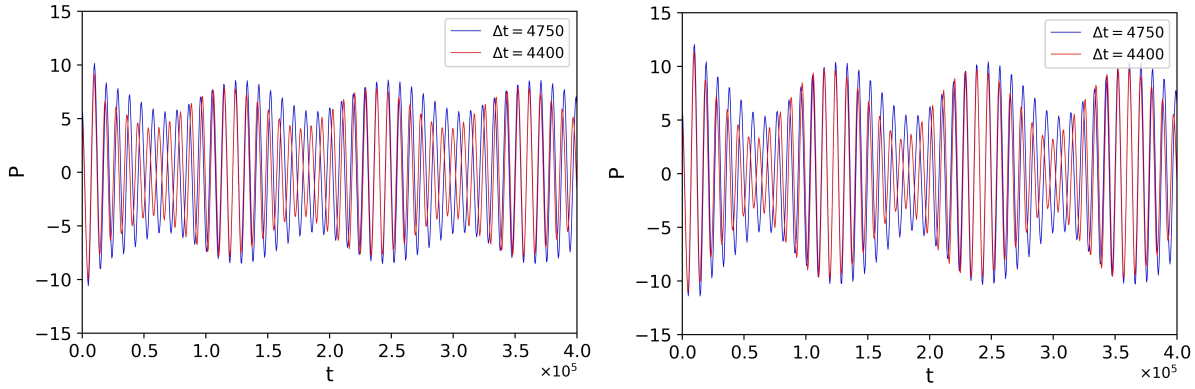

.

Figure 3.2: The system with particles whose acceleration changes direction after a fixed time interval, Δt, is present with each particle's position relative to their center of oscillation. The plot on the left corresponds to a system with dimensions 100×128, and the particle's centers of oscillation 50 lattice units apart; the plot on the right corresponds to a system with dimensions 80×128, and the particle's centers of oscillation 40 lattice units apart. In neither case do we have synchronization. The proximity of the centers of oscillation emphasizes the pulsating aspect

We saw that the displacement that each particle caused on the other was not enough to change their overall frequency, and thus, they did not synchronize in frequency. As the particles are not limited to predetermined positions, the displacement from the interaction between them results in something of an interference pattern. The aspect of the motion resembles that of two coupled oscillators attracted to each other and to nearest wall, in a system with 3 springs. In the coupled oscillators we also observe a pulsating pattern, or beats, through an envelope.

The system design which was ultimately chosen is as following: two particles oscillating on the horizontal axis due to: a body acceleration, A_x, with constant magnitude, but which direction changes every time a given particle passes beyond a certain point relative to the center of oscillation, to the right and to the left – we shall call the distance from the center of oscillation to these turning points the "turnabout amplitude", A; a spring-like force already cited above; and naturally, the drag force of the fluid. The fluid has period boundary conditions on the directions of the movement (i.e., to the right and to the left), and no-slip conditions on the top and the bottom boundaries. A schematic of the system is

presented in Figure 3.1.

This choice of system, with particles with constant magnitude body acceleration, has the desired consequence of making the particles achieve their terminal velocity.

Having established the model, we then studied what was the influence of a number of variables in the synchronization. These are divided in simulations with both particles with the same natural frequency and with the particles with different natural frequencies. On the first section, we will vary the initial phase shift, $\Delta\phi_i$, the distance between centers of oscillation, d, the viscosity of the fluid, ν, the body acceleration, A_x, and turnabout amplitude, A; on the second section, the distance, the viscosity and the frequency difference between particles (i.e., body acceleration of one of them, while maintaining the other one's constant).

From the LBM simulation we could retrieve quite some information about the system: from the particles' position, x_i (their relative position to their respective centers of oscillation is denoted P_i) we could retrieve their absolute phase, ϕ_i; and from this we could obtain the synchronization parameter R of the system. As said before, this parameter is a natural metric of the system's synchronization coherence, and from it we can easily determine the synchronization time of the system. Beyond these variables, we could determine the oscillation amplitude, the frequency, the linear velocity of each particle, and the phase shift of the system, at every time step.

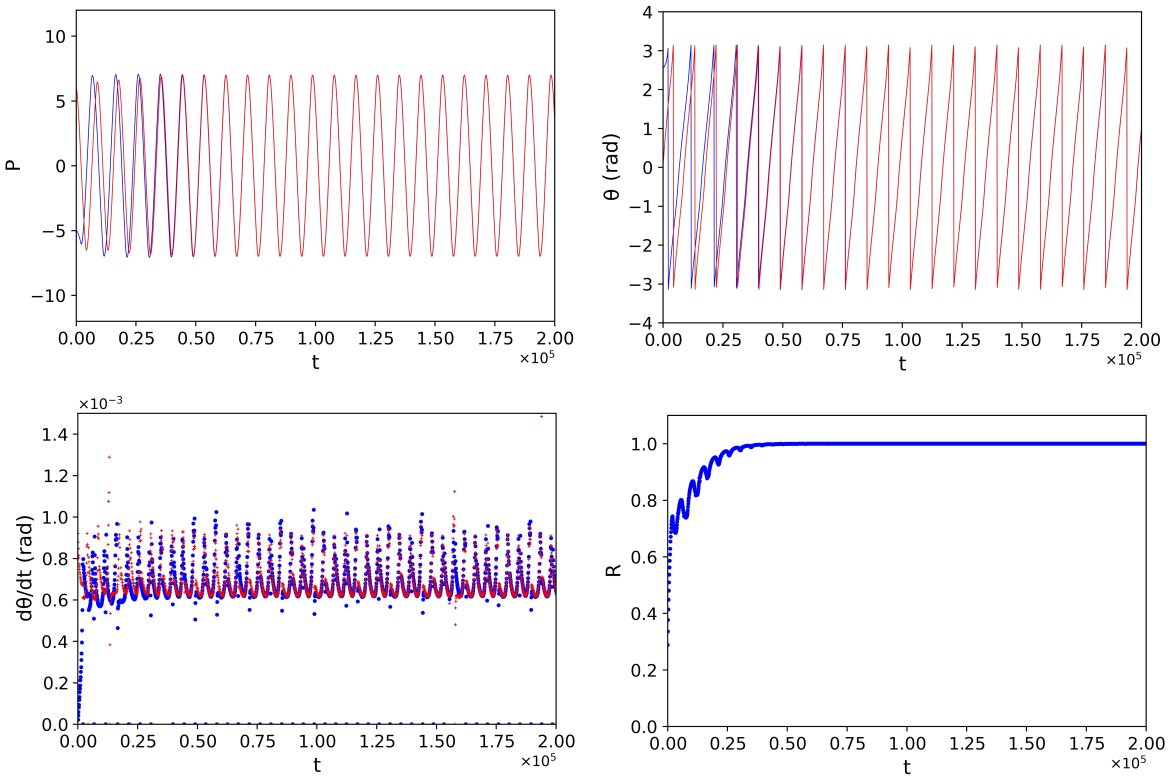

Figure 3.3: Example of a system that synchronizes seen by the particles' position in relation to their respective center of oscillation (top left), by their absolute phase (top right), by their frequency (bottom left) and the synchronization parameter R (bottom right). Each of the particles is represent by a color: blue and red (except for the R plot, which is a variable of the system). The dimensions of the system are 128×128 and the distance between the centers of oscillation of the particles is $d = 64$; the fluid viscosity is $\nu = 0.0333$; both particles have a body acceleration of $A_x = 6 \times 10^{-6}$ and a turnabout amplitude of $A = 6$. The synchronized state is achieved around $t = 35000$.

It should be noted that the argument of the trigonometric functions is expressed in rad, and, therefore,

the instantaneous phase, θ, and the phase shift, $\Delta\phi$, are expressed in this unit. Furthermore, the change in instantaneous phase, $d\theta/dt$, and the natural frequency, ω, are also expressed in rad, as we use the lattice unit of time, $\Delta t = 1$ (which is omitted).

In all the systems, we see that the particles' peak amplitude increases during the initial oscillations, reaching their final peak amplitude A_p. This final value is always larger than that of the turnabout amplitude that is a characteristic variable of each particle (i.e., $A_{pi} > A_i$)[2]. This was expected, as the turning motion of each particle is not instantaneous.

We also note that, as we can see in the bottom left plot of Figure 3.3, the change of frequency of the particles in time is not smooth, but has a periodic pattern around a mean value. This is also present in all systems, and it is intrinsic to our model.

Natural frequency

We will divide our study of the behavior of our system in two parts: 1) systems with oscillators have the same natural frequency; and 2) systems with oscillators with different natural frequencies. In the Kuramoto model (eq. 2.14), the natural frequency ω corresponds to the frequency at which a given oscillator oscillates when it is not influenced by any other (be it by the coupling factor K being zero, or by the particle being isolated in a system, $N = 1$). The way we determined this quantity was by placing a single oscillator in the system we have discussed before: between two parallel walls, with a height of $L_Y = 128$, and with periodic boundary conditions to the right and left. The center of oscillation of the particle was placed in the middle, $CO = L_X/2$ (and at $y = LY/2$); and the length was set large enough that the influence (through the periodic boundaries) was negligible compared to the other interactions (see the distance dependency subsection of the particles with the same natural frequency section of appendix A, more specifically the top right plot of Figure A.2) –, unless said otherwise, the length was $L_X = 1024$.[3] We let the particle oscillate long after it had reached its final periodic motion – and it is this motion's frequency that we consider the particle's natural frequency, ω. A schematic of such system is presented in Figure 3.4.

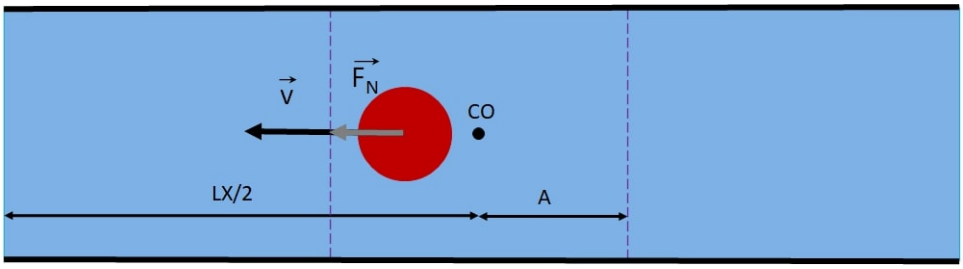

Figure 3.4: Scheme of the system used to determine the natural frequency. An isolated particle is placed in a large system, with its center of oscillation (CO) fixed in the middle of the system. It is subject to the same forces as the particle, in the system of 2 particles, whose natural frequency we intend to determine. The scheme is not to scale, as L_X should be considerably larger than A.

A particle's natural frequency is thus defined by: the fluid viscosity, ν, its turnabout amplitude, A, its body acceleration, A_x, and the spring-like force it is subject to, F_s. As this last force is constant

[2]The values of A_p of all our simulations can be consulted in the appendix A, as they are not the directed focus of the study that we intend to do.

[3]In section 3.1, we study the dependency of the distance between the centers of oscillation on the synchronization of the system, and we up to a system length of $L_X = 4096$, i.e., a distance of $d = 2048$. We direct the reader to Figure 3.8, in each we plot the synchronization time as a function of the distance –, where we see unexpected results for $d = 2048$

throughout our study, we can define the ω as a function of the other 3 variables. The initial position of the particle is not relevant to the natural frequency, as we are only interested in the final stable oscillatory motion –, which does not depend on the initial position, as long at it is in the range of the turnabout amplitude $P(0) \in [-A, A]$.

As an example, we present the natural frequency ω obtained on our study of the viscosity dependency, when both particles have the same natural frequency. The turnabout amplitude is $A = 6$ and the body acceleration $A_x = 6 \times 10^{-6}$. As we vary the viscosity, so does the natural frequency: in this case, as the viscosity increases, the natural frequency decreases. The values are presented in the following Figure 3.5.

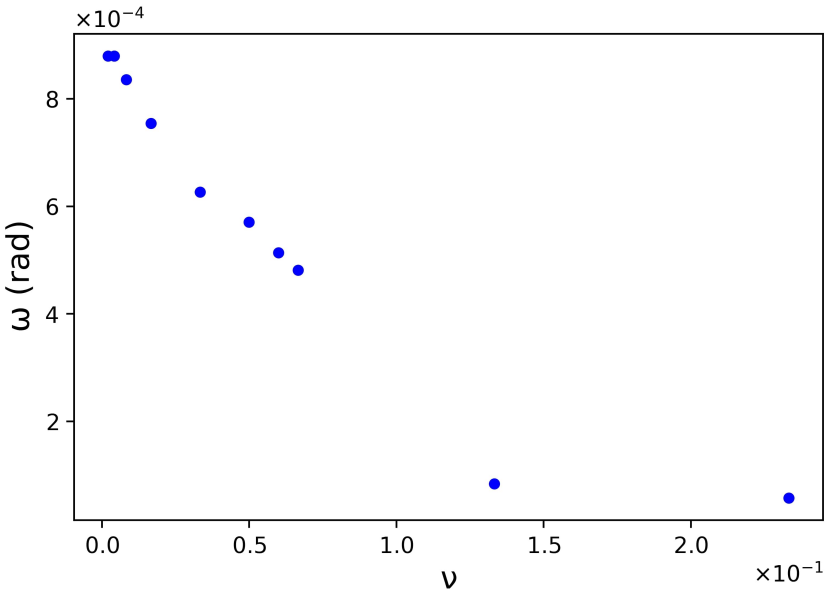

Figure 3.5: Plot of the natural frequency as a function of the viscosity. The turnabout amplitude is $A = 6$ and the body acceleration $A_x = 6 \times 10^{-6}$. The system's dimensions are 1024×128.

This setup can also be used to determine other "natural" variables of a particle's motion, like the oscillation amplitude or the linear velocity (being that the variable that we will use ahead in our study is actually the mean absolute linear velocity). These quantities are presented in the appendix A.

3.1 Particles with the same natural frequency

First we studied systems in which both particles have the same turnabout amplitude, A, and the same body acceleration, A_x. This results in both particles having the same natural frequency –, and this, in turn, means that the synchronized state has a null phase shift, $\Delta\phi = 0$ rad. This corresponds to a synchronization parameter equal to the unit, $R = 1$. However, for simplicity, and unless said otherwise, we consider that system has achieved the synchronized state if, and when, $R \geq 0.99$ – this is to say when the phase shift is $\Delta\phi \leq 0.283$ rad. The thresholds $R \geq 0.95$ ($\Delta\phi \leq 0.635$ rad) and $R \geq 0.999$ ($\Delta\phi \leq 0.0895$ rad) are also used as reference, but are not considered as the synchronization threshold.

Phase shift dependency

To study the influence of the initial phase shift between oscillators, we set the relaxation time of the

fluid to $\tau = 0.6$ (i.e., $\nu = 0.0333$), both the turnabout amplitudes to $A = 6$ and the magnitude of the acceleration to $A_x = 6 \times 10^{-6}$. The phase shift was set by placing the oscillators in different starting points in the interval $[CO - A, CO + A] = [CO - 6, CO + 6]$ – which correspond to the absolute phase shift of $[0, \pi]$ rad – and by changing the direction of the initial acceleration – which would then correspond to the full range of $[-\pi, \pi]$ rad.

First, we set the distance between the centers of oscillation at $d = 64$ – the same is to say that the system length was double that, $L_X = 128$, as the centers of oscillation are equidistant from each other and their closest periodic boundary. If the initial phase shift was in the range $[0, \pi]$ rad, the system converged to a state of synchronization; if the phase shift was in the range $]-\pi, 0[$ rad, then one of the particles would very quickly get stuck in an off-center oscillation, while the other one still oscillating around its predefined center of oscillation. These two cases are represent in the figure 3.6.

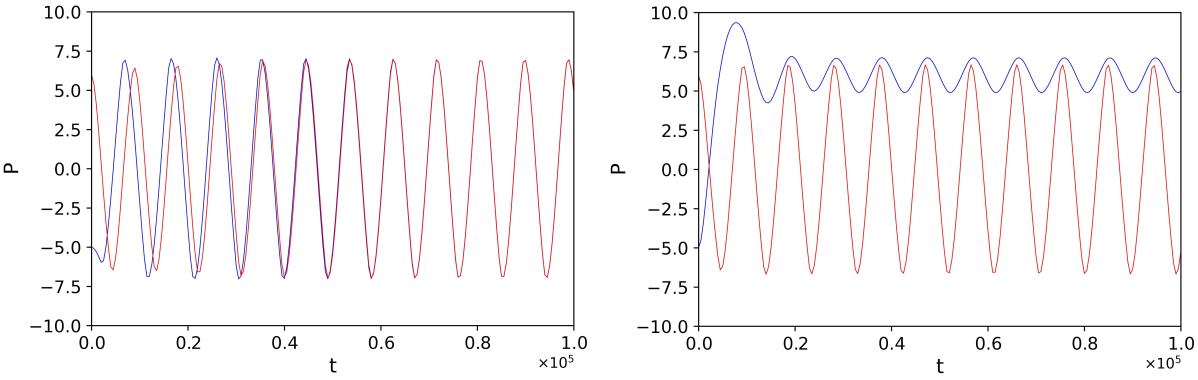

Figure 3.6: The plots of systems with dimensions 128×128, with distance between particles $d = 64$, fluid viscosity $\nu = 0.0333$; the particles have a body acceleration of $A_x = 6 \times 10^{-6}$ and turnabout amplitude of $A = 6$. On the left we have a system with initial phase shift of $\Delta\phi_i = 2.56$ rad, and on the plot on the right one with a initial phase shift of $\Delta\phi_i = -2.56$ rad. Each of the particles is represent by a color: blue and red. Only the system on the left has an on-center synchronization.

As we are interested in the cases of in-center synchronization, we set one of the particles' initial phase shift at $P_1(0) = A$ while varying the initial position of the other particle in the range $P_2(0) \in [-A, A] = [-6, 6]$; we also maintained the same initial direction of the body acceleration for both oscillators. This guaranteed that we were on the range of initial phase shifts $\Delta\phi_i \in [0, \pi]$ rad. In this range, we saw that the time needed to achieve the synchronized state was related to the phase shift itself. This relation is not linear, nor of any type immediately perceptible, as seen in Figure 3.7. In any case, the data points seem to be distributed in 3 regions: for $\Delta\phi_i \in [0, \pi/2[$ rad, the synchronization is almost instantaneous, and the time it takes increases very slightly; for $\Delta\phi_i \in [\pi/2, \pi[$ rad, the synchronization time increases linearly; and for $\Delta\phi_i = \pi$ rad, the system takes considerably longer to synchronize, taking more than 3 times longer than for the system with $\Delta\phi_i = 2.73$ rad.

It is intuitive why larger initial phase shifts correspond longer synchronization times: the closer the system is initially to synchronization, the least "effort" is required to get it to that state.

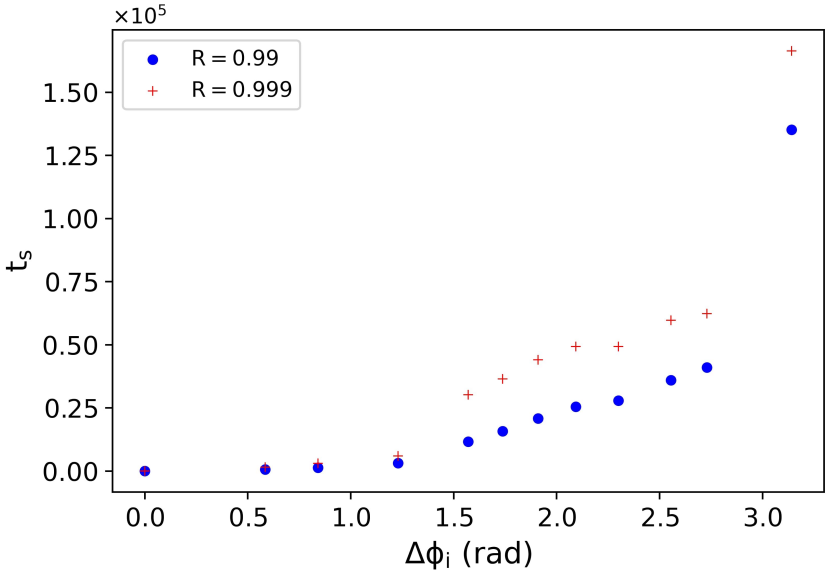

Figure 3.7: The time to achieve the at-center synchronized state, t_s, is proportional to the initial phase shift. Here we see the time taken for the system to achieve an synchronization parameter $R = 0.99$ (blue circles) and $R = 0.999$ (red crosses) for a series of initial phase shift values. There is no significant difference in the tendency of the two data sets, apart from the obvious characteristic of the larger R value taking longer to be reached.

Something that is also worth mentioning is the fact that systems with different initial phase shifts converge, in time, to the synchronized state in different ways. When looking at the time evolution of the synchronization parameter R, we see that the closer the initial phase shift is to $\Delta\phi_i = \pi$ rad, the closer is $R(t)$ (R as a function of time) to a sigmoid function; and the further it is from $\Delta\phi_i = \pi$ rad, the closer is $R(t)$ to an exponential function. When the system starts close to phase opposition, the change in the absolute phase of each particle is very small, and the phase of the system changes very little – this "semi-stable" phase opposition regime explains why the synchronization time increases drastically when $\Delta\phi_i \approx \pi$ rad.

These exponential and sigmoid tendencies can be fitted, and they have been, as they can be used to aid the determination of the synchronization time. The exponential fit has the following expression:

$$R(t) = 1 - A \cdot e^{-\lambda t}. \tag{3.2}$$

The sigmoid fit has the following expression:

$$R(t) = \frac{A}{A + e^{-\lambda t}}. \tag{3.3}$$

The A and λ parameters (for each of the previous function) have fitting proposes, and their physical meaning is not the focus of our study. This said, λ is related to the steepness of the function, i.e., how fast it goes from very close to zero to very close to the unit; A has a different meaning for each function: for the exponential function, it is related to the initial value of the function; for the sigmoid function, it is related to the time instant at which we achieve $R = 0.5$, akin to a time translation –, this can also be related to the initial value of the sigmoid, but, in general, it does not have this meaning in our study, as the sigmoid function is fitted to systems that start at (or very close to) phase opposition, $R = 0$. Regardless of this explanation, the parameters are adjusted with the sole goal of obtaining the best fit to the data points.

Distance dependency

Using the same setup as the one in the previous section, and by varying the length L_X, we studied the system's dependency on the distance between centers of oscillation. With the natural frequency of both particles the same – this is to say, both turnabout amplitudes and acceleration magnitudes are the same for both particles –, they tend to converge to a synchronized state with null phase shift (or a very small phase shift). The truth is that the phase shift increases slightly with distance, but this increase is small enough to be negligible.

The synchronization time t_s as a function of the distance between the centers of oscillation of the particles is shown in Figure 3.8. When considering the initial phase shift, there seemed to be two regimes: if $\Delta\phi_i \in [0, \pi/2[$ rad, then the synchronization time decreased with distance (this is more evident in the log-log scale of the right plot of Figure 3.8); if $\Delta\phi_i \in]\pi/2, \pi]$ rad, then the synchronization time increased with distance (up until $d = 1024$). For the latter range of $\Delta\phi_i$, up until $d = 512$, the synchronization time increased roughly linearly (in a logarithmic scale); then we had a sharp increase at $d = 1024$, from which peak the synchronization time then decreased. This is the most impressive fact, that the synchronization time decreased at $d = 2048$. It is counter-intuitive that at such a large distance the synchronization time would so considerably decrease, considering that the interaction is weaker with distance (the disturbance in the fluid made by one particle takes longer to reach the other one and loses more momentum).

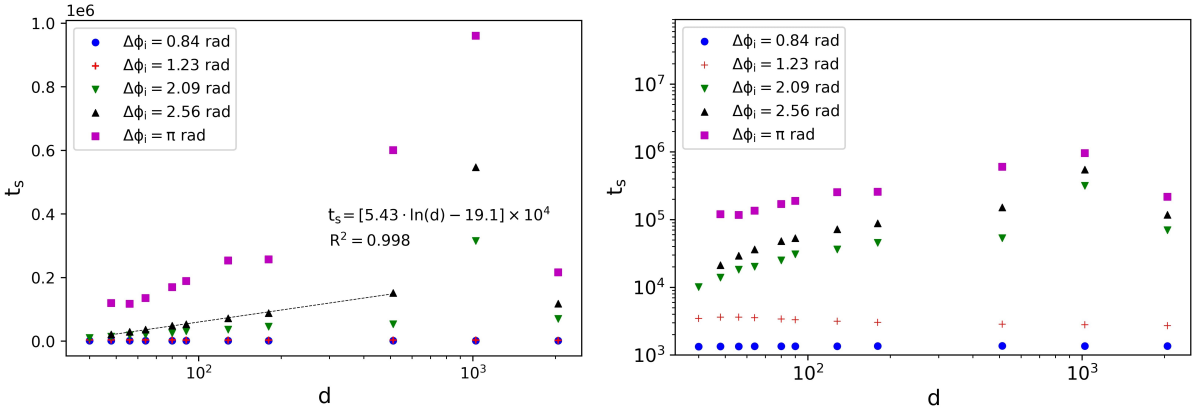

Figure 3.8: The synchronization time, t_s, as a function of the distance between the centers of oscillation, d, on a linear-log scale (left plot) and on log-log scale (right plot). Both particles have a turnabout amplitude of $A = 6$ and a body acceleration of $A_x = 6 \times 10^{-6}$; the fluid viscosity is $\nu = 0.0333$. On the left plot, we can see that (in this scale) the data points are displayed approximately in a line up until $d = 512$ – we also present a logarithmic fit of the $\Delta\phi_i = 2.56$ rad data set and its coefficient of determination, R^2. The scale of the plot on the right allows us to see the decreasing nature of the data points with $\Delta\phi_i = 1.23$ rad. We also clearly see that the synchronization time is essentially constant for $\Delta\phi_i = 0.84$ rad. The time to achieve the at-center synchronized state depends on the initial phase shift.

On the other hand, it's not inconceivable that, for smaller initial phase shifts ($\Delta\phi_i = 1.23$ rad and $\Delta\phi_i = 0.84$ rad), the synchronization time would decrease with the distance. These systems start somewhat close to synchronization already: it is possible that the interaction between particles tend to initially have a desynchronization effect, "overshooting" the synchronization, so to speak. Nevertheless, what we see is that the distance might be insignificant for the synchronization time (we can consider it reasonable constant); but this behavior will have to have a maximum distance, as there is a limit given by the speed of sound and the energy transmitted from one oscillator to the other dissipates with distance -

that is to say, they will be a distance beyond which the synchronization time will necessarily increase (or synchronization will not be possible). However, we redirect the reader to the Observations subsection to this section 3.1 we present a different perspective.

Viscosity dependency

Following a similar setup as above, but now varying the viscosity of the system, we get the results presented in Figure 3.9. As for the dependency of the synchronization time with viscosity, we can observe a power law. And just like with the dependency in distance, we have two regimes: if $\Delta\phi_i \in [0, \pi/2[$ rad, then the synchronization time increased with viscosity; if $\Delta\phi_i \in]\pi/2, \pi]$ rad, then the synchronization time decreased with viscosity. There is a deviation from this behavior for $\Delta\phi_i = \pi$ rad, in which the time synchronization increased with viscosity starting from $\nu = 0.00208$.

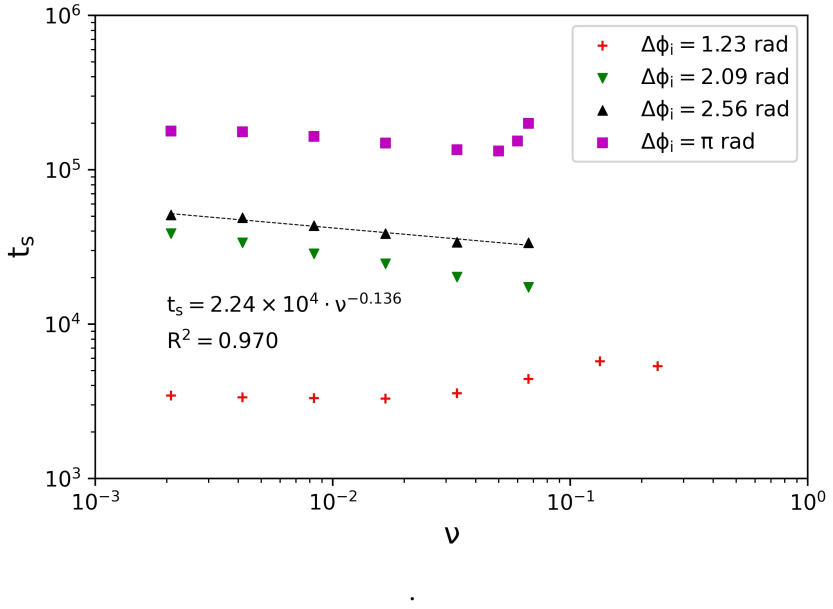

.

Figure 3.9: The synchronization time, t_s, as a function of the fluid viscosity. Both particles have a turnabout amplitude of $A = 6$ and a body acceleration of $A_x = 6 \times 10^{-6}$; the distance between the centers of oscillation of the particles is $d = 64$. The plot is in log-log scale, and we can see that in this scale the data point are displayed approximately in a line – we also present a power law fit of the $\Delta\phi_i = 2.56$ rad data set and its coefficient of determination, R^2. The time to achieve the at-center synchronized state depends on the initial phase shift.

Something that we could also observe was that for systems with initial phase $\Delta\phi_i \in [\pi/2, \pi]$ rad, the maximum viscosity at which they converge is the same, while for $\Delta\phi_i = 1.23$ rad this maximum viscosity was larger. However, the Reynolds Number is, in all case, in the range $Re \in [0.46, 2.34]$.

The reason why synchronization time decreases with viscosity is simple: the more viscous the fluid, the stronger the coupling of the oscillators - their motion is strongly conditioned by the fluid. This also corresponds to a more laminar flow (both oscillators and fluid also have a smaller velocity). Why the synchronization time increases for the system in phase opposition, is not so clear. It is possible that the more viscous fluid maintains the initial phase opposition semi-stable state for longer, for the initial disturbance that will get the system out of balance is less significant.

Viscosity dependency with constant frequency

Biologically, an organelle as a cilium or a living system with flagella would not change their acceleration at will, but would be subject to the changes in the fluid viscosity, and thus would not be able to maintain their frequency. But when we change the value of the viscosity, we are also changing the linear velocity and frequency. The linear velocity has negligible influence in the synchronization process (cf. the following subsection regarding the linear velocity), but the frequency does have a significant contribution. To see the real (isolated) influence of the viscosity in our systems, we changed the magnitude of the body acceleration accordingly so that the natural frequency of the oscillators remained close to $\omega = 8.55 \times 10^{-4}$ rad. The pair of values of ν and A_x used are presented in the table 3.1. We can imagine a situation where we could impose such condition on the oscillators, where they would try to maintain this frequency, or we can think that these are different organisms with different natural frequencies in different media.

Table 3.1: This table has the pair of used values of viscosity and body acceleration that assured constant natural, ω, and final frequencies, ω_f – this value is the mean over the 4 initial phase shifts studied: 1.23 rad, 2.09 rad, 2.56 rad and π rad. All the frequency values of this subsection can be consulted on the top right plot Figure A.4.

ν	$A_x(10^{-6})$	ω (10^{-4} rad)	ω_f (10^{-4} rad)
0.00208	6.00	8.55	8.98
0.00417	6.50	8.55	8.98
0.00833	8.00	8.55	8.98
0.0167	10.0	8.55	8.98
0.0333	13.5	8.55	8.98
0.0667	18.5	8.55	9.11
0.133	26.0	8.55	8.98
0.233	34.0	8.55	8.98

The results are presented in Figure 3.10. We no longer have a power law when we plot the synchronization time (for $R = 0.99$) against the viscosity, for the different initial phase shifts. When seen in a linear-log, however, the data points seem to follow a line, except for the system starting in phase opposition. These seems to indicate a logarithmic tendency between synchronization time and viscosity.

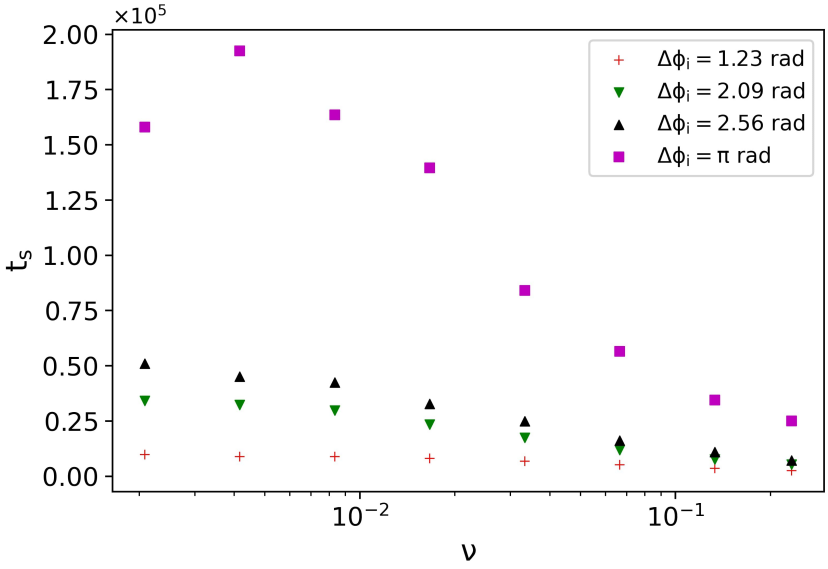

Figure 3.10: The plot is in log-linear scale. With constant natural frequency along all the values of viscosity we see decreasing tendency of the synchronization time across all initial phase shifts, apart from $\Delta\phi_i = \pi$ rad, which as peak at low values of viscosity. Both particles have a turnabout amplitude of $A = 6$, and the distance between the centers of oscillation is $d = 64$. The body acceleration of both particles is the same and given as a function of the fluid viscosity in the table 3.1.

Linear velocity dependency

To study the dependency of the synchronization time on the linear velocity, we varied the turnabout amplitude and the magnitude of acceleration of both particles in such a way that the frequency would not change, while increasing the oscillation amplitude of the particles – this would correspond necessarily to a change in the magnitude of the linear velocity. The body acceleration of both particles and the turnabout amplitude are related by $A_x = A \times 10^{-6}$. The natural frequency obtained was $\omega = 6.3 \times 10^{-4}$ rad.[4] The synchronization time was then compared to the linear velocity both particles – actually, its absolute mean value $v_n = \langle |v| \rangle$. For a given initial phase shift, the results being so close, the synchronization times are viewed as being the same. The values of the natural linear velocity are given as a function of the turnabout amplitude in table 3.2.

Table 3.2: This table has the correspondence between body acceleration and natural (mean absolute) linear velocity. This last one was determined by placing a single particle in a system of $L_X = 1024$ and find the linear velocity for each body acceleration.

A	$v_n(10^{-3})$
5	2.16
6	2.59
7	2.86
10	4.24
13	5.44
15	5.94

[4]There is a slight variation of both the final and the natural frequencies, but it is not relevant. These can be consulted on the top right plot of Figure A.5.

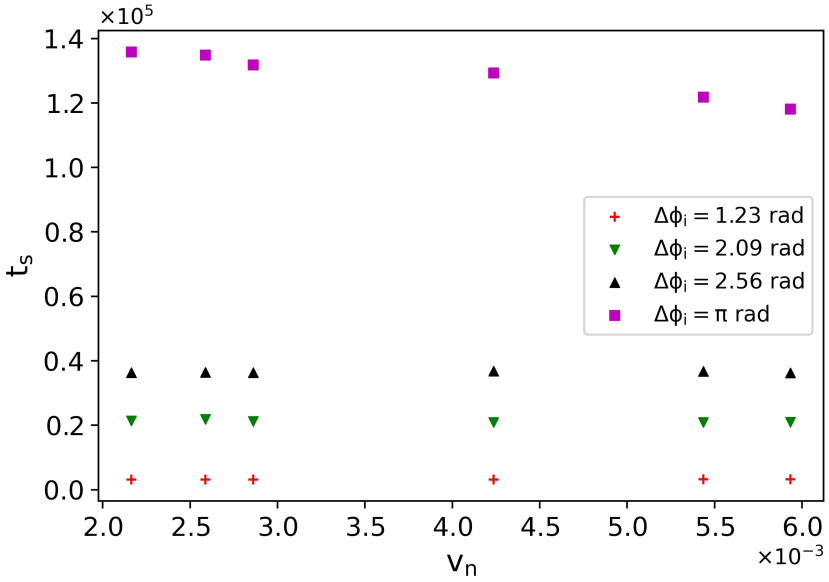

Figure 3.11: The time to achieve the at-center synchronized of one of the two particles depends very little on the linear velocity of the particles. The data presented is with respect to the linear velocity of a particle when isolated in a fluid. The fluid viscosity is $\nu = 0.0333$, and the distance between the centers of oscillation is $d = 64$; the turnabout amplitude, A, and the body acceleration, A_x, of both particles is the same is given by the expression $A_x = A \times 10^{-6}$. The correspondence between the linear velocity, v_n, and the turnabout amplitude is given by the table 3.2.

Once again, the linear velocity is not a variable that biological oscillators would, in principle, be able to control. But this study is useful as we can conclude, from the results presented in Figure 3.11, that there does not seem to be any strong relation between linear velocity and synchronization time –, apart from a slight decrease for the system starting in phase opposition; this means that we can neglect any alterations of the linear velocity that might result from the variation of some other characteristic of the system.

Body acceleration dependency

Finally, we studied the system's dependency on the body acceleration of the oscillators. This can be seen as the dependency in the natural frequency, as when we change the body acceleration of the particles, while maintaining their turnabout amplitude at $A = 6$, we effectively change the frequency at which the particles oscillate. We remember that the natural frequency of a particle is considered to be that at which it oscillates when isolated in a large system. We vary the acceleration magnitude in the range $A_x \in [5, 20]$ (the correspondence between body acceleration and natural frequency can be checked in the table 3.3).

What we see, from the results in Figure 3.12, that the synchronization time does depend on the frequency (i.e., body acceleration), with faster synchronization times for larger and smaller frequencies that $\omega = 6.72 \times 10^{-4}$ rad for all systems with initial phase shift larger that $\pi/2$.

Why do we have these two regimes? The larger the natural frequency, the stronger is the influence of the oscillator on the fluid (and thus on the other oscillator) and the faster the oscillators interact: this would indicate that the increase of natural frequency would result in a decrease of synchronization time. But the opposite happens in the first regime (up until $\omega = 6.72 \times 10^{-4}$ rad). How would increasing the natural frequency result in a longer synchronization? It could have to do with turbulence: it is

possible that at lower frequencies, the increase of the frequency (and thus of the fluid) would result in a turbulent flow that adds "noise" to the interaction; and that this turbulence because increasingly less significant with strength of the interaction between oscillators, as the frequency increases. Let us refer that the Reynolds number goes from $Re = 5.32$ up to $Re = 6.42$, between $\omega = 5.86 \times 10^{-4}$ and $\omega = 6.72 \times 10^{-4}$, and then up to $Re = 11.57$, at $\omega = 1.01 \times 10^{-3}$.

This is explanation should, however, be confronted with the result obtained in the previous subsection, where we saw that the linear velocity does not influence significantly the synchronization time.

Table 3.3: This table has the correspondence between body acceleration and natural frequency. This last one was determined by placing a single particle in a system of $L_X = 1024$ and find the final frequency for each body acceleration.

$A_x(10^{-6})$	$\omega(10^{-3}$ rad)
5	0.586
6	0.628
7	0.672
10	0.798
13	0.880
15	0.924
20	1.01

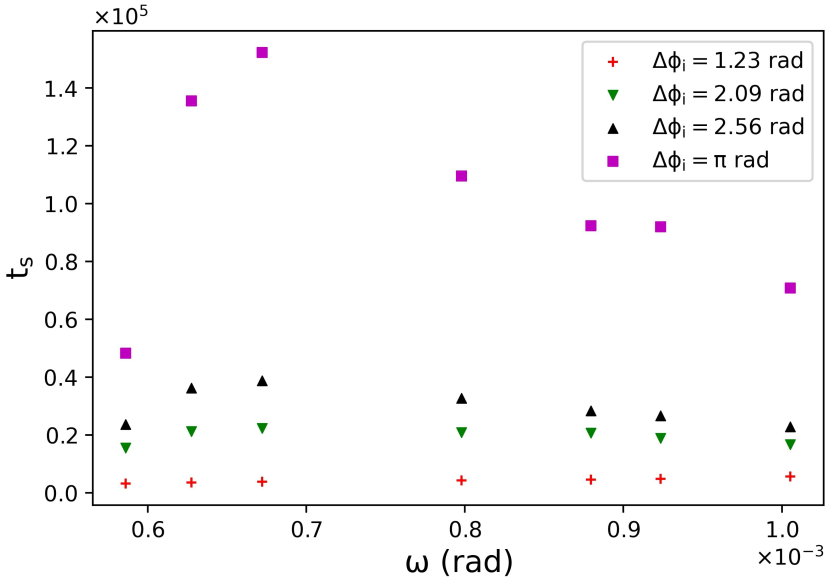

Figure 3.12: The time to achieve the at-center synchronized has a maximum around $\omega = 6.72 \times 10^{-4}$ rad. The data is presented with respect to the frequency of a particle when isolated in a fluid. Both particles have the same turnabout amplitude, $A = 6$, and the distance between the centers of oscillation of the particles is $d = 64$; the fluid viscosity is $\nu = 0.0333$. The correspondence between the natural frequency ω and the body acceleration is given by the table 3.3.

3.1.1 Initial phase shift or initial force ratio?

We have been discussing the initial phase shift, $\Delta\phi_i$, as one of the initial conditions of the system that we are studying. This, however, is nothing more than the relation between the particles' initial positions, which we turned into phases (as we are working in the context of phasors). But how important are the

particles' initial positions when compared to the system's initial phase shift? That is to say, what if, instead of having a particle always with an initial position $P(0) = 6$ (while varying the initial position of the other one), that particle's initial position was different? Would different combinations of initial positions would have different synchronization times, even when they would have the same initial phase shift? As we will see, the initial positions are very important.

To study what effect the initial positions would have in the system, we kept the same setup as that used in the study of the initial phase dependency ($LX = 128$, $\nu = 0.0333$, $A = 6$, $A_x = 6 \times 10^{-6}$), but now we did a total of 42 simulations in 6 series: each series had one of the particles with an initial position (in relation to its center of oscillation) $P_1(0) \in \{-5, -3, -1, 1, 3, 5\}$ and the other particle's initial position (in relation to its center of oscillation) was set, at each simulation, at a value of the series $P_2(0) \in \{-6, -5, -2, 0, 2, 4, 5\}$. The results of the synchronization time, considering the stable state when we achieved $R = 0.99$, is presented in Figure 3.13.

The reason why the initial position of the particles is so important is evident in Figure 3.13: the initial net force of each particle. Both particles have the same body acceleration (same magnitude and direction), and are subject to the same type of drag force; however, the spring-like force used to keep the particles around their centers of oscillation depends on their initial position P. We see a correlation between the initial force ratio and the synchronization time, except for the cases when one particle starts at $P_2 = 0$, which corresponds to a $F_{N2} = 0$ – and therefore a null ratio or an infinite one. And regardless if the force ratio is F_{N1}/F_{N2} or F_{N2}/F_{N1}, the synchronization times are distributed in a similar way. And the reason why the synchronization time tends to zero when $F_{N1}/F_{N2} = 1$ is because both particles start in similar conditions.

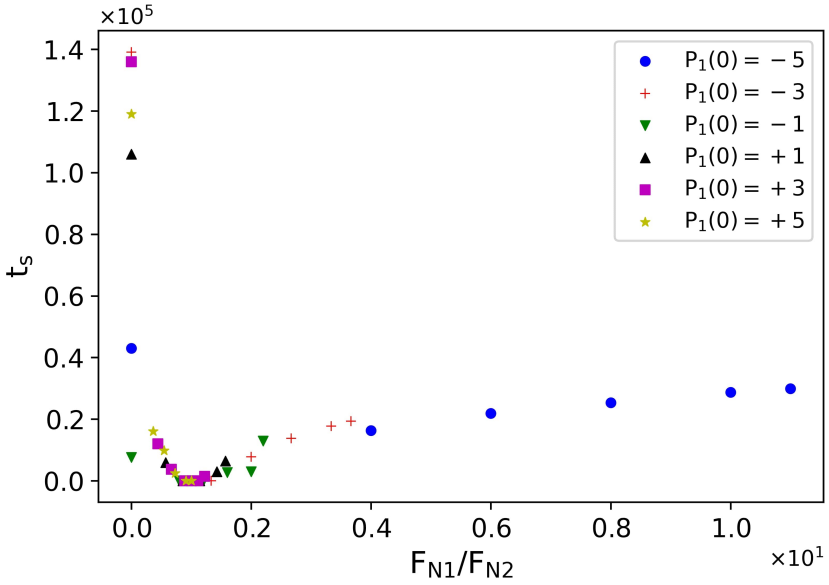

Figure 3.13: Synchronization time considering the stable state when $R = 0.99$. Each data set has a one particle with a constant initial position, given by $P_1(0)$, and the other one has a value of $P_2(0) \in \{-6, -5, -2, 0, 2, 4, 5\}$.

3.1.2 Observations on the system with particles with the same natural frequency

One of the situations that might seem odd in the previously presented results is the way that synchronization time of systems that start with a phase shift $\Delta\phi_i < \pi/2$ rad. These systems tend to have an opposite tendency than those with $\Delta\phi_i > \pi/2$ rad: the synchronization time decreases with distance, increases with viscosity (when we do not maintain the frequency constant), and increases with

frequency. This is due to the fact that the synchronization becomes somewhat "irregular" in its final moments. We show in the following plot 3.14, the evolution of the synchronization parameter R for the different distances that we simulated.

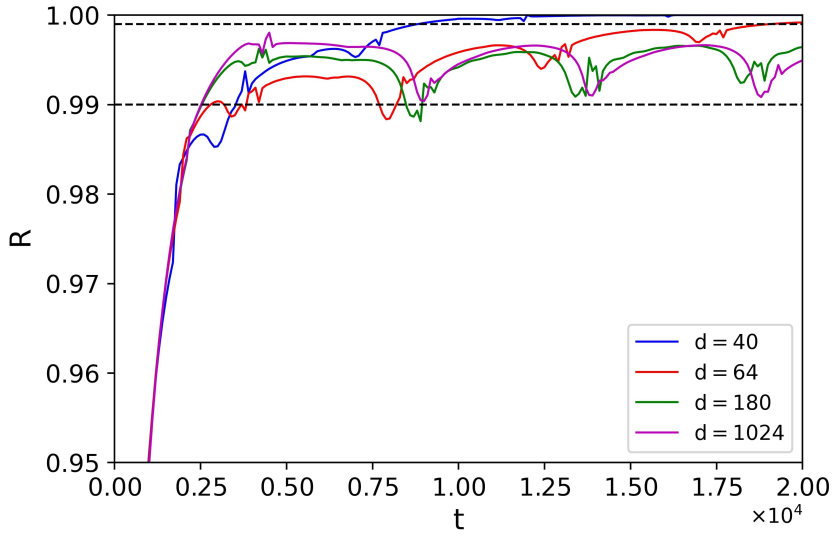

Figure 3.14: In the plot we have the synchronization parameter R evolution in time for some of the systems studied in distance dependency subsection of section 3.1, with $\Delta\phi_i = 1.23$ rad. There are two dashed lines for comparison: one for $R = 0.99$ and another for $R = 0.999$. We see that the smaller the system's size, the sooner it reaches $R = 0.99$; but the larger the system's size, the sooner it reaches $R = 0.999$.

The time to synchronization is essentially the same for any distance. However, there is a "bounce-back" – the increase of R slows down (and even decreases) around $t = 2000$, with this being more evident for smaller distances. But then the R increases faster for those same smaller distances. We can say that $R = 0.99$ is achieved around $t = 2700$, for all cases. But the fact remains that, if we consider $R = 0.99$ as the synchronization threshold, then the synchronization time decreases with distance; while if, on the other hand, we consider that $R = 0.999$ is the threshold, the synchronization time increases with distance – just like what we already observe for the systems with $\Delta\phi_i > \pi/2$ rad.

When we look at a position versus time plot of these systems (cf. Figure 3.15), what we see is that these R valleys correspond to the instant when the initially slower particle starts to decelerate near local maxima (or minima) of this particle's motion.

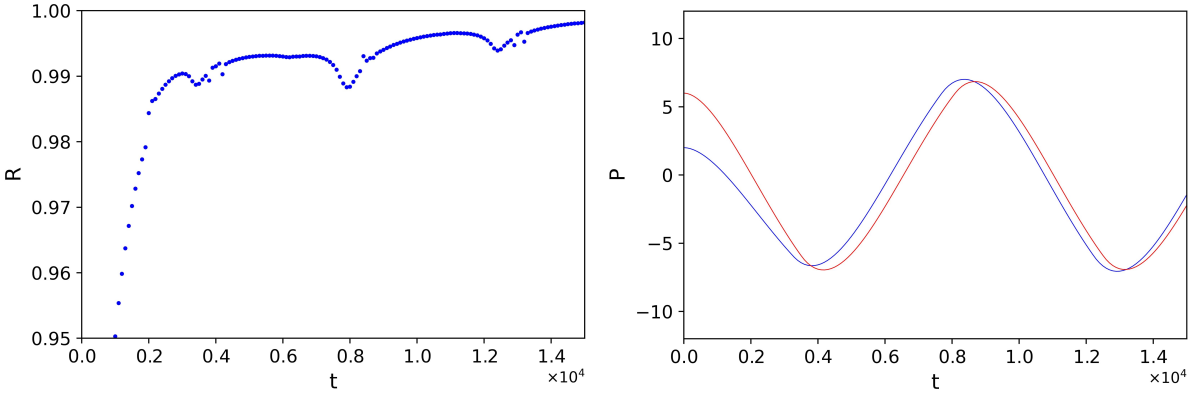

Figure 3.15: Side-by-side, the plot of the particles' position in relation to their respective centers of oscillation (left) and the synchronization parameter R (right) as a function of time. This system was studied in distance dependency subsection of section 3.1: it has $\Delta\phi_i = 1.23$ rad and $d = 64$.

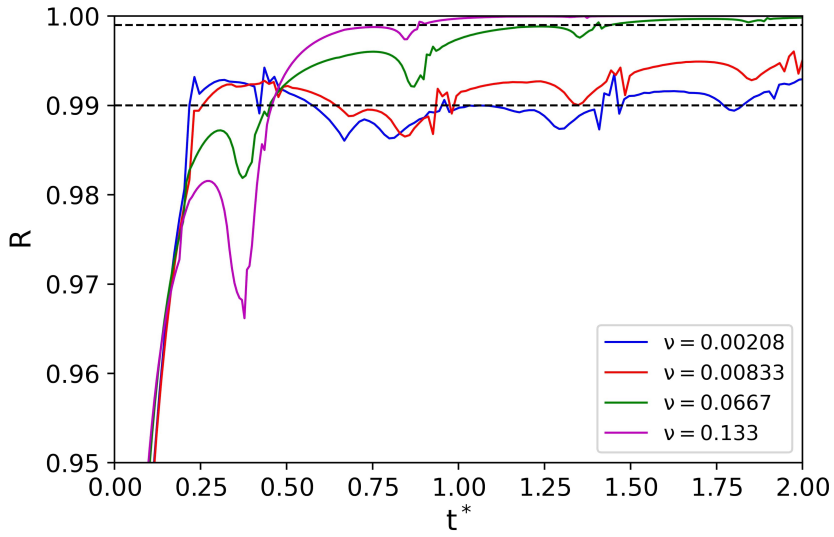

Figure 3.16: In the plot we have the synchronization parameter R evolution in normalized time ($t^* = t \times f_n$, where f_n is the ordinary natural frequency) for some of the systems studied for the dependency of the synchronization time in the viscosity, with $\Delta\phi_i = 1.23$ rad. There are two dashed lines for comparison: one for $R = 0.99$ and another for $R = 0.999$. We still have that the larger the fluid viscosity, the sooner it reaches $R = 0.99$, and the latter it reaches $R = 0.999$; but now we also see that the "R valleys" occurs approximately at the same instant of the oscillation for every viscosity value.

These fluctuations of the R value near synchronization are even more evident when we look at the viscosity dependency. In this case, the recessing of the R parameter is very clear. As the frequency of the particles is not the same, we can resort to plotting the results with the simulation time normalized by the natural frequency of the particles, i.e., $t^* = t \times f_n$ (where $f_n = \omega/(2\pi)$ is the ordinary natural frequency). These are presented in Figure 3.16. In this case, we clearly see that the R profile is identical for all viscosity, and the fluctuations tend to occurs at the same time instant for all values of viscosity – these occur around $t^* = 0.40, t^* = 0.85, t^* = 1.3$ and $t^* = 1.8$ (up until $t^* = 2.0$). The fluctuations are more accentuated for larger values of viscosity. We could say that all the systems synchronize around $t^* = 0.5$.

These fluctuations on the R parameter near the synchronization state is clearly evident for $\Delta\phi_i = 1.23$ rad, and clearly influences the instant when $R = 0.99$ is reached. And these fluctuations are also present for any initial phase shift, but for the cases when $\Delta\phi_i \geq \pi/2$ rad these do not alter the synchronization time significantly – and therefore, $R = 0.99$ is a good threshold for the final and synchronized state.

3.2 Particles with different natural frequencies

What if the two particles have different natural frequencies? While studying the dependency in the distance and in the viscosity for this new condition, the different natural frequencies were obtained by having both particles with be same body acceleration $A_x = 6 \times 10^{-6}$ but different turnabout amplitudes: one of them had $A = 5$ and the other had $A = 6$. Both of them had initial position relative to their center of oscillation at $P(0) = A$. Thus, they would start in-phase.

The other option to obtain different natural frequencies would be to change the body acceleration between oscillators. And that was exactly what was done next: both particles had the same turnabout amplitude $A = 6$, but one of them had a body acceleration of $A_x = 6 \times 10^{-6}$ while the other has a series

of values.

For all the previously mentioned systems, the height was $L_Y = 128$. And like the simulations of the section 3.1, the centers of oscillation were set at $CO_1 = L_X/4$ and $CO_2 = 3L_X/4$.

The aspect of the synchronization parameter R plot is now different. R starts at the unit, and then decreases in time to a smaller value, R_f – which, in general, is considered to be $\langle R \rangle$ when $t \to \infty$. That is, there is a final phase shift different from zero. In this case, the exponential fit was of the type:

$$R(t) = R_f + (1 - R_f) \cdot e^{-t \cdot \tau}. \tag{3.4}$$

Distance dependency

To study the behavior of the oscillators of different natural frequencies with distance, we varied the length of the system from $L_X = 76$ up to $L_X = 512$. As reference, we also made two simulations with a particle isolated in a fluid, with its center of oscillation at $CO = L_X/2$ in a system with $L_X = 512$: one of them with turnabout amplitude $A_1 = 5$, body acceleration $A_{x1} = 6 \times 10^{-6}$, and starting position $x(0) = L_X/2 - A$; and another with $A_2 = 6$, $A_{x2} = 6 \times 10^{-6}$ and again $x(0) = L_X/2 - A$. These were done so as to get an idea of what would the natural oscillation regime of the particle, i.e., its natural frequency and peak amplitude (these are presented in the second part of appendix A). All of these simulations had a relaxation time $\tau = 0.7$ ($\nu = 0.0667$).

The synchronization time, t_s, as a function of the distance between the centers of oscillation, d, is presented on the left plot of Figure 3.17. Such as when the particles had the same natural frequency, the synchronization time increased with the distance d. And if we were to discard the first two data points ($d = 38$ and $d = 40$), which have a t_s close to zero, we would see a clear exponentially tendency.

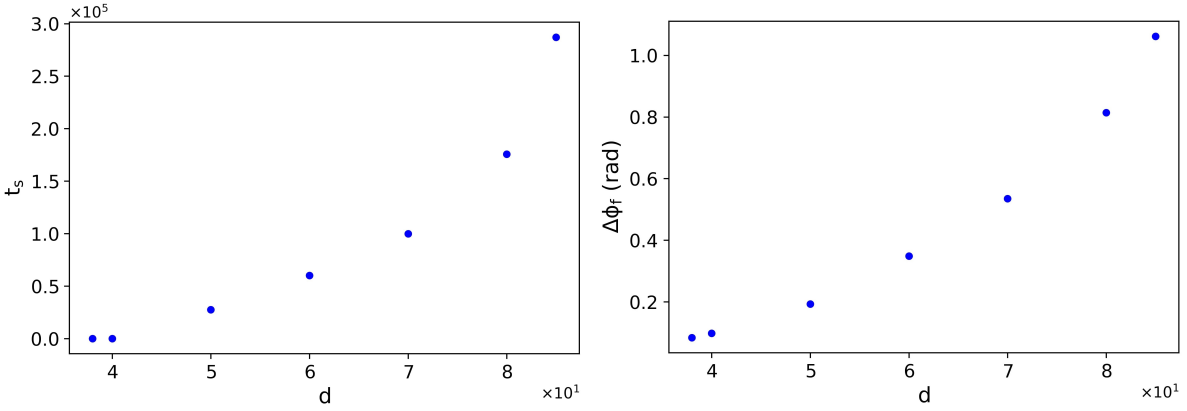

Figure 3.17: On the left, the plot of the synchronization time as a function of the distance between centers of oscillation. The synchronization is nearly instantaneous for small distances. On the right, the plot of the final phase shift as a function of the distance between centers of oscillation. The final phase shift is never zero, but close to zero for small distances. Both particles have a body acceleration of $A = 6 \times 10^{-6}$, while one has a turnabout amplitude of of $A_1 = 5$ and the other $A_2 = 6$. The fluid viscosity is $\nu = 0.0667$.

The particles may tend to and maintain the same final frequency, but, in general, their final state does not correspond to a in-phase synchronization. And in fact, the further away they are, the longer it takes the system to reach its final state and the larger the phase shift is (cf. right plot of Figure 3.17) – this tendency is also approximately exponential. But up until a certain distance, as beyond it the system is unable to maintain a synchronized state. The state we then observe is characterized by a slow

convergence to what seems like a synchronized state (with non-zero phase shift); but then the system quickly goes to phase opposition; and once again it slowly tends to that first pseudo-stable state – and this cycle repeats itself time and time again. This unstable state has a similar aspect to that observed in the system in 3 that is characterized by each oscillator having a set time interval for each direction of its body acceleration: the oscillation amplitude is inversely proportional to the instantaneous phase shift, and therefore there is a pulsating profile in the position-time plot.

We observe that the final synchronized state does not really have a fixed phase shift, but instead the phase shift varies slightly around a mean value. And the larger the distance, the wider is oscillation around the mean value – however, this oscillation isn't noticeable when we look at the position of the particles in time. These oscillations of the synchronization parameter (and necessarily the phase shift) becomes more noticeable with distance, and might be due to the difference of oscillation amplitude between the oscillators, which also increases with the distance (cf. left plot of Figure A.7).

Viscosity dependency

For the viscosity dependency, the setup is similar to that on the distance dependency, but here the system length was set at $L_X = 140$ and the viscosity was varied using a number of values for the relaxation time in the range $\tau \in [0.50625, 0.9]$, which corresponds to a viscosity in the range $\nu \in [0.002083, 0.1333]$. Like for the dependency on the distance, here we simulated a number of systems with a single particle with its center of oscillation at $x = L_X/2 = 70$, for all the viscosity values that we tested on the two particle system (cf. Figure A.8).

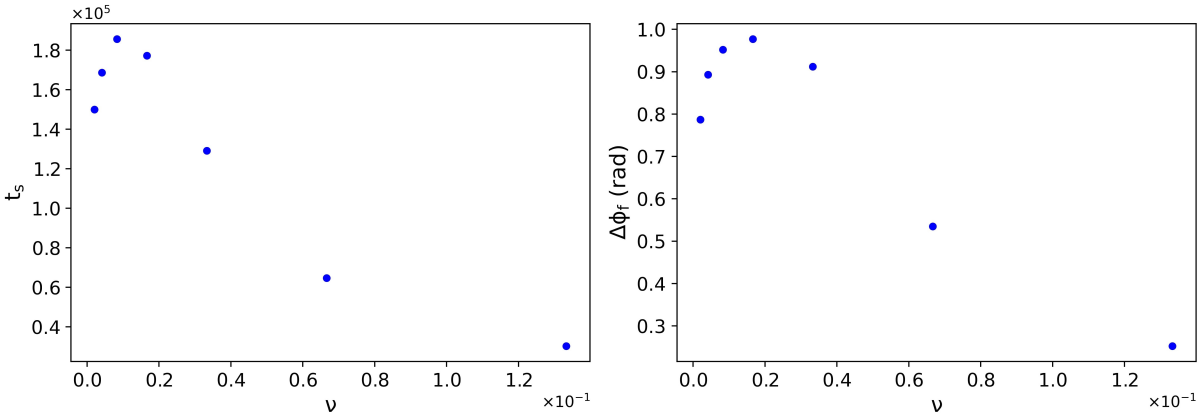

Figure 3.18: On the left, the plot of the synchronization time with the viscosity of the fluid. We can see the rise-and-fall shape of the plot, with the peak at $\nu = 0.00833$. On the right, the plot of the final phase shift with the viscosity of the fluid. We can see the rise-and-fall shape of the plot, with the peak at around $\nu = 0.0167$. Both particles have a body acceleration of $A = 6 \times 10^{-6}$, while one has a turnabout amplitude of of $A_1 = 5$ and the other $A_2 = 6$. The distance between the centers of oscillations is $d = 70$.

As it would have been expected, the increase in viscosity corresponds to a decrease in both oscillation amplitude and natural frequency, not only in the systems with a single particle but also on the systems with two particles (cf. Appendix A). But the most interesting results are those of the synchronization time (left plot of Figure 3.18) and final phase shift (right plot of Figure 3.18). What see is that, initially, the increase of viscosity corresponds to an increase in both synchronization time and in final phase shift; then we reach a peak, which for the synchronization time is at $\nu = 0.00833$ and for the final phase shift occurs at $\nu = 0.0167$; from beyond this point, both synchronization time and final phase shift decrease and reach values below those at $\nu = 0.00208$.

It is not immediately evident why this is the case. Moreover, because we do not see this behavior on the viscosity dependency when both particles have the same natural frequency (cf. Figure 3.9). Maybe, it is because it is the fluid that mediates the synchronization between the oscillators (the larger the viscosity, the stronger the drag force induced from one oscillator on the other), but it is also the viscosity that hinders the particles' individual motion (the larger the viscosity, the slower is the motion of a particle, and thus the less influence it has on the other), we get this unexpected behavior. The "push" (synchronization) and the "pull" (inertia) effects of the medium might have a different importance in different ranges of viscosity.

It can also be related to the natural frequency of the oscillators. When we look at the right plot of Figure A.8, we see that the natural frequencies tend to diverge with the increase in viscosity; however, the relative difference between natural frequencies follows the opposite tendency of the synchronization time and the final phase shift: it decreases between the 2 first data points (up to $\nu = 0.00417$), and increases from second data point onward. But we should note that the inflection of the synchronization time and the final phase shift occurs after that. Furthermore, this seems to contradict what we will see on the next subsection on the body acceleration difference dependency.

Another possibility is that of the distance between oscillators. The smaller the viscosity, the larger the oscillation amplitude. At $\nu = 0.00208$, the peak amplitudes are $A_{p1} = 10.2$ and $A_{p2} = 9.93$, and at $\nu = 0.133$ they are $A_{p1} = 6.63$ and $A_{p2} = 5.72$ – a drop of around 35% and 42% (cf. left plot of Figure A.8). It could be the case that at smaller viscosity, the larger amplitudes correspond to a effective decrease in the distance of the oscillators, which would increase the interaction; but then this amplitude effect would have to become essentially negligible for larger values of viscosity.

Body acceleration difference dependency

To study the influence on the system that a difference in body acceleration between particles has, we maintained one particle with its body acceleration constant at $A_1 = 6 \times 10^{-6}$, while varying the value of the other one in the range $A_{x2} \in [6, 15] \times 10^{-6}$. Both particles having a turnabout amplitude of $A = 6$. The system's length was set at $L_X = 140$ and the relaxation time at $\tau = 0.6$ ($\nu = 0.0333$).

What we observed from the simulations is that there is a point beyond which the difference in frequency does not allow the oscillators to reach a stable state. In our simulation, this point corresponded to the body accelerations $A_{x1} = 6 \times 10^{-6}$ and $A_{x2} = 7.30 \times 10^{-6}$; that is, a ratio of 1.217 or a difference of 21.7%. As for the synchronization time and final phase shift, we see that the larger the difference of body acceleration, the longer the system took to reach the stable state (cf. left plot of Figure 3.19) and larger was the final phase shift (cf. right plot of Figure 3.19). And if not for the two first data points, we would say that the synchronization time increases exponentially with the difference of body accelerations.

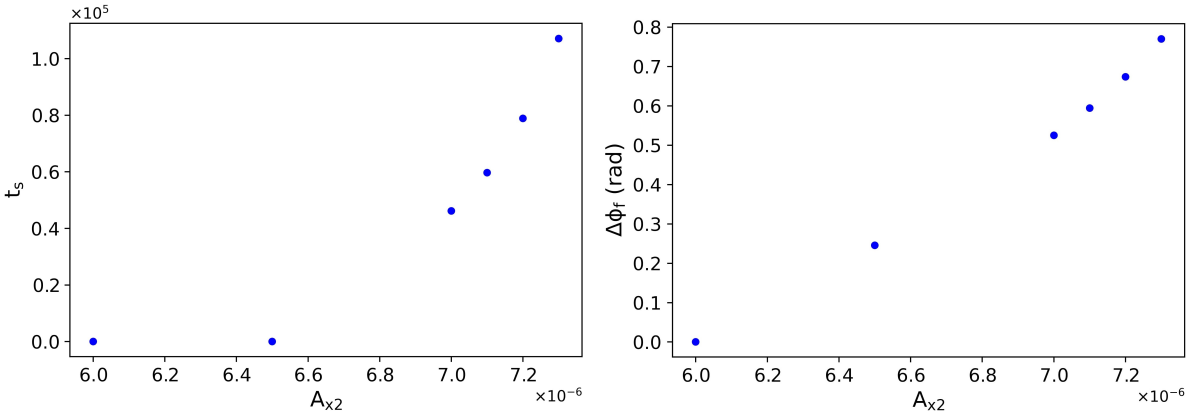

Figure 3.19: On the left, the plot of the synchronization time as a function to the value of the body acceleration of one of the particles, A_{x2}. On the right, the plot of the final phase shift as a function to the value of the body acceleration of one of the particles, A_{x2}. The other particle has a constant body acceleration of $A_{x1} = 6 \times 10^{-6}$. Both particles have a turnabout amplitude of $A = 6$ and the distance between the centers of oscillations is $d = 70$. The fluid viscosity is $\nu = 0.0333$.

3.2.1 Observations on the system with particles with different natural frequencies

One of the characteristics that differentiates the system of two particles with different natural frequencies and that with both particles with the same natural frequency is that the latter, when the stable state is achieved, the phase shift is null (or very close to zero), while for the former this is not guaranteed, and, in general, is not true. As was already shown, the final phase shift can be directly related to the synchronization parameter R. This result is already predicted by the KM, and is represented by the bifurcation diagrams, where we plot R as a function of K – in the case of different natural frequencies, there is a smooth transition from non-synchronized states (represented by $R = 0$) to a state where all the oscillators are phase-locked (represented by $R = 1$), and in between these two states there are the partial synchronization states; in the case of same natural frequencies, the transition from $R = 0$ to $R = 1$ is sharp, i.e., either the system does not synchronize, or it only synchronizes and is phase-locked. we will present these results also in the next chapter, once we have determined the coupling factor K of these simulations.

However, our simulations present a result that contradicts the KM, and that is the final frequency: in all of our simulations, the system never converges to the mean frequency value but is always larger. In fact, there is a clear dependency on the studied variables and the final frequency; moreover, even when the system does not synchronize, the final frequency of the particle with the smaller natural frequency is larger that this one.

Chapter 4

Kuramoto Model

Having simulated our system with the LBM, we now move to the Kuramoto model. Our system is, in essence, a biological system –, and as it has already been said, the Kuramoto model was firstly developed with chemical and biological systems in mind [15]. The idea is to compare the two models – the LBM and the KM –, and also to parameterize the latter with the results of the former. If we could map the results obtained in section 3 in terms of coupling factor, the KM would give us a general solution to the problem.

We did not observed any significant time delay in the interaction of our oscillator in the fluid simulations. So the time delay on our Kuramoto model should also be neglected. The KM for a system of 2 coupled oscillators without time delay is given as a pair of equations by 2.12. These equations can be written with $\Delta\theta(t) = \theta_1(t) - \theta_2(t)$, as:

$$\begin{cases} \dfrac{d\theta_1}{dt}(t) = \omega_1 - K\sin(\Delta\theta(t)) \\ \dfrac{d\theta_2}{dt}(t) = \omega_2 + K\sin(\Delta\theta(t)) \end{cases}. \tag{4.1}$$

If we consider that $\omega_1 = \omega_2 = \omega$, then we can define the system simply by the natural frequency ω, the initial phase shift – which is equivalent to $\Delta\theta(0) = \Delta\phi(0) = \Delta\phi_i$ [1] –, and the coupling constant K. If we know, or set, ω and $\Delta\phi_i$, the convergence of the system and the synchronization time depends only on K.

The Kuramoto model for a system with two oscillators has an analytical solution, given by the aforementioned model with delay in Ref. [35], but this solution does not specify the time development of the system. On the other hand, the KM (with noise and noiseless) has been solved numerically using a number of methods[2]: Euler, Heun, Taylor of order 3/2 and spectral [42][43][44][45]. As it was said before, as we have a finite (and small) number of oscillators, the exact solution of the KM for $N \to \infty$ cannot be used. But our system is relatively simple and we can solve it with the Euler method.

We simulated this system with the Euler method for $\omega = 4.81 \times 10^{-4}$ rad and for double that value, $\omega = 9.62 \times 10^{-4}$ rad. The results of the simulations were so close that we can say that for the range of $\omega \in [4.81, 9.62] \times 10^{-4}$ rad, the behavior of the system is essentially the same. Furthermore, these simulations were carried with time steps of $\Delta t = 1$, $\Delta t = 0.5$ and $\Delta t = 0.25$, and there was no significant gain in precision with the smaller time steps – thus, all the results presented have $\Delta t = 1$, as it reduces the computation time.

[1] This equivalency is due to the fact that we can express the instantaneous phase, θ, by the natural frequency, ω, and the absolute phase, ϕ.

[2] A comparison between these methods is presented in section VI of Ref. [34].

For a system that converges to a null phase shift synchronization, the synchronized state would be characterizes with $R = 1$. However, we will once again consider that we have achieved this state the instant that we reach $R = 0.99$ – this corresponds to a phase shift of 0.283 rad or $16.2°$. This is the value that we consider for the plots on Figure 4.1.

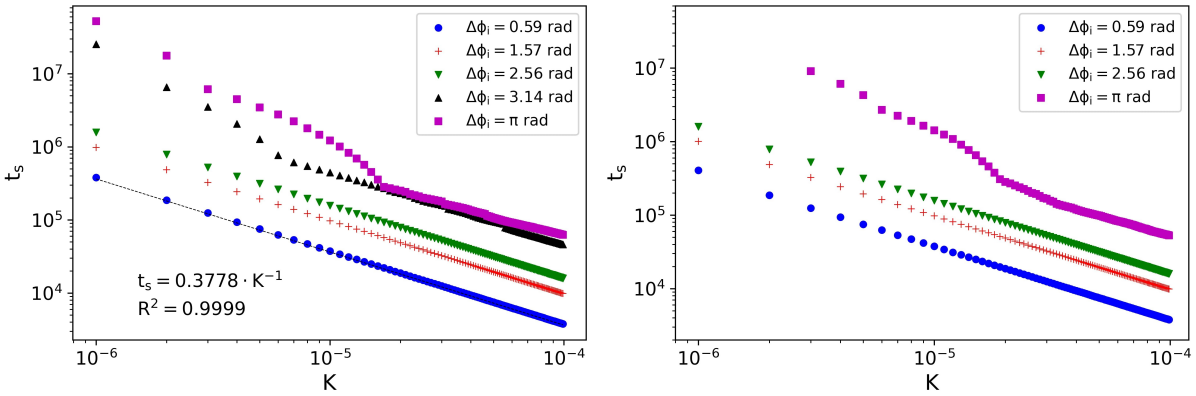

Figure 4.1: Plots of the synchronization time ($R = 0.99$) and the coupling constant K for different initial phase shift, with a natural frequency $\omega = 4.81 \times 10^{-4}$ rad (left) and $\omega = 9.62 \times 10^{-4}$ rad (right). These values were obtained by simulating the KM as referred above. The time interval is equal to the simulation time step $\Delta t = 1$. The dashed line on the left plot is the power law fit to the data set for $\Delta\phi_i = 0.59$ rad; as we see, this is a good fit (the determination coefficient is close to the unit) and corresponds to a slope of $c = -1$. The right plot is identical to the left one, which indicates that for this range of natural frequencies the relation between synchronization time and coupling factor is identical.

As we can see, apart from the systems with initial phase shift close to the phase opposition ($\Delta\phi_i \approx \pi$ rad), when plotted in a log-log scale, all sets of points for each of the initial phase shifts have a very similar slope: we have a power law, $t_s = a \cdot K^{-c}$; and it so happens that the slope is very close to the unit, $c \approx 1$. This means that – for a given given R threshold – we only need the a parameter to classify synchronization time for each phase shift:

$$t_s = \frac{a}{K}. \tag{4.2}$$

So, by knowing the initial phase shift and the natural frequency of the oscillators, we can easily estimate the a value. And with it, we can get either the synchronization time from the coupling factor K, and vice-versa. We calculated these proportionality values a for the natural frequencies used previously (that is, $\omega = 48.1 \times 10^{-4}$ rad and $\omega = 9.62 \times 10^{-4}$ rad); these are shown in the following Figure 4.2. As we can see, the values of a are similar for both frequencies and for each synchronization parameter R threshold.

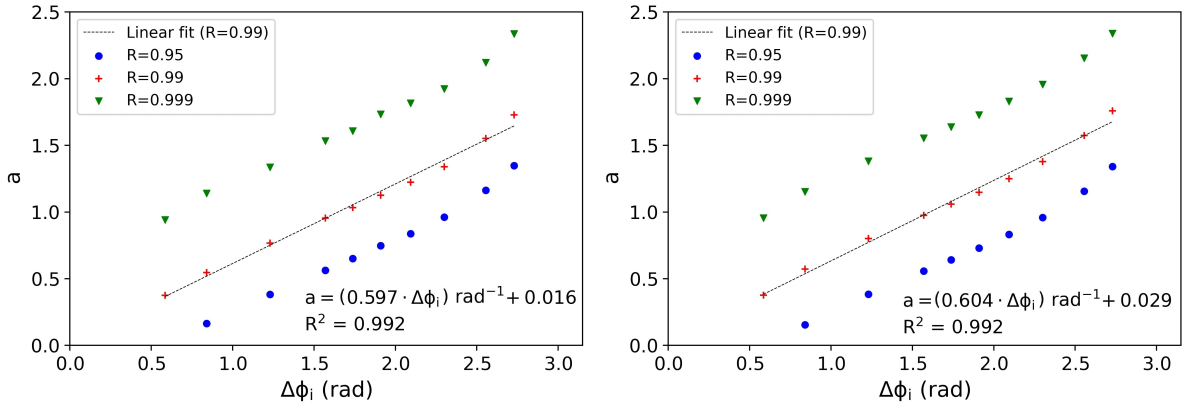

Figure 4.2: Plot of a value (eq. 4.2) for 3 different R values (0.95, 0.99 and 0.999) for different initial phase shift, with a natural frequency $\omega = 4.81 \times 10^{-4}$ rad (left plot) and $\omega = 4.81 \times 10^{-4}$ rad (right plot). We can make a linear fit of the data set of $R = 0.99$, which is presented on for each case and the corresponding coefficient of determination R^2. We see a considerable similarity between the two cases, also evident on the linear fit parameters.

The slope with the threshold $R = 0.99$, for both natural frequencies, is similar and approximately $m = (0.601 \pm 0.004)$ [3]. This means that we can get t_s from:

$$t_s = \frac{(m \cdot \Delta\phi_i) \ + b}{K}. \tag{4.3}$$

The same process can be used for the system of particles with different natural frequencies; but this added variable multiplies considerably the number of possible systems. For this reason, the simulations of the KM for systems of two particles with different natural frequencies do not run through two ranges of possible natural frequencies ω_j, but have fixed and known values of these variables, and we run only over the values of K.

4.1 Comparison with the fluid simulations

One of the objectives of this work is to map the results of oscillators in a fluid, obtained through the LBM, into the KM; and as said above, the synchronization parameter R and its evolution in time is a common metric to study the synchronization of such a system. In our first approach, we considered the simple formula given in the equation pair 4.1, with K and $\omega_{1,2}$ constant. This results in synchronization times of the type of eq. 4.2. The criterion of synchronization was the system achieving $R = 0.99$ – this is the criterion that we have been using up until now, and from which we get the plots in chapter 3.

We concentrate on fitting the KM to the system with 2 particles with the same natural frequency (cf. Section 3.1). The process was as following: 1) determine the a constant that corresponds to the initial phase shift of the system; 2) find $t(0.99)$, the instant at which the system achieves a value of $R \geq 0.99$ (often using a exponential or sigmoid fit to the data); 3) get the coupling constant K from the expression 4.2; 4) simulate the KM with K found in the previous step and plot the simulation alongside the R-time plot of the system; 5) assess the quality of the fit of the KM simulation to that of the fluid, using the coefficient of determination, R^2 (up until the point we reach $R = 0.99$).

For the initial phase shift dependency (cf. Figure 4.3), we see a drastic decrease of the coupling factor up until $\Delta\phi_i = \pi/2$ rad, from which point it decreases only slightly. For $\Delta\phi_i > \pi/2$ rad, the coupling factor K initially decreases, but then increases with the natural frequency; for $\Delta\phi_i = 1.23$ rad,

[3] If we want to be more precise, it is also possible to fit a 3rd order polynomial function to the data sets.

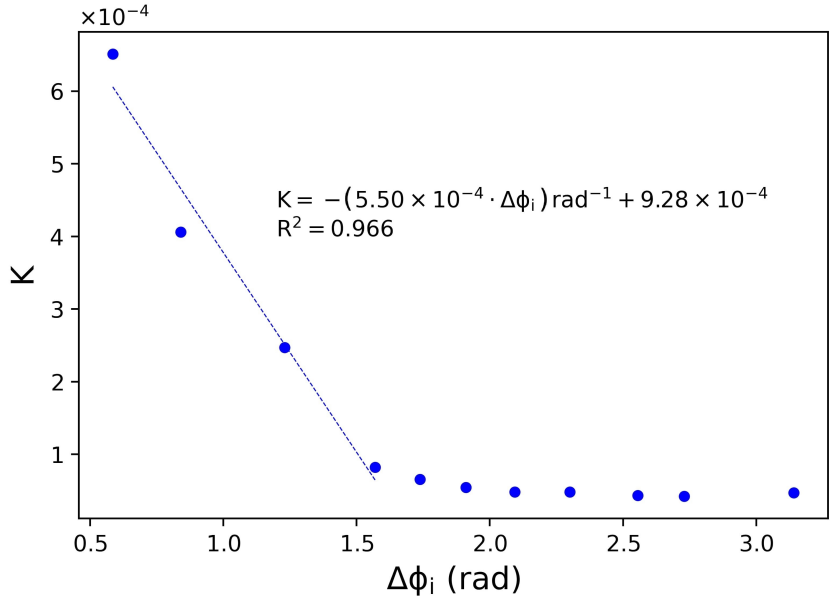

Figure 4.3: Coupling factor K as a function of the initial phase shift, obtained by the synchronization time. K decreases approximately linearly with $\Delta\phi_i$ up until $\Delta\phi_i = \pi/2$ rad (we present a linear fit as a dashed line, as well as its expression and coefficient of determination), and then only slightly decreases until $\Delta\phi_i = \pi$ rad.

decreases with the natural frequency, as seen on Figure 4.4. There is then no clear and general relation between the coupling factor and the natural frequency.

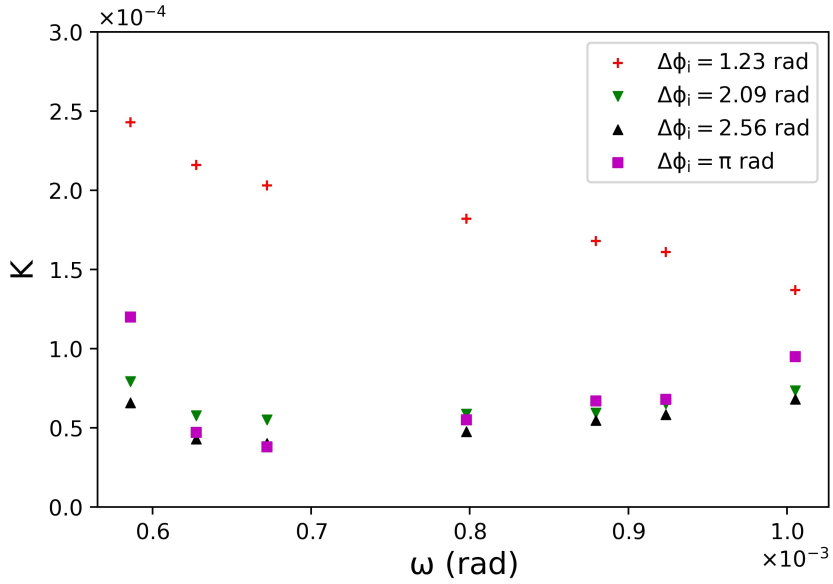

Figure 4.4: Coupling factor K as a function of the natural frequency, obtained by the synchronization time.

The cases in which the results are liable of being fitted are those for the viscosity dependency (cf. Figure 4.5), the distance dependency (cf. Figure 4.6), and for the viscosity dependency while maintaining a constant frequency (cf. Figure 4.7). In the first two cases, this was already expected, as there was already a clear relation between those quantities and the synchronization time (cf. Figures 3.9 and 3.8).

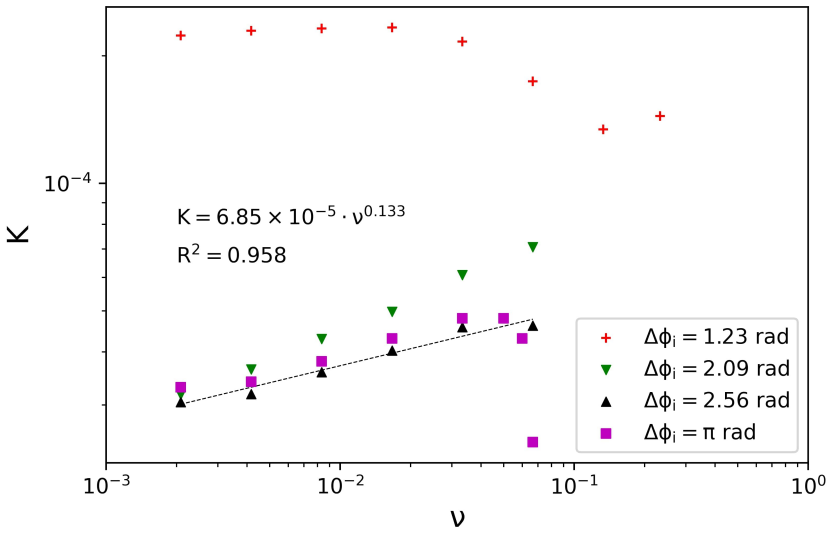

Figure 4.5: Coupling factor K as a function of the fluid viscosity, obtained by the synchronization time. We once again see a power law relation for $\Delta\phi_i \geq \pi/2$ rad. We present a power law fit to the points with $\Delta\phi_i = 2.56$ rad, with its expression and the corresponding coefficient of determination.

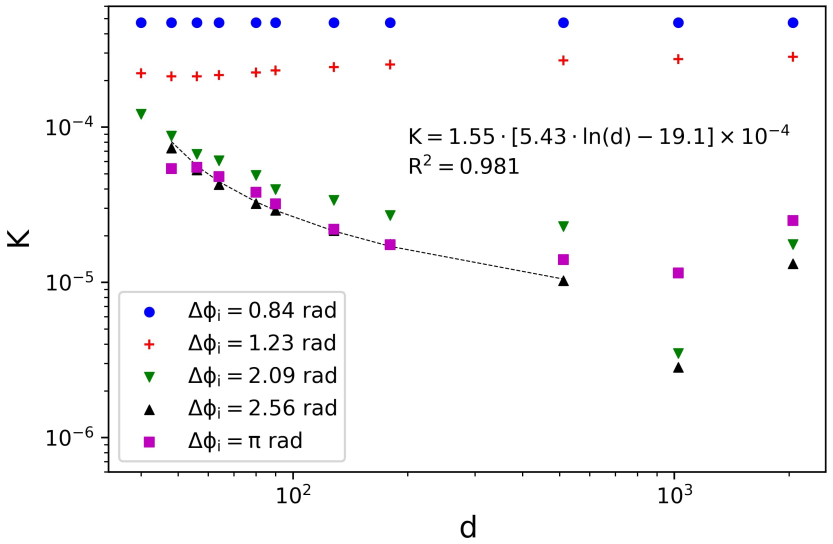

Figure 4.6: Coupling factor K as a function of the distance between the centers of oscillation of the particles, obtained by the synchronization time. The plot is in log-log scale. We see that the coupling factor for $\Delta\phi_i = 0.84$ rad and $\Delta\phi_i = 1.23$ rad is essentially constant. The fit for the data set of $\Delta\phi_i = 2.56$ rad is present along side its coefficient of determination R^2. The fit is given by equation 4.3 and the logarithmic expression found on Figure 3.8.

The quantity with the simplest and clearest relation with the coupling factor is the fluid viscosity, while maintaining a constant frequency (cf. Figure 4.7): across all data sets (for each of the initial phase shifts), the coupling factor is approximately linearly proportional to the viscosity.

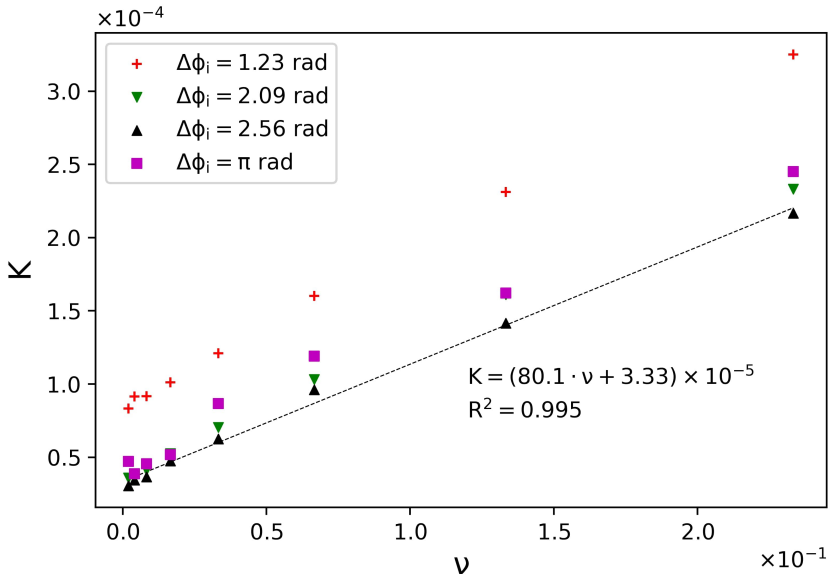

Figure 4.7: Coupling factor K as a function of the fluid viscosity, while maintaining a constant frequency, obtained by the synchronization time. The data sets are displayed approximately in line. We present the linear fit of the data set for $\Delta\phi_i = 2.56$ rad by the dashed line, alongside its expression and the corresponding coefficient of determination R^2.

When looking at the power fit in Figure 4.5, we verify that the coupling factor is given by equation 4.3, considering $\Delta\phi_i = 2.56$ rad (the characteristic variable is $a = 1.55$) and the power law fit for t_s present in Figure 3.9. Likewise, the values of the coupling factor, while varying the distance between the centers of oscillation, up until $d = 512$, is given by equation 4.3 and the logarithmic expression found on Figure 3.8. In the case of the distance dependency, we see that the coupling factor for $\Delta\phi_i = 0.84$ rad and $\Delta\phi_i = 1.23$ rad is essentially constant.

An interesting exercise is to obtain the synchronization time from the coupling factor, namely for the viscosity dependency (maintaining a constant frequency). We recall that it did not seem possible to fit the data presented in Figure 3.10. But now it seems that it was given by:

$$t_s = \frac{(m \cdot \Delta\phi_i) + b}{n \cdot \nu + p}, \tag{4.4}$$

where m and b are the parameters of the linear fit, dependent of the natural frequency and of the characteristic variable a (i.e., the initial phase shift) (cf. eq. 4.2), and n and p are the parameters of the linear fit to the results of coupling factor as a function of the viscosity, $K(\nu)$.

Limitations of the fitting

By fitting to the synchronization time we are ignoring how the system behaves until it achieves it. What is evidently apparent is that this simple model does not represent the synchronization process of the systems in study, specifically if the initial phase shift is larger that $\pi/2$ rad – for $\Delta\phi_i < \pi/2$ rad, the simple model gives reasonable results, but the closer we get to $\Delta\phi_i = \pi$ rad, the bigger is the discrepancy with the simulations. The comparison of the fluid simulation results with the KM, using the above process, for different initial phase shifts is presented in Figure 4.8.

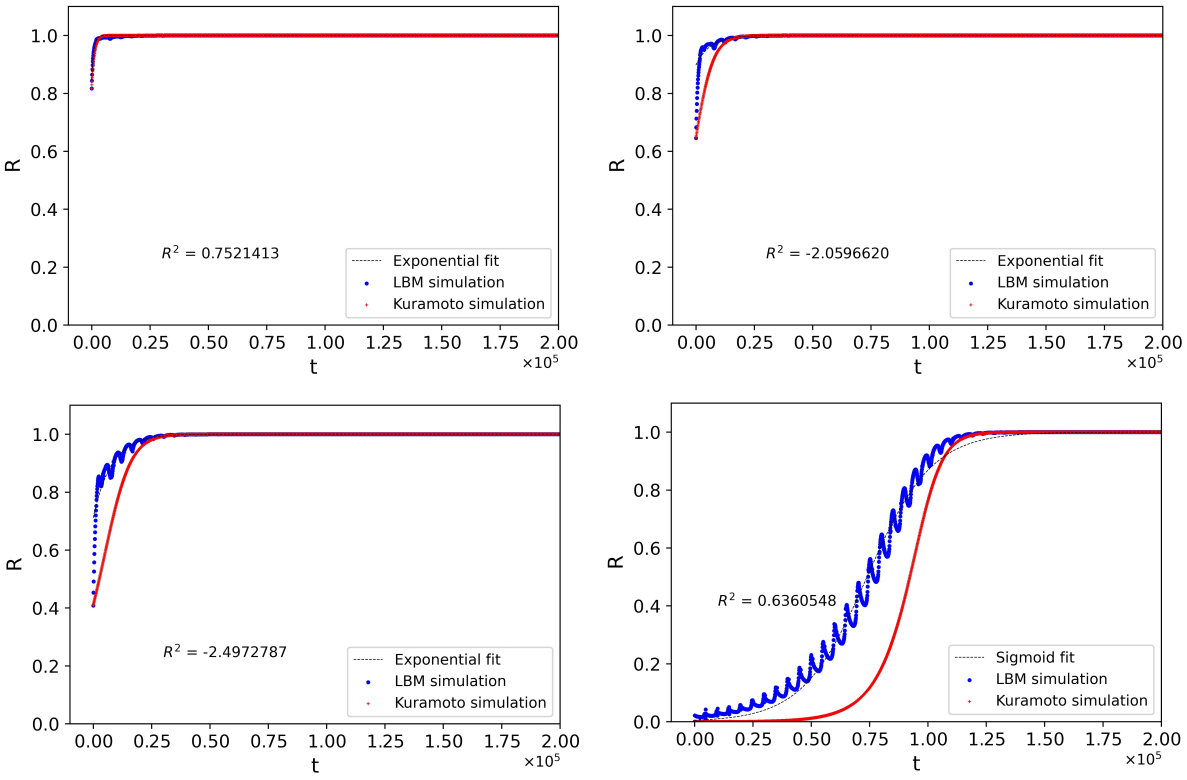

Figure 4.8: Comparison of the fluid simulation and the Kuramoto model simulation for the systems with $L_X = 128$ ($d = 64$), $\tau = 0.6$ ($\nu = 0.0333$), $A = 6$ and $A_x = 6 \times 10^{-6}$. Each of the four plots has a different initial phase shift: $\Delta\phi_i = 1.23$ rad (top left), $\Delta\phi_i = 1.74$ rad (top right), $\Delta\phi_i = 2.30$ rad (bottom left) and $\Delta\phi_i = \pi$ rad (bottom right). The coupling factors used for each of the cases is: $K = 2.47 \times 10^{-4}$ (top left), $K = 6.55 \times 10^{-5}$ (top right), $K = 4.81 \times 10^{-5}$ (bottom left) and $K = 4.70 \times 10^{-5}$ (bottom right). To assess the coherence between the LBM simulation and the model (up until the system reached $R = 0.99$), the coefficient of determination, R^2, is presented in each case. We see that the larger the initial phase shift, the more evident is the discrepancy between the two simulations.

The matter of the fact is that there are two synchronization regimes: the first one from $t = 0$ to a given $t = t_{min}$, and a second one from $t = t_{min}$ to $t \to \infty$. In the first regime, the synchronization parameter R increases very rapidly, and in the second regime it increases significantly slower. This is due to the fact that the systems in study has a very strong dependency in the initial conditions: the fluid is initially at rest and the particles start with different net forces. (This is essentially what we can concluded from the results on the initial net forces of section 3.1.1.)

The fluid is initially stationary and both particles start with null linear velocity and frequency; this results not only in the particles not starting with their natural frequency, ω_j, but also that they need to overcome the fluid resistance during the first half-period; the system is initially damped. The particles start moving and their frequency increases; when they get across the turnabout amplitude, their net force (which in the meanwhile had been decreasing in amplitude) quickly goes from null to a local maximum value, and from this point onward, the system is undamped and the natural frequency has been achieved (and is maintained). If a particle starts from a initial position at, or beyond, the turnabout amplitude, then particle's movement is already in an undamped regime.

This first regime is more evident if one of the particles starts at the turnabout amplitude and the other particle starts in a negative initial position, $P < 0$. The particle that starts in the position $P = A$ has a undamped oscillation (with both body acceleration and spring-like force pulling in the same direction),

while the other particle has the body acceleration pushing it away from the center of oscillation and the spring-like force pulling it towards the center of oscillation. This results in the second particle being considerable slower than the first one, which gives the impression that the second one is "waiting" for the first one to cross the turnabout amplitude – of course, this is not the cause, rather the second particle takes significantly longer to get to the turnabout amplitude the first time it does this. Alongside this, the first particle can and does propel the second one to the turnabout amplitude. The moment the slower particle crosses the turnabout amplitude we reach the t_{min} referred previously, which indicates the transition instant between regimes. While accelerating towards the acceleration turning point, the particle further away from the center of oscillation achieves its natural frequency, ω faster than the other particle (this one is closest to the turning point, but has a smaller net force). And by "natural frequency" we are referring to the value ω in the KM (that is generally considered constant).

If the slower particle's initial position is $x(0) \in [CO - A, CO]$ – that is, somewhere between its center of oscillation and the turning point (in the direction of the movement) –, then t_{min} is the instant the particle's linear velocity is null, after having its body acceleration changed direction: at this point, the particle is flung back with a local maximum net force. For particles with initial position $x(0) \in [CO, CO + A]$, t_{min} seems to be around the instant it crosses its center of oscillation – but if the particle starts very close to $x = A$, then t_{min} tends to be very close to the initial instant of the movement.

This effect is seen in all the simulations. In the next Figure 4.9, we can see the first instant of the slowest particle's oscillation for different distances between the particles, for a initial phase shift of $\Delta\phi_i = 2.56$ rad. The closer the particles are from each other, the sooner the slowest particle gets to the turnabout amplitude at the position $P = -6$.

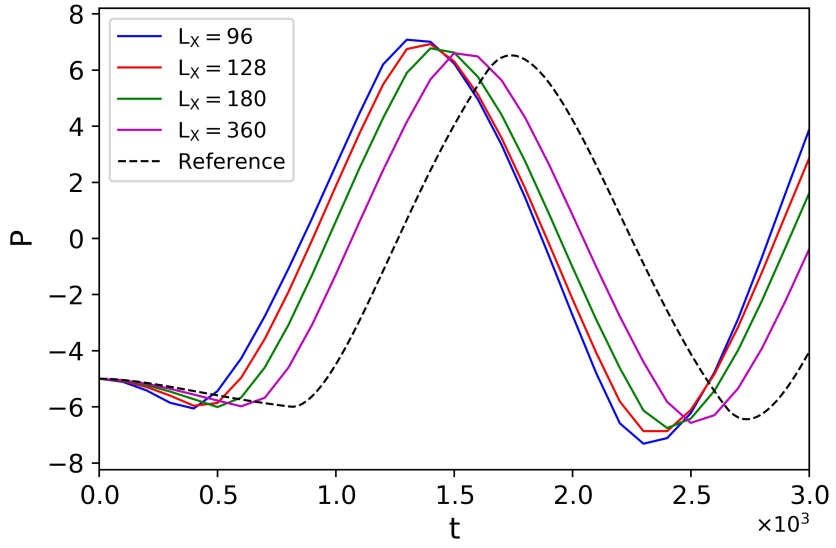

Figure 4.9: The trajectory of the particle that starts at $P = -5$ (the initial phase shift is $\Delta\phi_i = 2.56$ rad), for 4 different system sizes and as reference we have the positions of this particle isolated in a system of size $L_X = 1024$ (i.e., with no interaction with other oscillating particles). These systems are those studied in the distance dependency subsection of section 3.1, and the distance between the centers of oscillation are half of the length of the system ($d = 48$, $d = 64$, $d = 90$ and $d = 180$, respectively). We can see that the close the oscillators are from each other, the sooner the particle starting at $P = -5$ reaches the turnabout amplitude and oscillates at its natural frequency.

Another aspect that was observed was that the first synchronization regime becomes less and less relevant as the natural frequency of the particles becomes greater. When adjusting the "naive" coupling factor K, the fit becomes better for larger frequencies. And something similar occurs for the other

quantities of interest. The "naive" Kuramto model fits the data better for: shorter distances between the centers of oscillation; smaller initial phase shifts; larger viscosity values of the fluid; and (as was already said) larger values of natural frequency.

4.2 Modifying the Kuramoto model

The question that then arises is: what modifications can we then make to the Kuramoto model to better adjust it to our system? There are a number of already made modifications to the original KM. For example, in Ref. [46], two models are proposed: one with time-varying coupling strength and another with time-varying natural frequencies; in Ref. [47], we also see included varied connectivity between oscillators (on the context of neuronal synchronisation in the brain); some other studies have included non-constant natural frequencies [48][49]. However, all of these use periodic functions to model the time-varying parameters in study[4].

We know that the higher the value of the coupling factor, the faster the system synchronizes; we then propose to define the coupling factor K not as a constant, but as a function of time that goes from a higher value to a smaller (and final) one:

$$K(t) = K_{eff}\left(1 + A \cdot e^{-t/t_c}\right). \tag{4.5}$$

With this change, we guarantee the existence of the two regimes, being that for $t > t_{min}$ we should have $K(t) \approx K_{eff}$ – that is, from t_{min} we return to the KM with constant coupling factor. The question is then: what is the relation between these 3 new variables and the variables of our system?

The easiest to define is K_{eff}. As we have discussed already, if we remove the data points from the initial moments of the simulation (up to t_{min}), what we get is a system that converges to synchronization following the usual constant coupling factor model, with a different given initial phase shift. If we know this new phase shift, then we proceed as we did in the more simplistic approach. The effective K follows the same trend as the theoretical K (if the system had a constant K).

As for the first synchronization regime, we have two independent parameters, so it is not immediately evident what is the relation between these two parameters and the change in the synchronization parameter R; although, we can make a first assumption and consider that the multiplying constant of the exponential A defines the rate of change in R, and consider that the characteristic time constant t_c as defining the duration of the first regime.

Although we can use this method to model the change in R with high accuracy, we find two problems: 1) we can not easily explain why the coupling factor K would vary in time, when the system's variables are constant during all of the simulation, even if we consider the possibility that the first time the information from one of the particles is sent to the other one has some delay (maybe due to the initially stationary fluid); this hypothesis is not reasonable, because 2) the way the frequency changes in the fluid simulation and in the modified KM simulation do not coincide: as the KM simulation starts with a larger coupling factor, the initial change of the frequency of each particle relative to the their natural frequency is much larger than that of the LBM simulation (cf. left plot of Figure 4.12).

Another way to adjust the KM – which is more realistic, less dependent on the synchronization parameter R and models the frequency profiles more accurately – is based on the adjustment of the

[4] As it has already been said, the natural frequency of our oscillators is not constant, but fluctuates periodically around a mean value. Some of these models with time-varying natural frequencies would possibly model our system more accurately, but our main concern is the existence of the two synchronization regimes.

frequency (compare the plot of Figure 4.12). We know that the frequency of the particles starts from a null value and then converges its natural (and final) value (during the first regime). This is the effect discussed in section 4.1, and which can be observed for the non-sinusoidal first region of the plots in Figure 4.9. Well, this can be modelled by the pair of equations:

$$\begin{cases} \omega_1(t) = \omega_1^* \left(1 + e^{-t/t_{c1}}\right) \\ \omega_2(t) = \omega_2^* \left(1 + e^{-t/t_{c2}}\right) \end{cases}. \tag{4.6}$$

In this case, the characteristic time constant t_c is clearly related to t_{min}, as we know that $\omega(t_{min}) = \omega^*$. Once again, if a particle's initial position is at its turnabout amplitude, then we can assume that $\omega(t) = \omega^*$. While we have reduced the number of independent variables of our new model from 3 to 2, there is a new question that still hasn't been tackled: what is the relation between the t_{min} (and therefore t_c) and the system's variables? The answer is not as straightforward as one might wish. We will discuss this matter in subsection 4.2.1.

But by using one of these two modified Kuramoto models, we can obtain the effective coupling factor K_{eff}. As we shall see, this eliminates some of the odd behaviors observed on the synchronization time plots present above. And, in principle, the K_{eff} obtained by either of these models should be the same, as it always corresponds to the second regime. We compare these two modified models for the same fluid simulation: their synchronization parameter R evolution in time in Figure 4.11 and their phase change (frequency) evolution in time in Figure 4.12.

Overall, the second modified model (of variable natural frequency) is the best at fitting the fluid simulations, as it can reasonably predict the evolution of both the synchronization parameter R (and therefore, phase shift) and the frequency of both particles. However, we also need to say that this second model cannot fit the results when $\Delta\phi_i \approx \pi$ rad; the first model is able to fit the R plots of the system starting in phase opposition, but the frequency cannot be fitted appropriately by either model (cf. Figure 4.10).

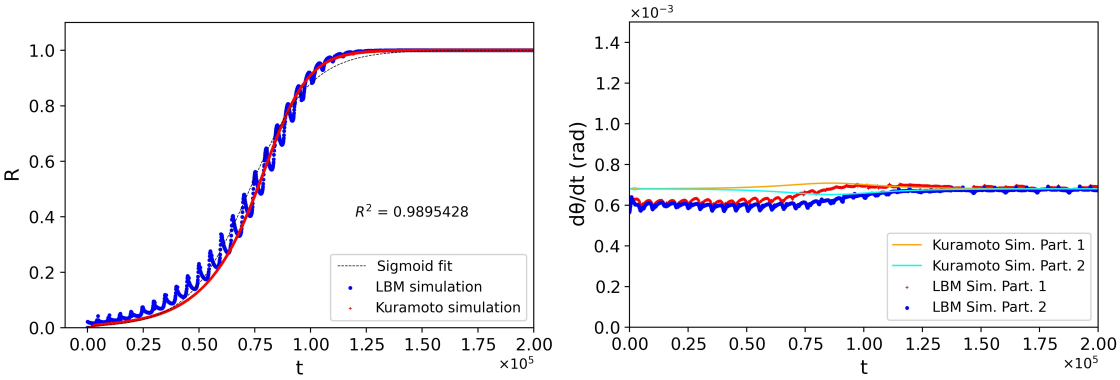

Figure 4.10: The fitting of the first modified KM (eq. 4.5) to a system with $L_X = 128$, and $\Delta\phi_i = \pi$ rad, studied in the phase dependency subsection of section 3.1. The coefficient of determination presented is calculated from the initial instant to the moment when it's reached the synchronization threshold ($R \geq 0.99$). On the left, we have the evolution of synchronization parameter R of the two simulations; and on the right fitting of the frequency of the modified model (orange and cyan lines) to the moving average of the velocity of the LBM model (red crosses and blue dots). The period used for the moving average was of 90 data points, i.e., 900 simulation time steps. The values of the modified KM were: $K_{eff} = 2.80 \times 10^{-5}$, $A = 215$ and $t_c = 840$. The synchronization parameter R is relatively well fitted, but the Kuramoto simulation does not predict the lower initial average frequency of the fluid simulation. The data point with $A_{x2} = 6 \times 10^{-6}$ is not included as it is not possible to determine its coupling factor.

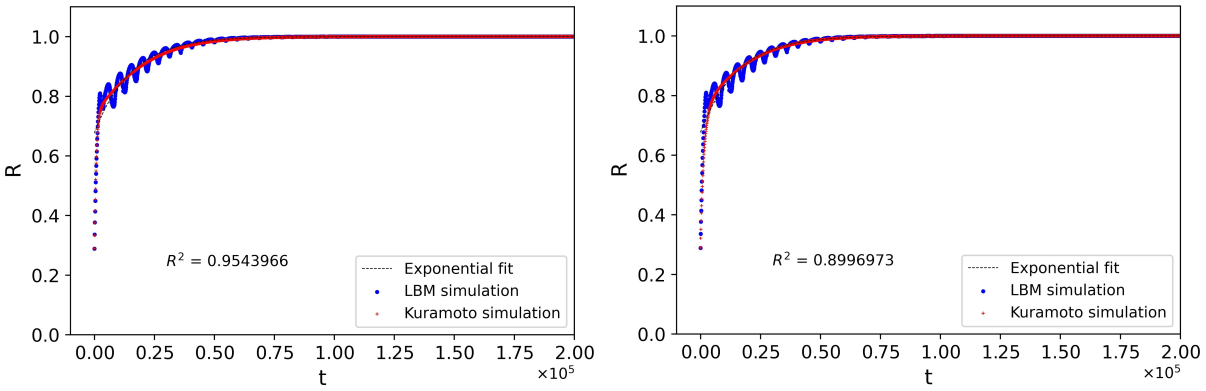

Figure 4.11: The fitting of frequency of the first modified Kuramoto model (left plot, eq. 4.5) and the second modified model (right plot, eqs. 4.6) to the moving average of the frequency of system with $L_X = 180$ ($d = 90$), and $\Delta\phi_i = 2.56$ rad, studied in the distance dependency subsection of section 3.1. The coefficient of determination presented is calculated from the initial instant to the moment when it is reached the synchronization threshold ($R \geq 0.99$). The parameters of the modified model are: for the first model, $K_{eff} = 1.62 \times 10^{-5}$, $A = 50$ and $t_c = 800$; for the second model, $K_{eff} = 1.67 \times 10^{-5}$ and $t_c = 1650$. We see that the first modification fits better prediction of the Kuramoto model, but the second modification is not much worse.

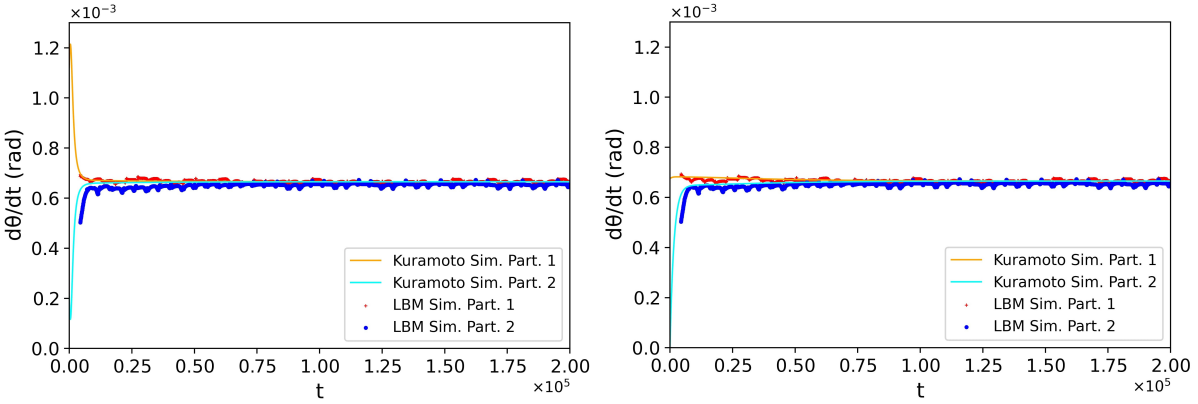

Figure 4.12: The fitting of frequency of the first modified Kuramoto model (eq. 4.5) and the second modified model (eqs. 4.6) to the moving average of the frequency of system with $L_X = 180$, and $\Delta\phi_i = 2.56$ rad, studied in the distance dependency subsection of section 3.1. The period used for the moving average was of 90 data points, i.e., 900 simulation time steps. On the left plot, the convergence of the frequency of the Kuramoto simulation is very drastic and occurs at around $t = 2500$, considerably sooner than that of the moving average value of the LBM simulation, that occurs at around $t = 6000$; the initial values for the particle 1 are noticeably different. On the right plot, the frequency of the Kuramoto simulation follows reasonably well the moving average of the frequency of the LBM simulation.

Because we define the natural frequency ω as the frequency of an oscillator isolated in a system with a large length L_X, and because the final frequency of the synchronized oscillators, in the LBM simulations, is (almost) always larger than the natural frequency, the LBM and Kuramoto simulations converge to different final frequencies. The two simulations converge to the same final frequency on the plots of Figure 4.12 because we considered as the natural frequency for the Kuramoto simulation the final frequency obtained from the LBM simulation. As it has been shown in section 4, this choice does not influence in any significant way the results, as both frequencies are close enough to each other (cf. Figure 4.1). The parameters of the fit (the effective coupling factor, the characteristic time constant t_c and the synchronization time) do not differ for each of the natural frequencies; the only difference is that the overall frequency would be smaller in the simulation of the KM than on the LBM simulation. The same

cannot be done for the system with particles with different natural frequencies, as when they synchronize they obtain the same final frequency –, and a difference in natural frequency between particles is essential for a non-zero final phase shift.

Effective coupling factor K

The transition from the first and faster regime of synchronization to the second and slower regime of synchronization occurs when both particles reach their final natural frequency – for most cases, this happens when the slower of particles crosses the turnabout amplitude [5]. We call the instant the transition occurs t_{min}. If we know what is t_{min}, then we can also recover the phase shift at this point $\Delta\phi(t_{min})$; and having the synchronization time, t_s, we can then determine the effective coupling factor simply by the formula derived previously for the synchronization time (eq. 4.2). In this case, we simply have:

$$K_{eff} = \frac{a}{t_s - t_{min}}. \tag{4.7}$$

We remember that a is defined by both initial phase shift (which is now effectively $\Delta\phi(t_{min})$) and the natural frequency.

So this is what we used to determine the K_{eff} for the data presented at 3.1, for the cases when $\Delta\phi_i = \{1.23, 2.09, 2.56\}$ rad. We then fitted our results using the second modified model (eqs. 4.6). The only instance in which we used the first modified model of equation 4.5 was to determine the K_{eff} for the system with $\Delta\phi_i = \pi$ rad from the phase dependency data set presented in the phase dependency subsection of section 3. The K_{eff} for the linear velocity dependency is not presented because, as the synchronization is constant, so is the coupling factor and the t_c variable of the modified KM.

Not much changes when we look at plot of K_{eff} as a function the initial phase dependency in Figure 4.13, when compared with the plot obtained during our first approach (cf. Figure 4.3). In fact, for $\Delta\phi_i < 1.23$ rad, the values of the coupling factor obtained by the original KM is identical to that obtain by using one of the modified KMs; and for $\Delta\phi_i \geq 1.23$ rad, K_{eff} is mostly only slightly smaller than the "naive" K, with most significant difference at $\Delta\phi_i = 1.23$ rad.

What see now is a clearer relation between the quantities of interest and the coupling factor K_{eff}. The most obvious relation is observed for viscosity (with constant natural frequency) on the top right plot of Figure 4.14: there is an obvious linear proportionality. This is also the case for the viscosity (without maintaining the frequency constant) on the top left plot of Figure 4.14: for the cases that $\Delta\phi_i = 2.09$ rad and $\Delta\phi_i = 2.56$ rad; as for the system with $\Delta\phi_i = 1.23$ rad, the variation of the synchronization with viscosity is the most irregular one of all the cases presented.

There is also a more linear dependency with regards to frequency, or body acceleration (bottom right plot of Figure 4.14): the maximum of synchronization time around $\omega = 6.9 \times 10^{-4}$ rad (cf. Figure 3.12) has all but disappeared: for $\Delta\phi_i = 2.09$ rad, we can see the corresponding minimum, but this is not as accentuated.

The results for the dependency on the distance between centers of oscillation is plotted on bottom left plot of Figure 4.14. In this case, there seems to be an inverse-square law at play.

[5] The exact instant which corresponds to t_{min} and the transition between the two regimes is further elaborated in the next subsection 4.2.1.

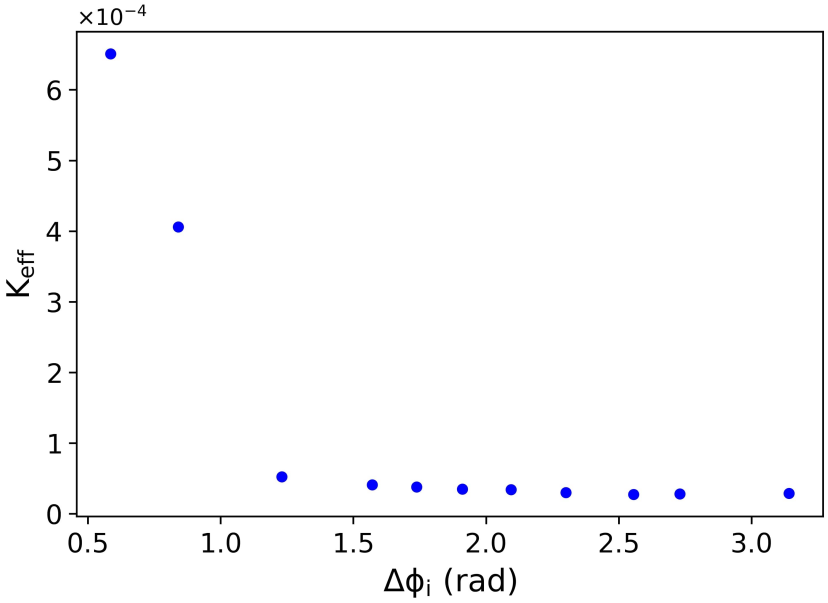

Figure 4.13: Values of K_{eff} obtained as a function of the initial phase shift. The results were obtained through the expression 4.7 for the phase shift dependency subsection of section 3.1.

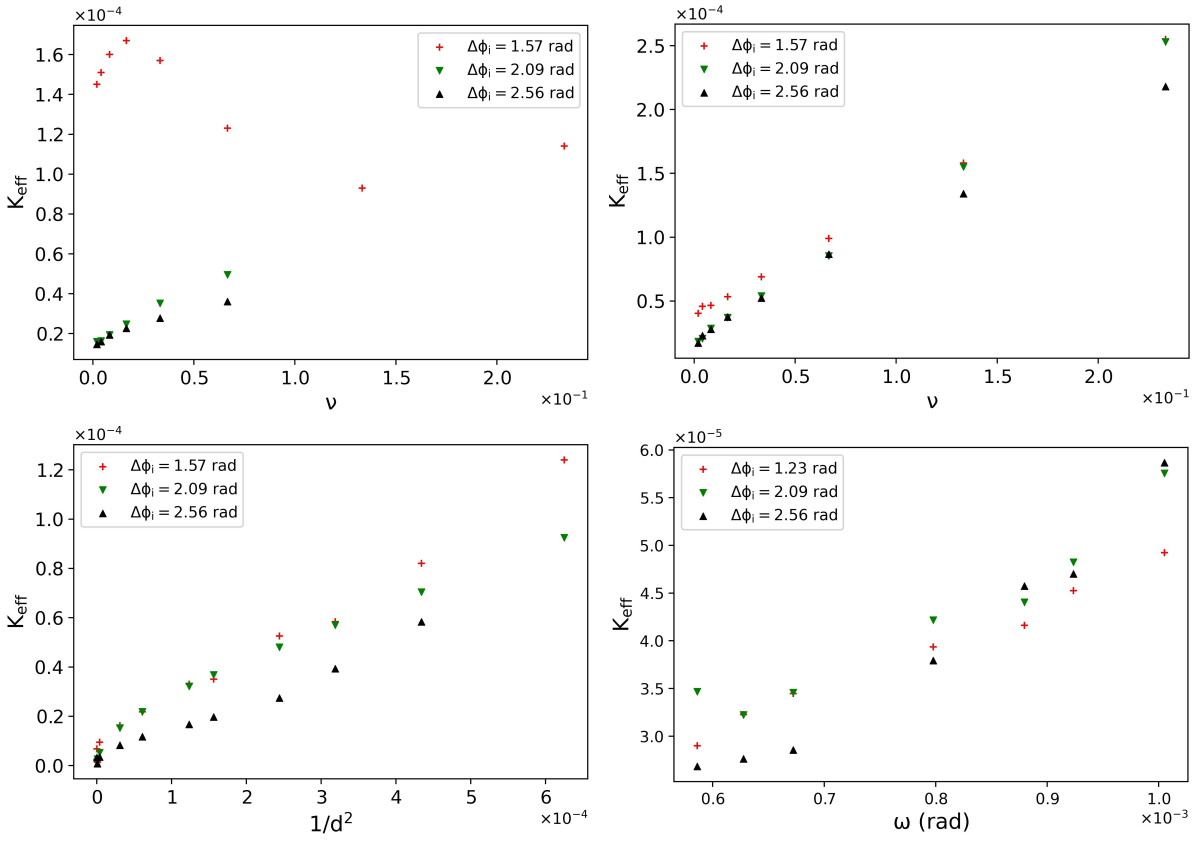

Figure 4.14: The plot of the values of K_{eff} as a function of 4 quantities of interest, for the different initial phase shifts. On the top left plot, the values of K_{eff} as a function of the fluid viscosity, with constant natural frequency. On the top right plot, the values of K_{eff} as a function of the fluid viscosity. On the bottom left plot, the values of K_{eff} as a function of the inverse square of of the distance between centers of oscillation. On the bottom right plot, the values of K_{eff} as a function of the frequency. The results were obtained through the expression 4.7 for the viscosity dependency with constant frequency subsection of section 3.1. The data points for the viscosity (with constant frequency), the inverse square of the distance and the frequency are displayed approximately in lines, which indicates a linear proportionality between K_{eff} and the variables.

From what is said above, for a given initial phase shift, we should expect to symbolically represent these relations as:

$$K_{eff} \propto \frac{\omega\nu}{d^2}. \tag{4.8}$$

We present the results of the effective coupling factor as a function of this quantity, for the distance, body acceleration and viscosity (with and without maintaining constant frequency) dependency data sets. This is what we see in Figure 4.15, in which plot the K_{eff} of the previously mentioned data sets for $\Delta\phi_i = 2.56$ rad. The results present an overall linear tendency, but there is still a observable difference between each of the fits. This seems to indicate two things: 1) that our proportionality assumption in 4.8 is reasonable, but 2) there are more variables that determine the coupling factor (that we did not consider), which vary as these three quantities of interest vary (natural frequency, fluid viscosity and distance between centers of oscillation).

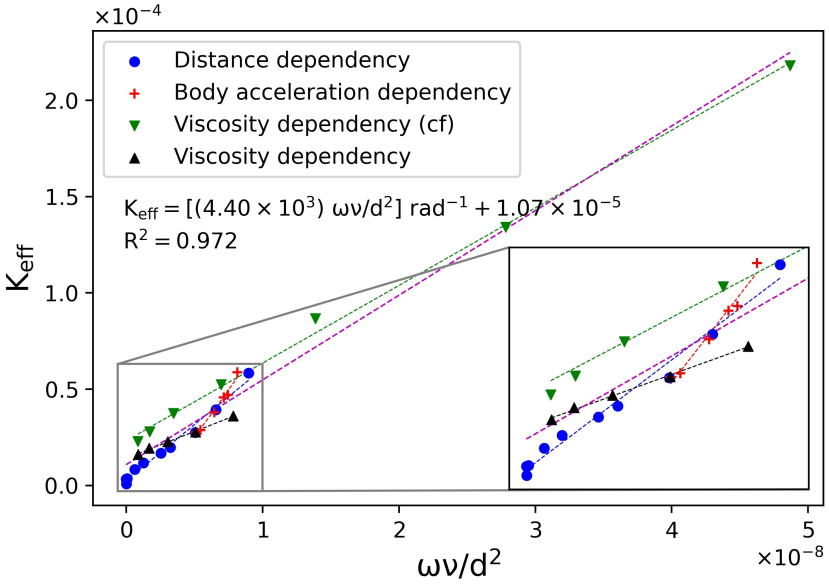

Figure 4.15: Values of K_{eff} obtained as a function of $\omega\nu/d^2$, for $\Delta\phi_i = 2.56$ rad. Each data set corresponds the sets of simulations: distance, body acceleration, viscosity with constant frequency (cf) and viscosity dependency. We zoom in on the plot for the smaller values of the effective coupling ($K_{eff} \leq 0.6 \times 10^{-4}$), where the majority of the data points are located. We also present the linear tendency of all the data sets as dashed lines of the same color as the respective marks. We see that there is an overall linear tendency across all data sets, fitted by the purple dashed line –, and its expression and coefficient of determination are those presented.

We should note that the relation presented in eq. 4.8 is obtained from fitting. And as K_{eff} is a dimensionless quantity, so should the the right-hand side of that equation. We did study the possibility of K_{eff} being related to dimensionless quantities used in fluid dynamics, like the Reynolds number and the Strouhal number; however, this was not possible. This has the consequence of not making the K_{eff} a dimensionless quantity. How definition is then clearly incomplete.

This, despite the physical arguments that can be made to justify each quantity of interest in eq. 4.8: the greater the natural frequency, the faster and stronger is the interaction between oscillators; the greater the viscosity, the stronger is the influence of the fluid (and thus the influence of an oscillator on another); and like other inverse-square laws, the greater the distance, the weaker the interaction between oscillators and the longer the disturbance from one oscillator takes to influence the other.

4.2.1 Observations on the modified models

Something only touched briefly in the discussion so far was the question of the division between the first and the second synchronization regimes. We characterized them, and we called the instant when we go from the first to the second t_{min} – but we just observed where that point was and fitted the results of the simulations according to the modified model. We also briefly showed that t_{min} is dependent on the position (cf. Figure 4.9). But what is the dependency of the system's variables and this transition point?

What we observe is that this transition point has a clear correlation with distance, viscosity and frequency, and – as was already alluded when we first discussed t_{min} – this correlation is accentuated by the initial phase shift. From the fittings of the second modified model (eqs. 4.6), we see that t_{min} is proportional to the distance between the centers of oscillation (cf. left plot of the first row of Figure 4.16), inversely proportional to frequency (cf. right plot of the first row of Figure 4.16), and inversely proportional to the fluid viscosity (while maintaining constant frequency) (cf. left plot of the second row of Figure 4.16).

Interestingly enough, t_{min} is proportional to the viscosity, when the frequency is not maintained constant (cf. right plot of the second row of Figure 4.16) –, this makes sense, as the increase in viscosity reduces the frequency of both particles. However, it makes it unclear what is the general tendency of the transition point and the fluid viscosity (while maintaining and not a constant frequency). What seems apparent is that the influence of the frequency on t_{min} is more significant than that of the viscosity (at least in the range of values that we simulated).

When we look at the last row plot of Figure 4.16, we see a more complex relation between t_{min} and the initial phase shift: if $\Delta\phi_i < \pi/2$ rad, then the t_{min} is very close to null, and is smaller the closer we are to $\Delta\phi_i = 0$ rad; if $\Delta\phi_i > \pi/2$ rad, then t_{min} decreases the closer we get to $\Delta\phi_i = \pi$ rad. We should recall that body acceleration is an important factor in the initial net force on the particles: if $\Delta\phi_i < \pi/2$ rad, then both the spring-like force that fixes the particles' motion around their center of oscillation and the body acceleration have the same direction; if $\Delta\phi_i > \pi/2$ rad, these two forces have opposite directions – the closer $\Delta\phi_i$ is to π rad the bigger the difference between these forces, but also the closer the particles are to changing their body acceleration direction. For $\Delta\phi_i > \pi/2$ rad, the proximity to the turnabout amplitude is more important than the diminishing magnitude of the initial net force.

We also plotted the characteristic time constant t_c (the characteristic time value we fitted using the second modified model of eqs. 4.6) as a function of t_{min} for all the quantities of interest (cf. Figure 4.17). The plot with the most regular tendency is that of the frequency dependency, plotted on the left side of the first row of Figure 4.17: here, the characteristic time constant t_c seems linearly proportional to the transition instant t_{min}.

When we look at the results for the fitting of the distance dependency, plotted on the right side of the first row of Figure 4.17, and of the viscosity dependency, with constant frequency, plotted on the last row of Figure 4.17, the tendency is not so clear: we still see that t_c increases with quantities of interest, but the relation is somewhere between linear and logarithmic. In truth, the plot of the distance dependency has a general logarithmic tendency; while the one of the viscosity dependency, with constant frequency, seems to have a linear tendency, but with a have "cutoff points": for example, for $\Delta\phi_i = 2.56$ rad, t_c increases sharply at $t_{min} = 1500$, and then increases approximately linearly.

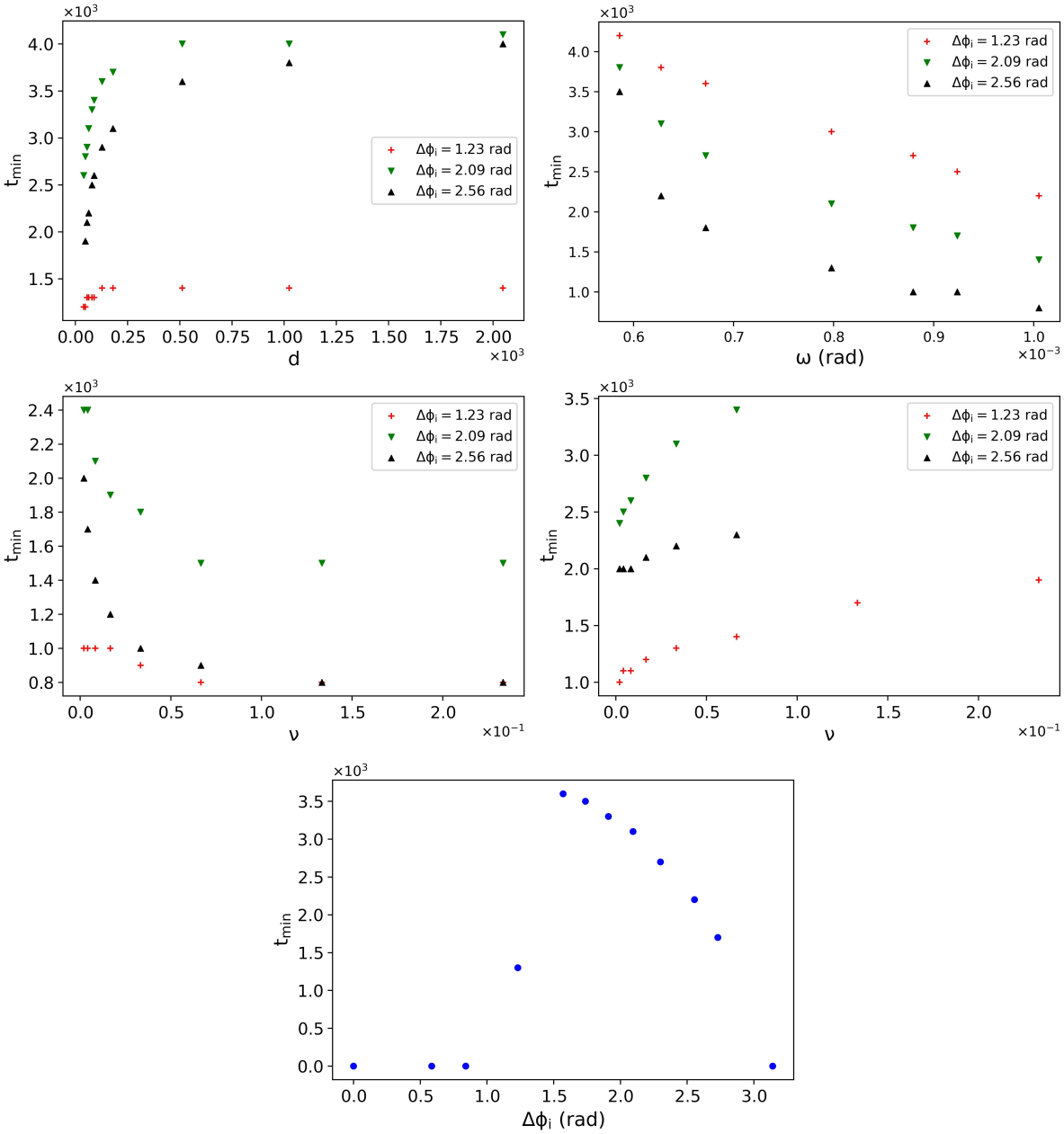

Figure 4.16: Plots of transition instant as a function of the quantities of interest for the different initial phase shifts: first row left, t_{min} as a function of the distance between centers of oscillation; first row right, t_{min} as a function of the frequency; second row left, t_{min} as a function of the fluid's viscosity, and maintaining a constant natural frequency; second row right, t_{min} as a function of the fluid's viscosity. And the last row, t_{min} as a function of the initial phase shift. The results were obtained through the expression 4.7 for the distance dependency subsection of section 3.1.

As for the initial phase shift and the viscosity, there does not seem to be any clear tendencies, as t_c might increases as much as it might decrease with t_{min}. For the phase dependency, the relation being the most irregular of all the cases presented.[6]

It is true that the behavior of t_{min} as a function of the system's variables is, to some extent, regular: like we said, it increases with distance and with the fluid viscosity; decreases with the fluid viscosity, if the frequency is maintained constant, and with the frequency. This gives us an idea of the physical arguments to situate the transition instant: the distance between the centers of oscillation reduces the

[6]These last three cases are not plotted.

interaction between the particles, and thus they do not increase each others' frequency and take longer to reach their final natural frequency; the viscosity presents more resistance to the particles, and thus they take longer to reach their final natural frequency; but if the frequency is maintained, then the fluid viscosity increases the interaction between the particles and they reach their final frequency quicker; and the larger the natural frequency, the sooner and the stronger is the interaction between the particles, and they converge to their final natural frequency sooner.

But on the other hand, the relation between the characteristic time constant t_c and the transition instant t_{min} is not so clear; thus we can say with a very high degree of certainty that t_c cannot be predicted directly from t_{min}. For each of the quantities of interest, the plot of t_c vs. t_{min} has a different aspect. This makes it more difficult to establish a physical meaning to the characteristic time constant.

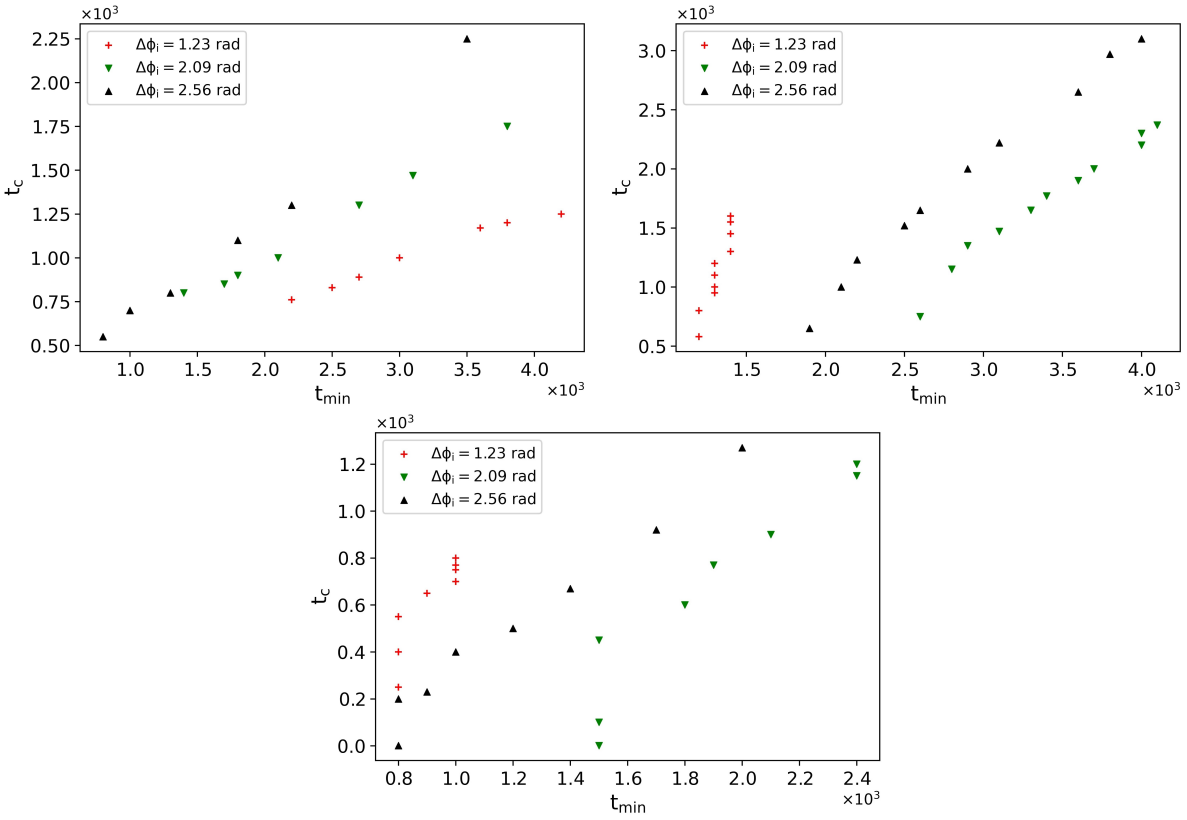

Figure 4.17: Plots of characteristic time constant t_c as a function of the transition instant t_{min}, for the different initial phase shifts, and for the 3 variables of interest data sets that show somewhat regular tendencies: first row left, for the study of the frequency; first row right, for the study of the distance between centers of oscillation; last row, for the study of the fluid's viscosity, and maintaining a constant natural frequency. For all of the cases above, t_c is proportional to t_{min}, but each with different degrees of linearity.

4.3 Fitting the system with particles with different natural frequencies

We also tried to fit the KM to the second set of simulations, those in which the natural frequency of each particle was different. As both particles start their motion at $P(0) = A$ in all of the setups, there should not be two synchronization regimes, but just one – the effective regime. This means that the original KM, with constant natural frequencies ω_j and constant coupling factor K, is the most appropriate to describe the synchronization. And, in principle, the fitting of the data should be easier than the one we did in the previous section: we know that the final phase shift is non-zero –, therefore we would only need to simulate the KM with null initial phase shift, $\Delta\phi_i = 0$ rad, with each particle with its

natural frequency, ω_1 and ω_2, and the coupling factor K would be the one that guaranteed that the system synchronized with our known final phase shift. The values of the coupling factor for the three quantities studied (distance between centers of oscillation, viscosity and body acceleration difference) are presented on Figures 4.18-4.20.

The data presented for the distance and body acceleration difference dependencies are plotted in a log-log scale; this suggests that there is a power law in the data. We present these on the right plots in Figures 4.18 and 4.19, where we also can see the power law expression and the corresponding coefficient of determination R^2; the left plots of these Figure have the data in linear scale.

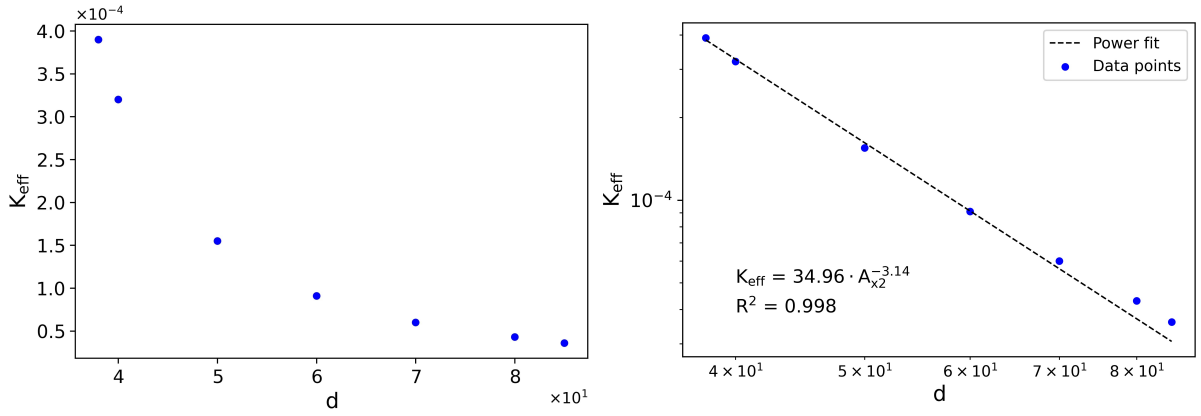

Figure 4.18: Values of K_{eff} as a function to the distance between centers of oscillation, in linear scale (left plot) and in log-log scale (right plot). These results were obtained by fitting the simulation of pair of equations 4.1, for the distance dependency subsection of section 3.2. The criterion of the fit was the final phase shift $\Delta\phi_f$, represented on the right plot of Figure 3.17. In the right plot we have a power law fit and the corresponding coefficient of determination.

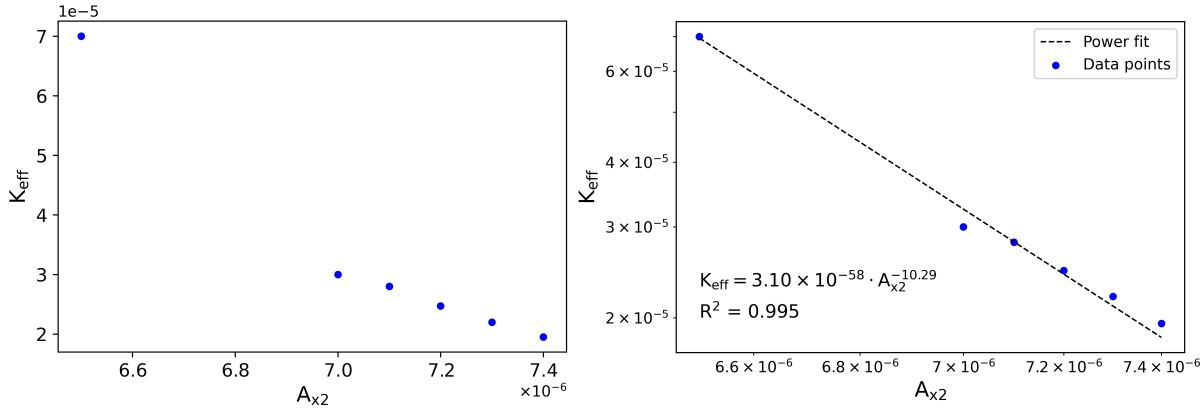

Figure 4.19: Values of K_{eff} as a function of the body acceleration of one of the particles, in linear scale (left plot) and in log-log scale (right plot). The other particle has a constant body acceleration of $A_{x1} = 6 \times 10^{-6}$. These results were obtained by fitting the simulation of pair of equations 4.1, for the body difference dependency subsection of section 3.2. The criterion of the fit was the final phase shift $\Delta\phi_f$, represented on the right plot of Figure 3.19. In the right plot we have a power law fit and the corresponding coefficient of determination.

A problem arises from this process: the original KM does not predict that a system with particles starting with the same natural frequency, and with a null initial phase shift, find their stable state with a final phase shift different from zero – it should be in the synchronized state from the start. In our simulations to study the viscosity effect, despite each particle having a different turnabout amplitude A, we find two cases in which the natural frequency is the same (or very similar) for both particles and the

final phase shift is non-zero: these are for $\nu = 0.00417$ and $\nu = 0.00833$. The frequencies might not be the same, but are certainly so close in value that it is impossible to determine the coupling factor. For this reason, the K_{eff} values for the aforementioned viscosity values are not presented in Figure 4.20. From the remaining values, the general aspect of the plot suggests that the value of K_{eff} for these two data points ($\nu = 0.00417$ and $\nu = 0.00833$) is in the range $[2.35, 2.80] \times 10^{-5}$.

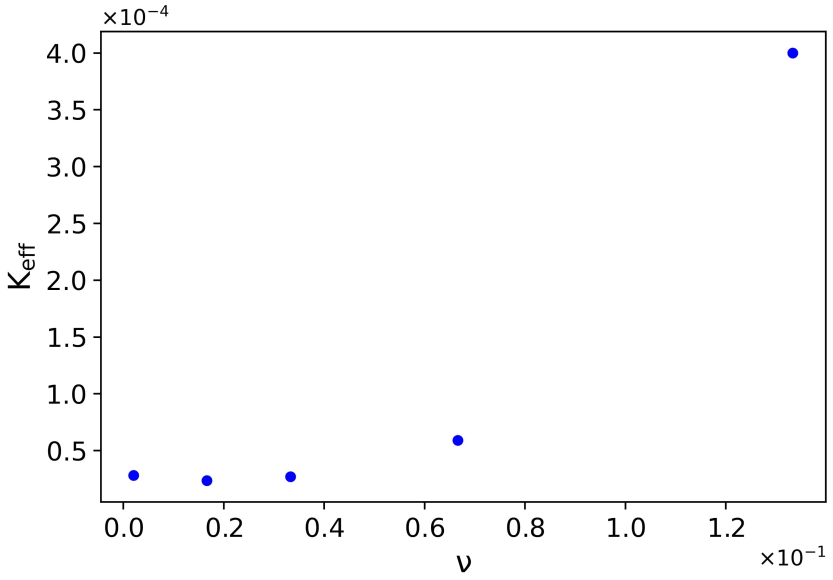

Figure 4.20: Values of K_{eff} as a function to the viscosity of the fluid. It was not possible to determine the value of K_{eff} for 2 data points, as these had (as far we could determine) the same natural frequency but non-zero final phase shift – if is not predicted by the Kuramoto model. These results were obtained by fitting the simulation of pair of equations 4.1, for the viscosity dependency subsection of section 3.2.

The process of fitting these results using the final phase shift sounds like a reasonable assessment. And for most cases, like that of the viscosity dependency and the frequency dependency, it can actually give us some reasonable results. However, we are considering that the transition from the initially null phase shift to the final phase shift of the systems simulated with LBM will coincide exactly with the prediction made by the KM – and this is not necessarily the case. This last case is mostly evident when the distance between centers of oscillation is bigger (cf. Figure 4.21) – here, the synchronization time predicted by the KM is smaller than that of the simulations (becoming more evident as the distance increases), for the same predicted final phase shift. Furthermore (and as was already mentioned in the beginning of section 3.2), unlike when the natural frequencies are the same, the final R value is not constant – which means that the final state of the system has a variable phase shift, albeit regular and periodic.

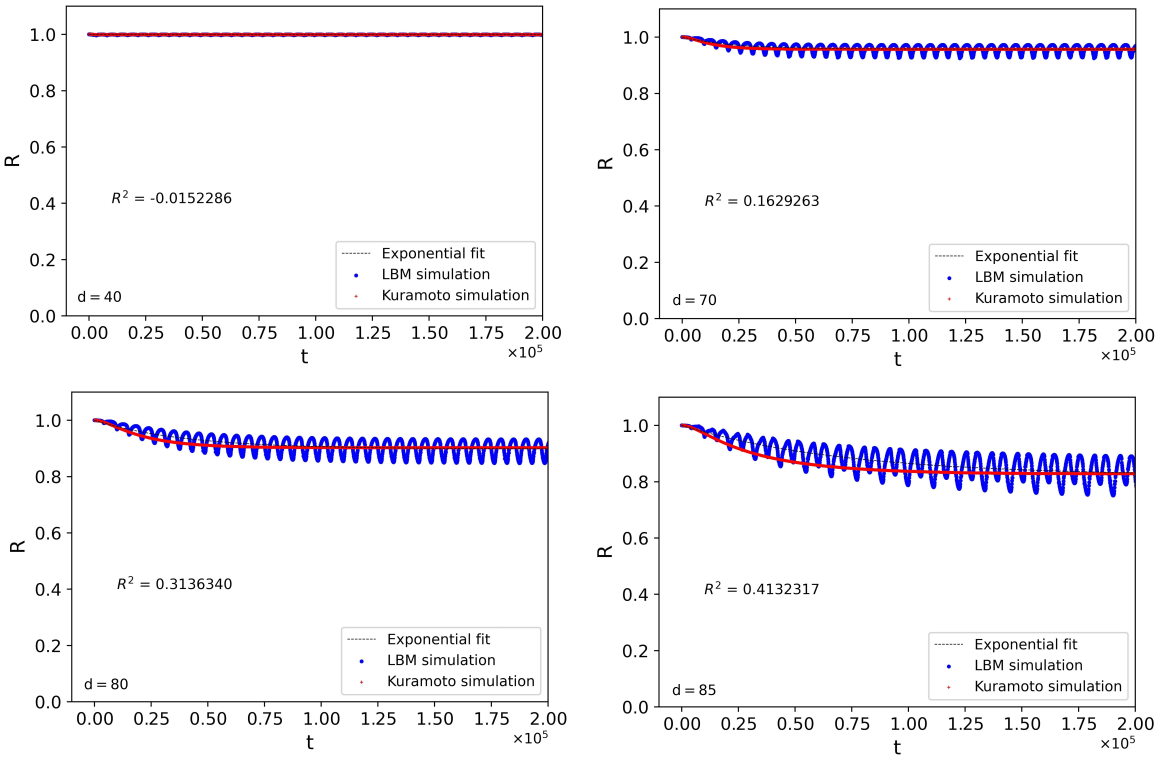

Figure 4.21: Evolution of the synchronization parameter R for the systems with particles with different natural frequency, and the Kuramoto simulations fitted by the final phase shift $\Delta\phi_f$. These four plot present 4 different distances between centers of oscillation: $d = 40$ (top left); $d = 70$ (top right); $d = 80$ (bottom left); $d = 85$ (bottom right). As the distance increases, the synchronization time predicted by the Kuramoto simulation is smaller than that of the LBM simulation.

Bifurcation diagrams

A common result presented when studying the Kuramoto model is that of the bifurcation diagram, which plots the order parameter R (in our case, the synchronization parameter) against the coupling factor K. We represent the bifurcation diagrams for the three dependencies studied for the particles with different natural frequencies (Figure 4.22). As the values of the coupling factor for the distance and the body acceleration difference dependency can be fitted using a power law (cf. Figures 4.18-4.19), we also predicted what would be the coupling factor for the values of these variables for the simulated systems that did not synchronize, as we always have an R value[7]. These are indicated in the plots as x's. Even if we ignore the data points with coupling factors determined by fitting, we can clearly see that the transition to complete coherence is a smooth one.

Each case has a different diagram, and its not quite possible to determine the critical coupling factor K_c. In the large ensemble scenario, K_c corresponds to the solution of the KM where bifurcations of groups of synchronized oscillators is so big that no oscillator is synchronized with any other, i.e., the coherence of the system is null, $R = 0$. In the case of two oscillators, as we discussed in subsection 2.2.1, the mean value of the synchronization parameter when two oscillators with different natural frequencies

[7]These being unstable cases, there is no synchronization of the particles, and the synchronization parameter R varies considerably (and periodically) in its full range of values. We remember that the R value presented is in fact the mean value, $\langle R \rangle$, over a long period of time, i.e., $t \to \infty$

oscillate independent of each other is $\langle R \rangle \approx 0.637$ – and indeed, this is the value to which the R value tends to for small coupling factor values. What we can say is the smallest value K for which the system synchronizes: $K = 3.60 \times 10^{-5}$, for the distance; $K = 2.35 \times 10^{-5}$, for the viscosity; $K = 1.95 \times 10^{-5}$, for the body acceleration difference.

What the different diagrams seem to indicate is that none of these variables alone (distance between centers of oscillation, fluid viscosity or body acceleration difference) is enough to determine the critical coupling factor K_c, as we would expect to have obtained similar synchronization parameter R values for the same values of K.

Another aspect that is worth mentioning is how regular the R-K diagram for the viscosity dependency becomes, despite the irregularity of the plot of the K as a function of the viscosity (cf. Figure 4.20).

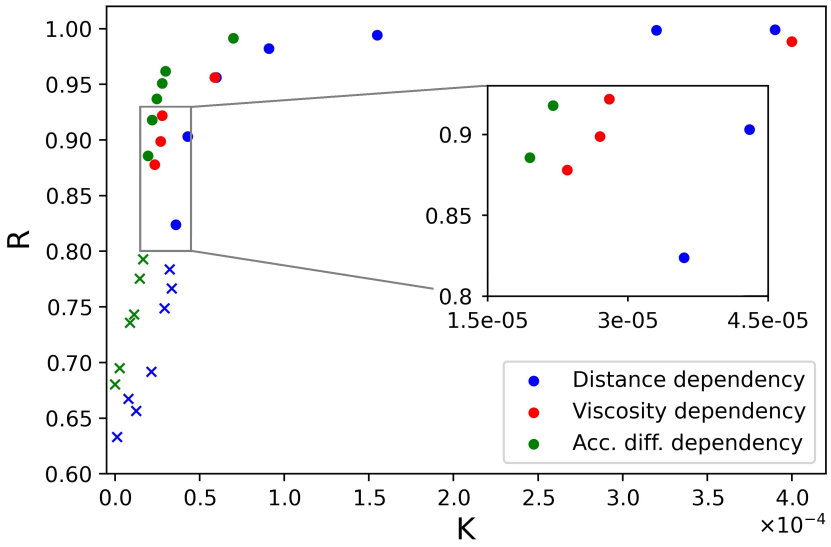

Figure 4.22: Bifurcation diagrams for the distance, viscosity and body acceleration difference dependencies. The x's represent the cases in which there was no synchronization, while the dots those that synchronized. The coupling factor of former where obtained predicting their values from the fitting of the synchronized states (dots) presented on the right plots of Figures 4.18 and 4.20. The synchronization parameter R only goes down to 0.637, when the order parameter usually starts from 0 (cf. subsection 2.2.1). Each data set has a different diagram, with different values of coupling factor below which there is no longer synchronization; if we look at the inset, we see that these are: $K = 3.60 \times 10^{-5}$, for the distance; $K = 2.35 \times 10^{-5}$, for the viscosity; $K = 1.95 \times 10^{-5}$, for the body acceleration difference.

Chapter 5

Conclusions

We developed our study on a 2D system based on the Lattice-Boltzmann method, consisting of two oscillators immersed in a fluid enclosed between two parallel walls with no-slip condition (at the top and at the bottom) and with periodic boundary conditions to the left and right; each particle was fixed to their center of oscillation through a spring-like force, and their one dimensional motion was propelled by a external force, which changed direction every time the particles' center went beyond a certain distance from their center of oscillation. The interaction between the oscillators was established through the fluid's drag force. This setup allowed us to see how important were the model parameters, namely: the distance between the centers of oscillation of the particles, body acceleration and linear velocity of these particles, the fluid viscosity and the initial phase shift. We saw that the particles with the same natural frequency, when able to synchronize, did so in a in-phase stable state, while the particles with different natural frequencies synchronize to a stable state with a non-zero final phase shift.

When the natural frequency was the same for both particles, we saw that the synchronization time: 1) increased with the initial phase shift; 2) increased logarithmically with distance between the centers of oscillations of the particles; 3) decreased with the fluid viscosity, in a power law relation; 4) if the natural frequency was maintained constant, it decreased with viscosity; 5) did not depend on the linear velocity of the particles; and 6) initially increased but then decreased with the body acceleration.

For when the particles had different natural frequencies, we saw that both the synchronization time and final phase shift had the same behavior: 1) they increased with the distance between centers of oscillation; 2) increased with the difference between the body acceleration of the oscillators; 3) initially increased but then decreased with viscosity.

Our first approach of defining our system by assigning the coupling factor look at the synchronization time of the simulations with particles with the same frequency proved to be simplistic. Besides, it did not help much in parameterizing the Kuramoto model, as the relations found between the coupling factor and the variables of the system did not correspond to regular functions. Our second approach, in which we modified the Kuramoto model and focused in the second regime of synchronization observed in our system, was a more successful endeavor, providing us with better and more realistic predictions. Finally, the systems with particles with different natural frequencies turned out to be liable of being defined by the original Kuramoto model.

But we could see that the variables of the system in study are, for one, not independent from each other and, for another, their codependency is non-linear and seems somewhat complex. It is clear that the Kuramoto model, in its simplest form, does not predict the full complexity of our system. Nonetheless, with some minor modifications, it seems to be able to make reasonable predictions. However, the dependency of the quantities of interest on the coupling factor K and the natural frequency ω is not

clear cut. We can say with a certain degree of confidence that, when the particles have the same natural frequency, the coupling factor is directly proportional to the fluid viscosity and to their natural frequency, while being inversely proportional to the square of the distance between the centers of oscillation. And when the particles have different natural frequencies, we can say that both distance between the centers of oscillation and the difference between the body acceleration of the particles decreases the coupling factor, and it is suggested that this relation follows a power law.

The modified models worked quite well for initial phase shifts in the range $\Delta\phi_i \in [\pi/2, \pi[$ rad. But what about when we have $\Delta\phi_i \in]0, \pi/2[$ rad? We present K_{eff} values for $\Delta\phi_i = 1.23$ rad in section 4.2, but these should be viewed with scepticism. As we said in that section, t_{min} tends to be null for $\Delta\phi_i \to 0$ rad and tends to be equal to the instant of time when the particle crosses $P = 0$ for $\Delta\phi_i \to \pi/2$ rad. However, it might be possible to ignore the second case, and consider that $t_{min} \approx 0$ if $\Delta\phi_i \in]0, \pi/2[$ rad. In this case, the values of the coupling factor are essentially those predicted by the original Kuramoto model - and the values for $\Delta\phi_i = 1.23$ rad are one order of magnitude larger that those presented. This is not that small of a difference.

One of the most difficult setups to analyze in our model was that of particles starting in phase opposition. Despite the fact that we could obtain a value of effective coupling factor K_{eff} considering a latter point of the synchronization, neither of the two modified models used could completely describe the way the frequency of the particles evolved in time. For this reason, we chose not to include the value of K_{eff} in the results in the effective coupling factor K subsection of section 4.2, apart from the case of the phase dependency in the Figure 4.13. In this case, we used the model with time-varying coupling factor in 4.5.

Despite presenting two modifications to the Kuramoto model, there are still some behaviors that these do not predict: the first model can predict quite well the evolution of the order parameter R in time for a system initially in phase opposition; however, it does not predict well the change in frequency of such system. What would then be the modification to the Kuramoto model that would predict such changes? According to the Kuramoto model, two oscillators in phase opposition do not influence each others' frequency; but we clearly see that, in the initial state, the frequency of both oscillators is smaller than that when they reach the synchronized stable state. In other words, there has to be some factor that reduces the frequency when $\Delta\phi = \pi$ rad (or $R = 0$) - or effectively the natural frequency ω_i of the particles. This factor is only relevant for very small R. What is then this factor?

From the results obtained in the lattice Boltzmann method simulations, we observed the existence of tendencies and tried to fit the results to the Kuramoto model. Something that could also be done would be the development of a more rigorous physical argument for the synchronization phenomenon. This is to say, to coarse grain the interactions and derive the equivalent to the Kuramoto model. In this case, more than likely many of the unexpected behaviors observed in our study would be present in the final model. But all indicates that this is a very difficult task, beyond the scope of this thesis.

Something that was also not explored were the states for which a given system does not synchronize. We did see that there are values of distance, viscosity and body acceleration difference beyond which the system did not synchronize. But these systems would also have a theoretical coupling factor, which we could not predicted from the original Kuramoto model. We saw clearly that the oscillators still interact with each other (the unstable state referred at distance dependency subsection of section 3.2). Besides this, there is the question of how would the variation in oscillation amplitude would be accounted for. If it were possible to determine the coupling of the unstable cases of the fluid simulation, then it would be possible to present a complete bifurcation diagram.

By simulating a interaction of a small number of oscillators (two) in a physical medium, we would expect to see some time delay in the interaction of the oscillators, which would then be present in the

way of a non-zero final phase shift in the synchronized state. However, this was not the case, being the Kuramoto model with no time delay the one that fitted best the systems simulated. As we had periodic boundary conditions on the direction of the motion, this system could be seen as having infinite particles, with half of all particles always phase-locked in one phase and the other half phase-locked in another phase –, and such a system would not have a time delay in the synchronized state.

There is also the question of the natural frequency itself. What should be the value of this quantity? Should it be the value of the frequency for a given oscillator when not influenced by any other oscillator? If so, then these lattice Boltzmann method simulations do not coincide with the prediction of the Kuramoto model, in which the final frequency of particles is the mean of their natural frequencies. In fact, the final frequency is almost always larger that the one obtain by the unobstructed motion of a single particle (the supposed natural frequency). This can be seen in the frequency plots in appendix A. This happened even in the case when both particles had the same turnabout amplitude and body acceleration (which corresponds necessarily to the same frequency).

It would also be interesting to see some different configurations, namely regarding the number of oscillators: we know that our setup of 2 oscillators synchronizes, but (as said before) its behavior is not exactly predicted by the Kuramoto model – would ensembles of more and more oscillators tend to behave as predicted by this model? What would be a threshold at which N oscillators could be considered $N \to \infty$? We could also had particles moving parallel to each other (in columns), just like those we observe in biological system (as oppose to the single row of two oscillators of the system that we simulated), and see if these columns aid the synchronization. This last scenario would make our setup fully two dimensional.

Bibliographic References

[1] C. Huygens. *Oeuvres complètes de Christiaan Huygens*, volume 17. La Haye, M. Nijhoff, 1932. (Works from 1651-1666).

[2] M. Bennett, M. Schatz, H. Rockwood, and K. Wiesenfeld. Huygens's clocks. *Proceedings of The Royal Society A: Mathematical, Physical and Engineering Sciences*, 458:563–579, Mar 2002.

[3] A. R. Willms, P. M. Kitanov, and W. F. Langford. Huygens' clocks revisited. *Royal Society Open Science*, 4, Set 2017.

[4] J. Pantaleone. Synchronization of metronomes. *American Journal of Physics*, 70:992–1000, Set 2002.

[5] S. L. Tamm and G. A. Horridge. The relation between the orientation of the central fibrils and the direction of beat in cilia of opalina. *Proceedings of the Royal Society B: Biological Sciences*, 175: 219–233, Aug 1970.

[6] R. E. Mirollo and S. H. Strogatz. Synchronization of pulse-coupled biological oscillators. *SIAM Journal on Applied Mathematics*, 50(6):1645–1662, Dec 1990.

[7] S. Gueron, K. Levit-Gurevich, N. Liron , and J. Blum. Cilia internal mechanism and metachronal coordination as the result of hydrodynamical coupling. *Proceedings of the National Academy of Sciences of the United States of America*, 94:6001–6006, Jul 1997.

[8] L. Gheber and Z. Priel. Metachronal activity of cultured mucociliary epithelium under normal and stimulated conditions. *Cell Motility*, 28(4):333–345, 1994.

[9] N. Sarkar, A. Basu, and J. Toner. Hydrodynamic theory of flocking at a solid-liquid interface: Long-range order and giant number fluctuations. *Physical Review E*, 104:064611, Dec 2021.

[10] M. Polin, I. Tuval, K. Drescher, J. P. Gollub, and R. E. Goldstein. *Chlamydomonas* swims with two "gears" in a eukaryotic version of run-and-tumble locomotion. *Science*, 325(5939):487–490, Jul 2009.

[11] R. E. Goldstein, M. Polin, and I. Tuval. Noise and synchronization in pairs of beating eukaryotic flagella. *Physical Review Letters*, 103:168103, Oct 2009.

[12] D. R. Brumley, N. Bruot, J. Kotar, R. E. Goldstein, P. Cicuta, and M. Polin. Long-range interactions, wobbles, and phase defects in chains of model cilia. *Physical Review Fluids*, 1:081201, Dec 2016.

[13] D. R. Brumley, K. Y. Wan, M. Polin, and R. E. Goldstein. Flagellar synchronization through direct hydrodynamic interactions. *eLife*, 3, Jul 2014.

[14] M. Tătulea-Codrean and E. Lauga. Elastohydrodynamic synchronization of rotating bacterial flagella. *Physical Review Letters*, 128:208101, May 2022.

[15] Y. Kuramoto and T. Tsuzuki. Reductive perturbation approach to chemical instabilities. *Progress of Theoretical Physics*, 52(4):1399–1401, Oct 1974.

[16] A. T. Winfree. Biological rhythms and the behavior of populations of coupled oscillators. *Journal of Theoretical Biology*, 16(1):15–42, Jul 1967.

[17] K. Wiesenfeld, P. Colet, and S. H. Strogatz. Frequency locking in Josephson arrays: Connection with the Kuramoto model. *Physical Review E*, 57:1563–1569, Feb 1998.

[18] G. Kozyreff, A. G. Vladimirov, and P. Mandel. Global coupling with time delay in an array of semiconductor lasers. *Physical Review Letters*, 85:3809–3812, Oct 2000.

[19] G. Kozyreff, A. G. Vladimirov, and P. Mandel. Dynamics of a semiconductor laser array with delayed global coupling. *Physical Review E*, 64:016613, Jun 2001.

[20] T. Krüger, H. Kusumaatmaja, A. Kuzmin, O. Shardt, G. Silva, and E. Viggen. *The Lattice Boltzmann Method: Principles and Practice*. Graduate Texts in Physics. Springer International Publishing, 2017. ISBN 9783319446479.

[21] P. L. Bhatnagar, E. P. Gross, and M. Krook. A model for collision processes in gases. I. Small amplitude processes in charged and neutral one-component systems. *Physical Review*, 94:511–525, May 1954.

[22] S. Chapman and T. Cowling. *The Mathematical Theory of Non-uniform Gases: An Account of the Kinetic Theory of Viscosity, Thermal Conduction and Diffusion in Gases*. Cambridge Mathematical Library. Cambridge University Press, Feb 1991. ISBN 9780521408448.

[23] Z. Guo, C. Zheng, and B. Shi. Discrete lattice effects on the forcing term in the lattice Boltzmann method. *Physical Review E*, 65:046308, Apr 2002.

[24] X. Shan and H. Chen. Lattice Boltzmann model for simulating flows with multiple phases and components. *Physical Review E*, 47:1815–1819, Mar 1993.

[25] A. J. C. Ladd. Numerical simulations of particulate suspensions via a discretized Boltzmann equation. Part 1. Theoretical foundation. *Journal of Fluid Mechanics*, 271:285–309, Jul 1994.

[26] R. Jäger, M. Mendoza, and H. J. Herrmann. Clogging at pore scale and pressure-induced erosion. *Physical Review Fluids*, 3:074302, Jul 2018.

[27] R. Mei, D. Yu, W. Shyy, and L.-S. Luo. Force evaluation in the lattice Boltzmann method involving curved geometry. *Physical Review E*, 65:041203, Apr 2002.

[28] R. C. V. Coelho, D. P. F. Silva, A. M. R. Maschio, M. M. Telo da Gama, and N. A. M. Araújo. Collective transport of droplets through porous media. *Physics of Fluids*, Jan 2023.

[29] A. S. Nunes, R. C. V. Coelho, V. C. Braz, M. M. Telo da Gama, and N. A. M. Araújo. Dynamical demixing of a binary mixture under sedimentation. *Communications in Computational Physics*, 33 (1):1–21, Feb 2023.

[30] L. Verlet. Computer "experiments" on classical fluids. I. Thermodynamical properties of Lennard-Jones molecules. *Physical Review*, 159:98–103, Jul 1967.

[31] H. Daido. Quasientrainment and slow relaxation in a population of oscillators with random and frustrated interactions. *Physical Review Letters*, 68:1073–1076, Feb 1992.

[32] V. H. P. Louzada, N. A. M. Araújo, J. S. Andrade, and H. J. Herrmann. *The Cacophony of Interconnected Networks*, pages 141–148. Springer International Publishing, Cham, Feb 2016. ISBN 9783319239477.

[33] V. H. P. Louzada, N. A. M. Araújo, J. S. Andrade, and H. J. Herrmann. Breathing synchronization in interconnected networks. *Scientific reports*, 3:3289, Apr 2013.

[34] J. A. Acebrón, L. L. Bonilla, C. J. Pérez Vicente, F. Ritort, and R. Spigler. The Kuramoto model: A simple paradigm for synchronization phenomena. *Reviews of Modern Physics*, 77:137–185, Apr 2005.

[35] H. G. Schuster and P. Wagner. Mutual entrainment of two limit cycle oscillators with time delayed coupling. *Progress of Theoretical Physics*, 81(5):939–945, May 1989.

[36] A. Takamatsu, T. Fujii, and I. Endo. Time delay effect in a living coupled oscillator system with the plasmodium of physarum polycephalum. *Physical Review Letters*, 85:2026–2029, Aug 2000.

[37] A. Vilfan and F. Jülicher. Hydrodynamic flow patterns and synchronization of beating cilia. *Physical Review Letters*, 96:058102, Feb 2006.

[38] N. Uchida and R. Golestanian. Generic conditions for hydrodynamic synchronization. *Physical Review Letters*, 106:058104, Feb 2011.

[39] B. M. Friedrich and F. Jülicher. Flagellar synchronization independent of hydrodynamic interactions. *Physical Review Letters*, 109:138102, Sep 2012.

[40] G. S. Klindt, C. Ruloff, C. Wagner, and B. M. Friedrich. Load response of the flagellar beat. *Physical Review Letters*, 117:258101, Dec 2016.

[41] G. S. Klindt, C. Ruloff, C. Wagner, and B. M. Friedrich. In-phase and anti-phase flagellar synchronization by waveform compliance and basal coupling. *New Journal of Physics*, 19(11):113052, Nov 2017.

[42] J. A. Acebrón, J. Lavrentiev, Mikhail M., and R. Spigler. Spectral analysis and computation for the Kuramoto–Sakaguchi integroparabolic equation. *IMA Journal of Numerical Analysis*, 21(1): 239–263, Jan 2001.

[43] J. A. Acebrón, L. L. Bonilla, and R. Spigler. Synchronization in populations of globally coupled oscillators with inertial effects. *Physical Review E*, 62:3437–3454, Sep 2000.

[44] J. A. Acebrón and R. Spigler. Adaptive frequency model for phase-frequency synchronization in large populations of globally coupled nonlinear oscillators. *Physical Review Letters*, 81:2229–2232, Sep 1998.

[45] F. Sartoretto, R. Spigler, and C. Vicente. Numerical solution of the Kuramoto-Sakaguchi equation governing populations of coupled oscillators. *Mathematical Models and Methods in Applied Sciences*, 8, Nov 2011.

[46] S. Petkoski and A. Stefanovska. Kuramoto model with time-varying parameters. *Physical Review E*, 86:046212, Oct 2012.

[47] D. Cumin and C. Unsworth. Generalising the Kuramoto model for the study of neuronal synchronisation in the brain. *Physica D: Nonlinear Phenomena*, 226(2):181–196, Feb 2007.

[48] D. R. Khatiwada. Numerical solution of finite Kuramoto model with time-dependent coupling strength: Addressing synchronization events of nature. *Mathematics*, 10(19), Oct 2022.

[49] A. Franci, A. Chaillet, and W. Pasillas-Lépine. Phase-locking between kuramoto oscillators: Robustness to time-varying natural frequencies. *49th IEEE Conference on Decision and Control (CDC)*, pages 1587–1592, Dec 2010.

Appendix A

Supplementary results

In this appendix we present supporting information for the results in section 3. We include data about the final peak amplitude, the frequency and the absolute mean linear velocity (which we, for simplicity, call "linear velocity") of the simulated systems. We also present the natural values of these quantities. We also recall that we use lattice units for time steps, $\Delta t = 1$, and lattice units for space $\Delta x = 1$; as the argument of the trigonometric functions are in rad, the frequency is also expressed in rad (for we use $\Delta t = 1$, which is omitted).

Particles with the same frequency

Phase shift dependency

The initial phase shift does not influence in any significant (and constant) way the peak amplitude (top left plot of Figure A.1), nor the frequency (top right plot of Figure A.1), nor the linear velocity (bottom plot of Figure A.1) of the particles motion on the synchronous state. The variations are small in magnitude, thus not physically relevant. The mean values of the variables are: $A_p = 7.0$, $\omega_f = 6.85 \times 10^{-4}$ rad and $v = 3.07 \times 10^{-3}$. The initial phase shift does not affect the natural values.

We also note that the peak amplitude, the frequency and the linear velocity for a system with 2 particles are always larger than their natural values (i.e., when we have an isolated particles) –, this is constant throughout the simulations[1]. This seems to be due to the constructive interference of both oscillators when in synchronization (we remember that we only present results for the cases when we have in- or out-of-phase synchronization). When one particle moves in the same direction as the other, the former is simultaneously pushed by the fluid pushed ahead of the latter (which is behind), and is pulled too, as the fluid in wake of the latter also "follows" it. This facilitates the the motion of both particles, who can now move further and faster, increasing their amplitude and reducing their period.

[1] There an exception in the next section, when the particles have different natural frequencies. It can be seen the frequency plot of Figure A.9.

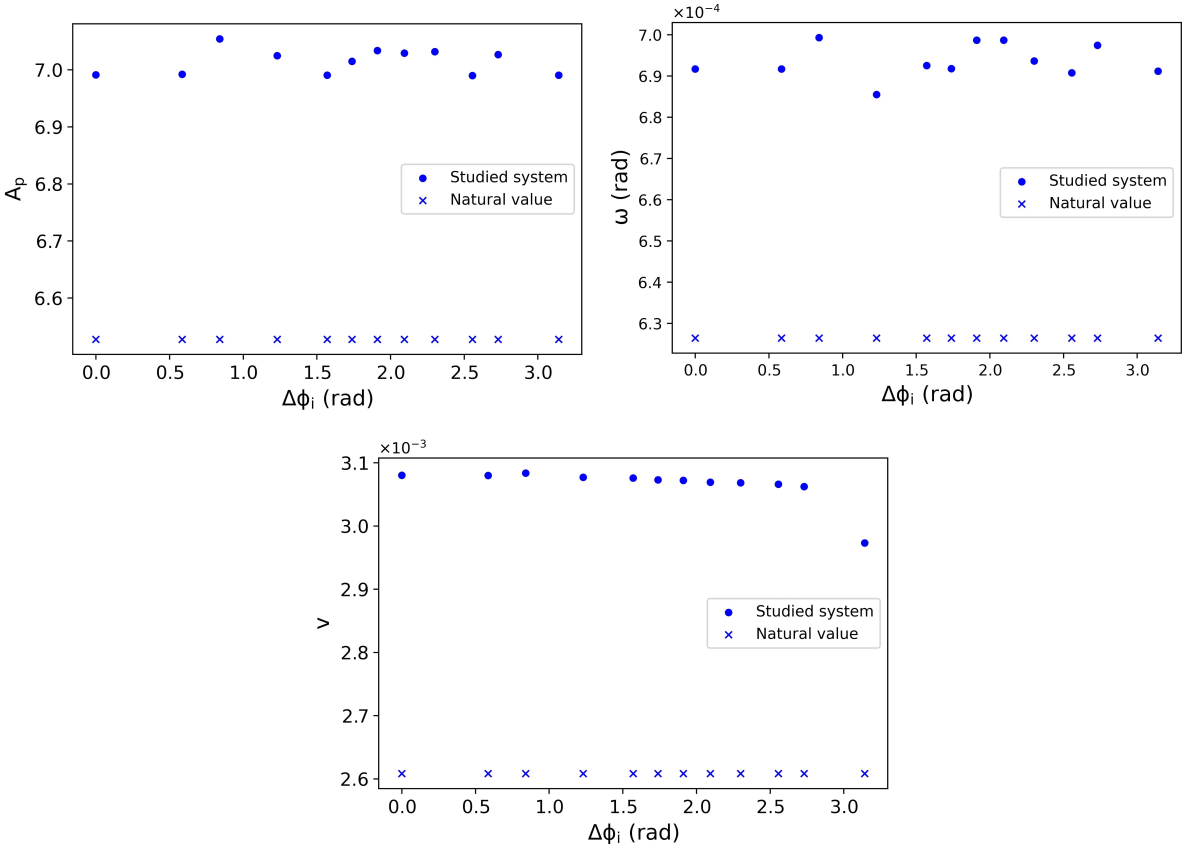

Figure A.1: Top left plot: final amplitude of both particles (blue dots) and the natural amplitude (blue x's) as a function of the initial phase shift. Top right plot: final frequency of both particles (blue dots) and the natural frequency (blue x's) as a function of the initial phase shift. Bottom plot: linear velocity (absolute mean linear velocity) of both particles (blue dots) and the natural linear velocity (blue x's) as a function of the initial phase shift. The initial phase shift does not affect neither the final nor the natural amplitude.

Distance dependency

The peak amplitude (top left plot of Figure A.2), the frequency (top right plot of Figure A.2) and the linear velocity (bottom plot of Figure A.2) of the particles in the synchronous state all have the same general tendency with distance: all these variables decreases with distance, tending to a long-distance value. This happens for all initial phase shift, with the outlier being the frequency for $\Delta\phi_i = 0.84$ rad: the frequency is mostly constant at $\omega = 6.28 \times 10^{-4}$ rad with some significantly higher values at $d = 40$, $d = 48$ and $d = 2048$. The approximate long-distance values are: $A_p = 6.5$, $\omega_f = 6.41 \times 10^{-4}$ rad and $v = 2.6 \times 10^{-3}$. These variables, by definition, tend towards their natural values (and the natural values of these variables do not depend on the distance).

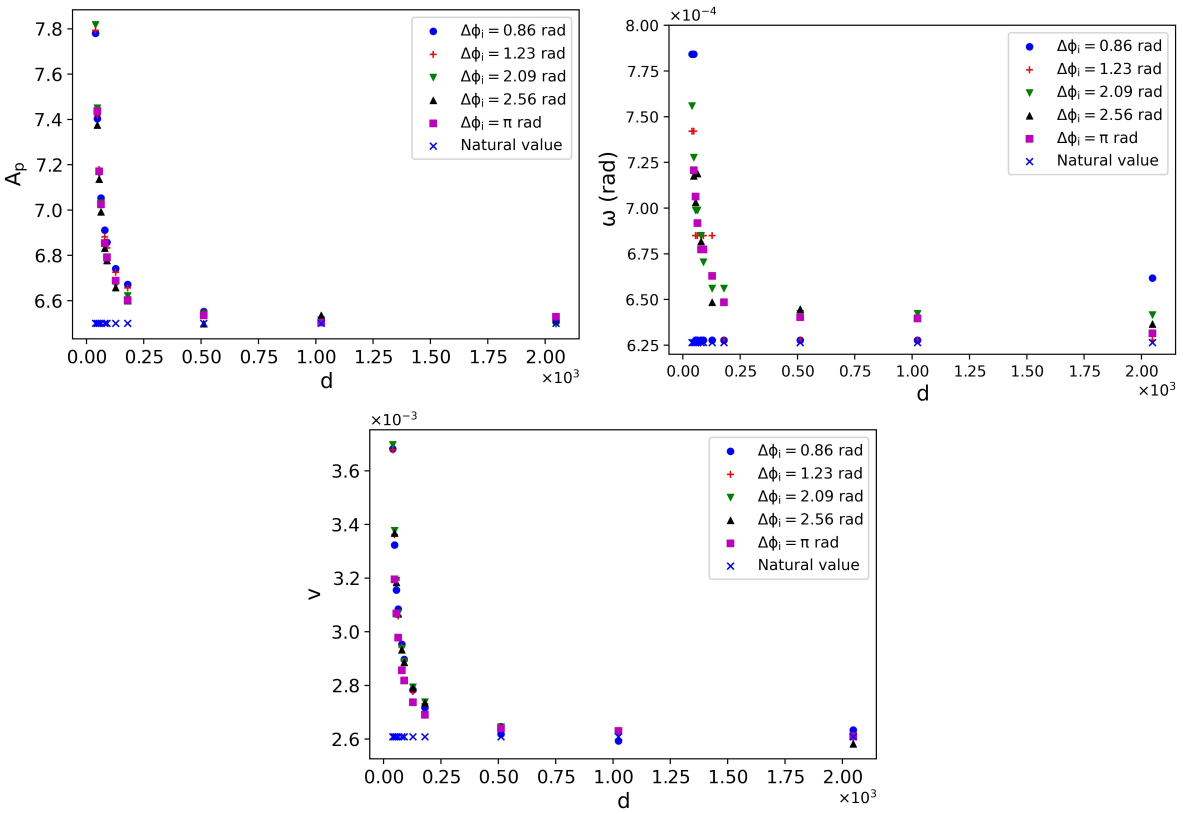

Figure A.2: Top left plot: final amplitude of both particles as a function of the distance between the centers of oscillation, for each of the initial phase shifts. The natural oscillation amplitude is also presented by the blue x's. The final amplitude (for all cases) tends towards the natural amplitude. Top right plot: final frequency of both particles as a function of the distance between the centers of oscillation, for each of the initial phase shifts. The natural frequency is also presented by the blue x's. The final frequency of the system tends towards the natural frequency. Curiously, for most of the distances the frequency of the system with $\Delta\phi_i = 0.86$ rad (blue dots) is identical to the natural frequency. Bottom plot: linear velocity (absolute mean linear velocity) of both particles as a function of the distance between the centers of oscillation, for each of the initial phase shifts. The natural linear velocity is also presented by the blue x's. The final linear velocity (for all cases) tends towards the natural linear velocity.

Viscosity dependency

Just as with the distance between centers of oscillation, the peak amplitude (top left plot of Figure A.3), the frequency (top right plot of Figure A.3) and the linear velocity (bottom plot of Figure A.3) of the particles in synchronization seem to decreases with viscosity. The end value of the peak amplitude is close to that of the long-distance, $A_p = 6.6$ (note that the different initial phase shifts have different values of viscosity beyond with the system does not synchronize). The end values (and mainly considering the set of results with $\Delta\phi_i = \pi$ rad) for the frequency and for the linear velocity are: $\omega_f = 4.00 \times 10^{-5}$ rad and $v = 1.7 \times 10^{-3}$. This is somewhat expected as for the larger resistance of the fluid to motion.

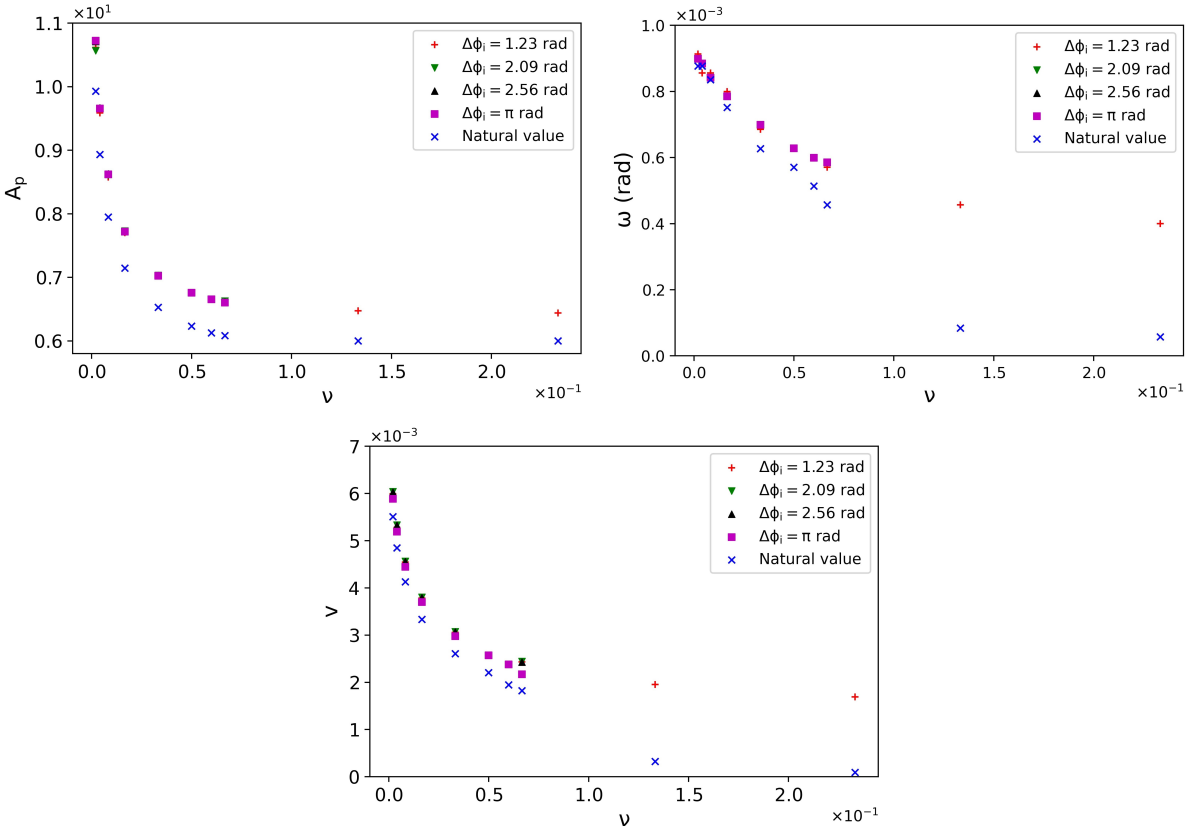

Figure A.3: Top left plot: final amplitude of both particles and the natural amplitude as a function of the fluid viscosity. The different initial phase shifts data sets have different sizes. Both final and natural amplitudes decrease with viscosity but are always different. Top right plot: final frequency of both particles and the natural frequency as a function of the fluid viscosity. The different initial phase shifts data sets have different sizes. The final and natural frequencies tend to the same values as the viscosity decreases. Bottom plot: linear velocity (absolute mean linear velocity) of both particles and the natural linear velocity as a function of the fluid viscosity. The different initial phase shifts data sets have different sizes. The final and natural linear velocities tend to the same values as the viscosity decreases.

Viscosity dependency with constant frequency

The tendencies of the peak amplitude (top left plot of Figure A.4) and the linear velocity (bottom plot of Figure A.4) are the same as they when we consider the distance and the viscosity dependencies: they decrease – which they both have to, as the frequency is constant. The end values of these quantities are: $A_p = 7.9$ and $v = 4.4 \times 10^{-3}$. As for prerequisite it is constant and equal to $\omega = 8.55 \times 10^{-4}$ rad (top right plot of Figure A.4). We recall that this is obtained by increasing the body acceleration along with the viscosity; the pair of values of these quantities that result in the same frequency was included in table 3.1.

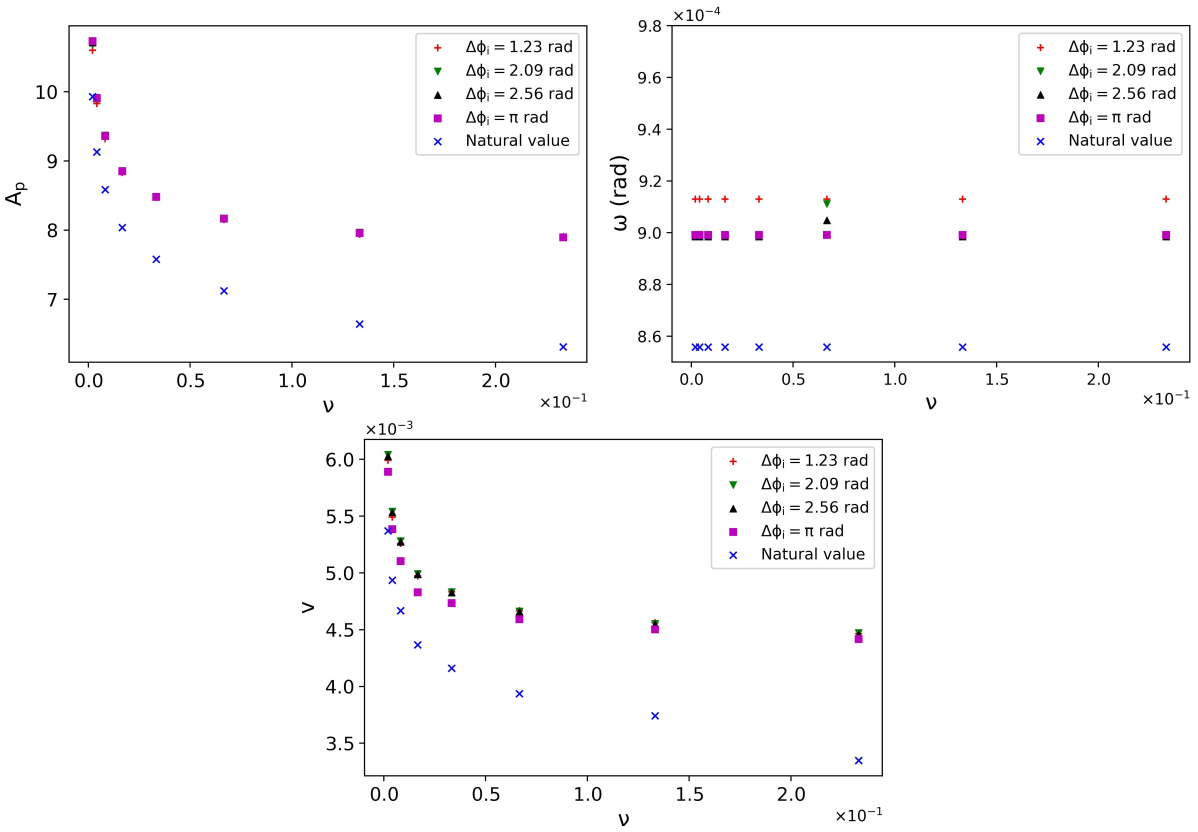

Figure A.4: Top left plot: final amplitude of both particles, for each of the initial phase shifts, and the natural amplitude as a function of the fluid viscosity, when the frequency is maintained constant. Top right plot: final frequency of both particles, for each of the initial phase shifts, and the natural frequency as a function of the fluid viscosity, when the frequency is maintained constant. The natural frequency is constant, as for prerequisite, and the final frequency is also mostly constant for each initial phase shift – it is slightly larger, $\omega = 9.11 \times 10^{-4}$ rad for $\Delta\phi_i = 1.23$ rad. Bottom plot: final linear velocity (absolute mean linear velocity) of both particles, for each of the initial phase shifts, and the natural linear velocity as a function of the fluid viscosity, when the frequency is maintained constant.

Linear velocity dependency

The linear velocity (its absolute mean value) dependency supposes that the natural frequency is constant, as to not have two variables at play. Its value oscillates slightly, but is essentially $\omega = 6.28 \times 10^{-4}$ rad (cf. top right plot of Figure A.5).

Both peak amplitude (top left plot of Figure A.5) and linear velocity (bottom plot of Figure A.5) increase linearly with the natural linear velocity. The peak amplitude is independent of the initial phase shift, and the proportionality of the linear velocity is only slightly different for each phase shift. The final frequency (top right plot of Figure A.5) varies both with the natural velocity and initial phase shift, but it hovers around with $\omega_f = 6.9 \times 10^{-4}$ rad. The final linear velocity is always larger than the natural linear velocity.

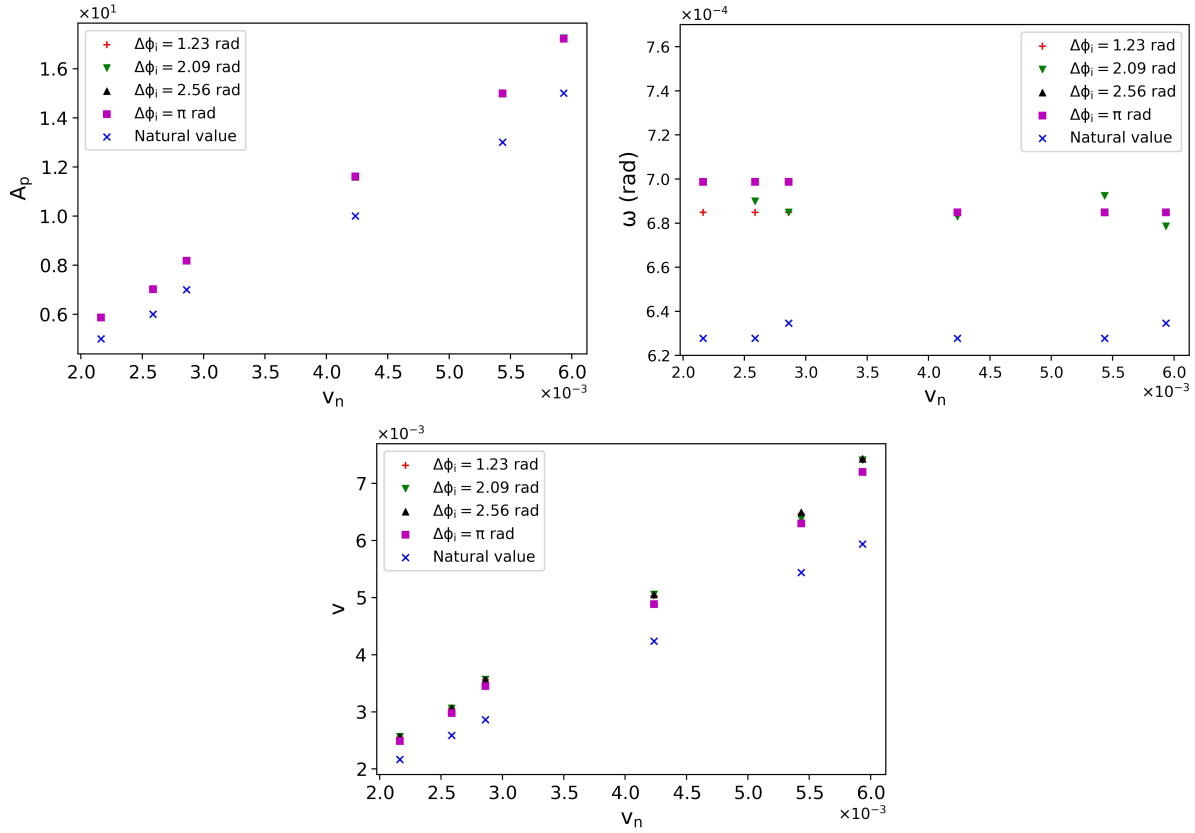

Figure A.5: Top left plot: final amplitude of both particles, for each of the initial phase shifts, and the natural amplitude as a function of the linear velocity (natural absolute mean linear velocity). The data sets for all the initial phase shifts overlap. Top right plot: final frequency of both particles, for each of the initial phase shifts, and the natural frequency as a function of the linear velocity (natural absolute mean linear velocity). The frequencies of the systems studied and the natural frequency vary slightly, being that the latter's oscillation is smaller; nonetheless, these variations are negligible. Bottom plot: linear velocity (absolute mean linear velocity) of both particles, for each of the initial phase shifts, and the natural linear velocity as a function of the natural absolute mean linear velocity. This last set is redundant, but helps to see that the linear velocity is always larger than its natural counterpart; it also has a larger slope.

Body acceleration dependency

Like with the linear velocity, both peak amplitude (top left plot of Figure A.6) and linear velocity (bottom plot of Figure A.6) increase with body acceleration (i.e., frequency, or natural frequency), and so does the final frequency (top right plot of Figure A.6). Once again the peak amplitude does not depend on the initial phase shift; the final frequency varies slightly only for $\Delta\phi_i = \pi$ rad. The final frequency is larger than the natural frequency; there is only one case in which this is not true: for $\Delta\phi_i = 1.23$ rad and $A_x = 1.0 \times 10^{-5}$, the final frequency is equal to the system's natural frequency. Besides that, this is the only instance, of all the simulations that we ran, that this happens. This would be the behavior that the Kuramoto model predicts: as both particles have the same natural frequency, in the synchronous stable state their frequency would be equal to their natural value (strictly speaking, equal to the average of the natural frequency of all particles).

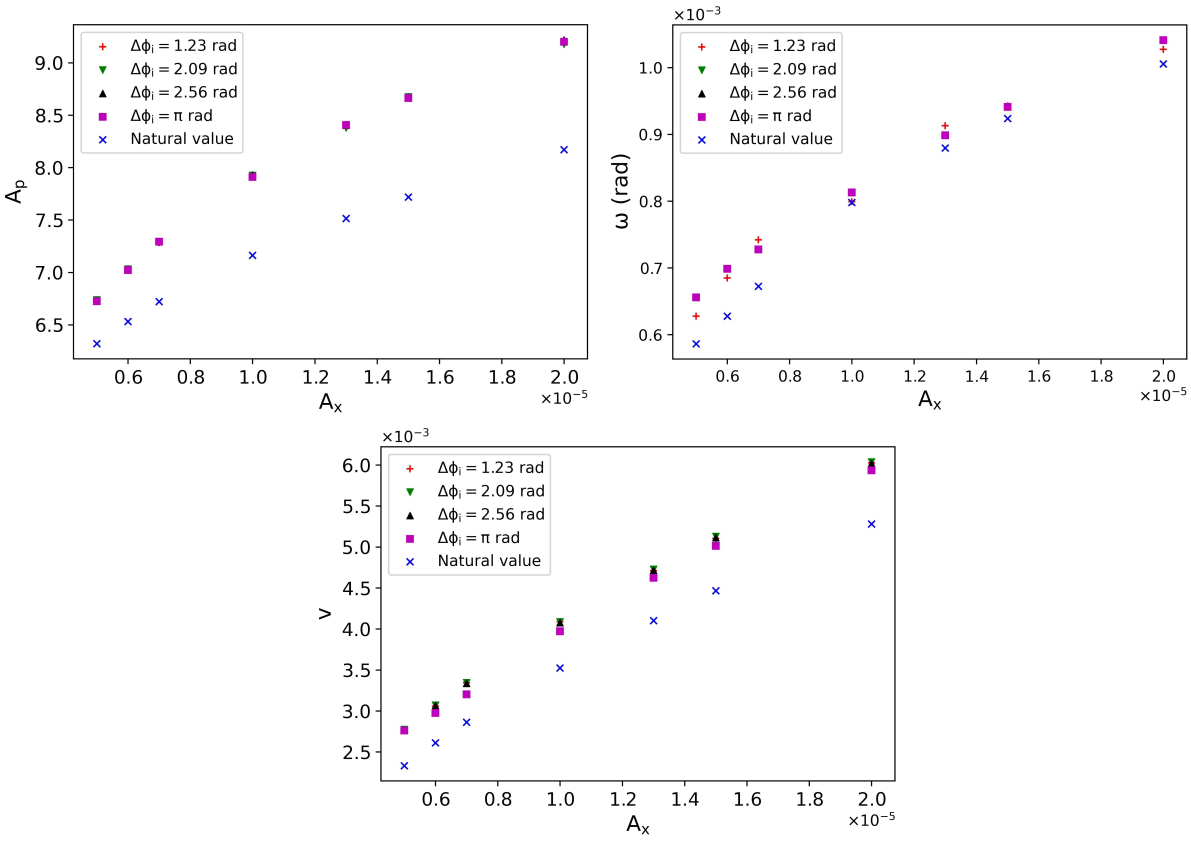

Figure A.6: Top left plot: final amplitude of both particles, for each of the initial phase shifts, and the natural amplitude as a function of the body acceleration of both particles. The difference between the amplitudes of the systems studied and their natural amplitude increases with the body acceleration. Top right plot: final frequency of both particles, for each of the initial phase shifts, and the natural frequency as a function of their body acceleration, for each of the initial phase shifts. The data points for all the initial phase shifts coincide, except for the data set of $\Delta\phi_i = 1.23$ rad – for $A_x = 1.0 \times 10^{-5}$, its data point coincides with that of the natural frequency. Bottom plot: linear velocity (absolute mean linear velocity) of both particles, for each of the initial phase shifts, and natural frequency as a function of the body acceleration of both particles. The linear velocity of the systems and its natural value mostly follow the same increasing tendency.

Particles with different frequencies

Distance dependency

The tendency of peak amplitude (left plot of Figure A.7) and final frequency (right plot of Figure A.7) is that of an decrease, here where each particles has a different natural frequency, as it is the case when they have the same frequency. The particle with $A = 6$ has a natural amplitude of $A_p = 6.07$ and a natural frequency of $\omega = 4.81 \times 10^{-4}$ rad, the particle with $A_p = 5$ has a natural amplitude of $A = 5.14$ and a natural frequency of $\omega = 5.49 \times 10^{-4}$ rad.

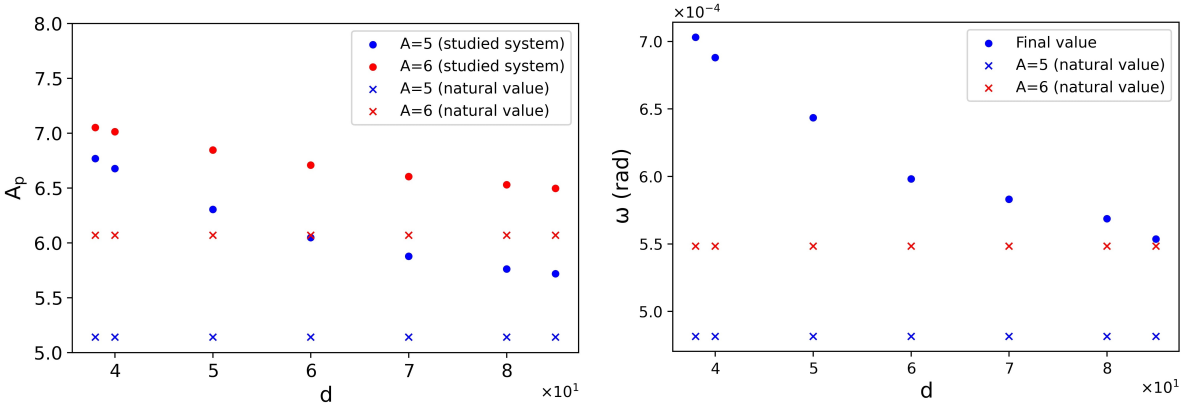

Figure A.7: Left plot: final (dots) and natural (x's) amplitudes of each particle as a function of the fluid viscosity. As expected, the final amplitude of each particle tends towards their natural amplitude, but we can also see that the closer the particles are, the smaller the difference between their motion's amplitude. Right plot: final (dots) and natural (x's) frequency of both particles as a function of the fluid viscosity. As we represent the systems that synchronize, the final frequency of both particles is the same. The final frequency decreases with distance, but it is always larger than any of the natural frequencies.

Viscosity dependency

What has been said for the distance is valid for the viscosity: both peak amplitude (left plot of Figure A.8) and final frequency (right plot of Figure A.8) decay with viscosity. But here we see that natural frequency of each particle and the final frequency of the system all tend to the same value as the viscosity becomes smaller and smaller.

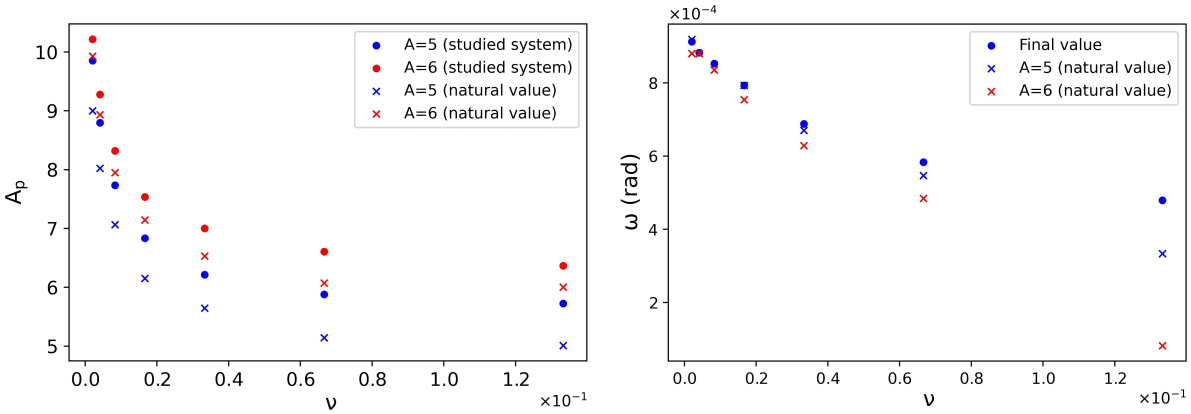

Figure A.8: Left plot: peak amplitude of both particles as a function of the fluid viscosity. Right plot: final frequency of both particles as a function of the fluid viscosity. As the viscosity becomes smaller, the closer the natural frequencies get to each other, and these to the final frequency of the system. As the system synchronizes, the frequency of both particles is the same.

Body acceleration difference dependency

The variation on the body acceleration difference probably has the most peculiar influences in the peak amplitude (left plot of Figure A.9) and final frequency (right plot of Figure A.9). There is a divergence in peak amplitude from $A_{x2} = 6.5 \times 10^{-6}$ onward, with the peak amplitude of both particles coinciding for this pair of body acceleration values. The final frequency of the synchronous state increases slightly; the natural frequency of one of the particles is necessarily constant (as both turnabout

amplitude and body acceleration are maintained constant); the natural frequency of the particle whose body acceleration is being increased has a large jump at $A_{x2} = 6.5 \times 10^{-6}$ and then increases slightly at $A_{x2} = 7.3 \times 10^{-6}$. One of the most curious results is the fact that for $A_{x2} = 7.4 \times 10^{-6}$ and $A_{x2} = 7.4 \times 10^{-6}$, the final frequency is between the natural frequency of both particles. This is the only time this happens in our simulations - in all other cases, the value of the final frequency is larger than the natural frequency of the particles. Despite this, the values at these points, $\omega_2 = 7.10 \times 10^{-4}$ rad is very close to the value of the final frequency, $\omega_{f1} = \omega_{f2} = 7.04 \times 10^{-4}$ rad. This seems to indicate that the final frequency is largely dominated by the particle with the larger body acceleration - so much so that from $A_{x2} = 7.4 \times 10^{-6}$ onward the the system does not synchronize.

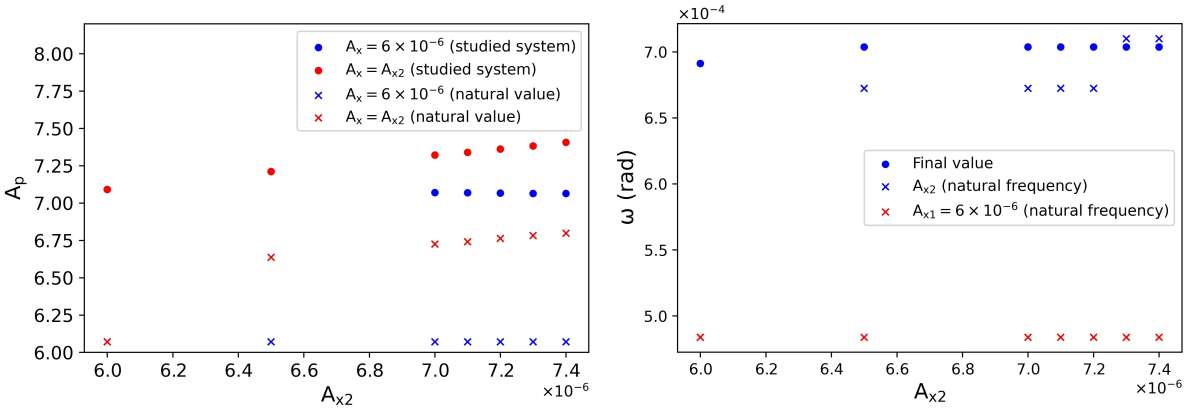

Figure A.9: Left plot: natural (x's) and final (dots) amplitude of each particle as a function of the body acceleration of the particle whose body acceleration was change between simulations, A_{x2}. The peak amplitude of the particles are the same up until $A_{x2} = 6.5 \times 10^{-6}$. Right plot: final frequency of each particle in the synchronous state (dots) and the natural frequency (x's) of each particle as a function of the body acceleration of the particle whose body acceleration was change between simulations, A_{x2}. As the system synchronizes, the frequency of both particles is the same and their data sets overlap. ω_{f2} is constant as the body acceleration of this particle is constant – $A_x = 6 \times 10^{-6}$.

Appendix B

Synchronization parameter calculations

When we write the expression 2.13, what we are saying is that the synchronization parameter R is the module and ψ is the argument of the average of all the N phasors of our system. This means that, for 2 oscillators, R is immediately given by:

$$R = \left| \frac{e^{i\theta_1} + e^{i\theta_2}}{2} \right| = \left| \frac{\cos(\theta_1) + i\ \sin(\theta_1) + \cos(\theta_2) + i\ \sin(\theta_1)}{2} \right|, \tag{B.1}$$

$$R = \frac{1}{2}\sqrt{[\cos(\theta_1) + \cos(\theta_2)]^2 + [\sin(\theta_1) + \sin(\theta_1)]^2}. \tag{B.2}$$

But by the end of this appendix we will have arrived at a much simpler expression for R.

Once again for 2 oscillators, we have that ψ is given by:

$$\psi = Arg\left(\frac{e^{i\theta_1} + e^{i\theta_2}}{2}\right) = Arg\left[\frac{\cos(\theta_1) + i\ \sin(\theta_1) + \cos(\theta_2) + i\ \sin(\theta_1)}{2}\right], \tag{B.3}$$

$$\psi = Arg\left[\frac{\cos(\theta_1) + \cos(\theta_2)}{2} + i\frac{\sin(\theta_1) + \sin(\theta_2)}{2}\right]. \tag{B.4}$$

At this point we recall the identities for the sum of two sine and two cosine functions:

$$\sin(\alpha) + \sin(\beta) = 2\sin\left(\frac{\alpha+\beta}{2}\right)\cos\left(\frac{\alpha-\beta}{2}\right), \tag{B.5}$$

$$\cos(\alpha) + \cos(\beta) = 2\cos\left(\frac{\alpha+\beta}{2}\right)\cos\left(\frac{\alpha-\beta}{2}\right). \tag{B.6}$$

The argument is calculated then from the 2-argument arctangent function $atan2$, which can take one of these 3 results, depending if the real, x, and complex, y, components of the argument are positive or negative:

$$\psi = \arctan\left[\frac{\sin\left(\frac{\theta_1+\theta_2}{2}\right)}{\cos\left(\frac{\theta_1+\theta_2}{2}\right)}\right] = \arctan\left[\tan\left(\frac{\theta_1+\theta_2}{2}\right)\right] = \frac{\theta_1+\theta_2}{2},\ \text{if } x > 0, \tag{B.7}$$

$$\psi = \arctan\left[\frac{\sin\left(\frac{\theta_1+\theta_2}{2}\right)}{\cos\left(\frac{\theta_1+\theta_2}{2}\right)}\right] + \pi = \arctan\left[\tan\left(\frac{\theta_1+\theta_2}{2}\right)\right] + \pi = \frac{\theta_1+\theta_2}{2} + \pi, \text{ if } x < 0 \text{ and } y \geq 0, \tag{B.8}$$

$$\psi = \arctan\left[\frac{\sin\left(\frac{\theta_1+\theta_2}{2}\right)}{\cos\left(\frac{\theta_1+\theta_2}{2}\right)}\right] - \pi = \arctan\left[\tan\left(\frac{\theta_1+\theta_2}{2}\right)\right] - \pi = \frac{\theta_1+\theta_2}{2} - \pi, \text{ if } x < 0 \text{ and } y < 0. \tag{B.9}$$

It goes without saying that if the real component, x, is zero, then argument ψ is $\pi/2$ rad, if $y > 0$, and it is $-\pi/2$ rad, if $y < 0$.

For now, let us consider the case where we have $x > 0$. We can write 2.13 for 2 oscillators as:

$$R\, e^{i\left(\frac{\theta_1+\theta_2}{2}\right)} = \frac{1}{2}\left(e^{i\theta_1} + e^{i\theta_2}\right), \tag{B.10}$$

and from this expression we make the final developments:

$$R = \frac{1}{2}\left(e^{i\theta_1} + e^{i\theta_2}\right) e^{-i\left(\frac{\theta_1+\theta_2}{2}\right)} = \frac{1}{2}\left\{e^{i\left[\theta_1 - \left(\frac{\theta_1+\theta_2}{2}\right)\right]} + e^{i\left[\theta_2 - \left(\frac{\theta_1+\theta_2}{2}\right)\right]}\right\}, \tag{B.11}$$

$$R = \frac{1}{2}\left[e^{i\left(\frac{\theta_1-\theta_2}{2}\right)} + e^{i\left(\frac{\theta_2+\theta_1}{2}\right)}\right] = \frac{1}{2}\left[e^{i\left(\frac{\theta_1-\theta_2}{2}\right)} + e^{-i\left(\frac{\theta_1+\theta_2}{2}\right)}\right], \tag{B.12}$$

being that the last expression is equivalent to the cosine function:

$$R = \cos\left(\frac{\theta_1-\theta_2}{2}\right) = \cos\left(\frac{\Delta\theta}{2}\right). \tag{B.13}$$

The two cases B.8 and B.9 result in having $e^{\pm i\pi} = -1$ on the left-hand side of the equality on B.10. In reality, as R is always taken as being non-negative, we can ignore the $\pm\pi$ rad that we get from the $atan2$ function in B.8 and B.9, and arrive to our final expression for R:

$$R \equiv |\pm R| = \left|\pm\cos\left(\frac{\Delta\theta}{2}\right)\right| = \left|\cos\left(\frac{\Delta\theta}{2}\right)\right|. \tag{B.14}$$

And recalling the cases in which the real component is zero, we would get $e^{\pm i\pi/2} = \pm i$; but this also would mean that the real component of R would have to be zero: $\cos(\theta_1) + \cos(\theta_2) = 0$. This only happens when $\theta_1 = (\theta_2 + \pi + 2\pi n)$ rad, with $n \in \mathbb{Z}$, i.e., when the system is in phase opposition –, which means that the synchronization parameter is zero. This result is already predicted by B.14:

$$R = \left|\cos\left(\frac{\pi \pm 2\pi n}{2}\right)\right| = \left|\cos\left(\frac{\pi}{2} \pm \pi n\right)\right| = 0. \tag{B.15}$$